The Effects of Adherence to Antiretroviral Therapy for HIV-1 Infection

Lauren Clara Browning McKenzie

Thesis submitted in partial fulfillment of the requirements for the degree of
Master of Science Mathematics and Statistics[1]

Department of Mathematics and Statistics
Faculty of Science
University of Ottawa

© Lauren Clara Browning McKenzie, Ottawa, Canada, 2021

[1]The M.Sc. program is a joint program with Carleton University, administered by the Ottawa-Carleton Institute of Mathematics and Statistics

Abstract

The emergence of drug resistance is a serious threat to the long-term virologic success and durability of HIV-1 therapy. Adherence has been shown to be a major determinant of drug resistance; however, each pharmacologic class of antiretroviral drugs has a unique adherence–resistance relationship. We develop an immunological model of the HIV-1 infected human immune system that integrates the unique mechanisms of action of reverse transcriptase and protease inhibiting drugs. A system of impulsive differential equations is used to examine the drug kinetics within $CD4^+$ T cells. Stability analysis was preformed to determine the long-term dynamics of the model. Using the endpoints of an impulsive periodic orbit in the drug levels, the maximal length of a drug holiday while avoiding drug resistance is theoretically determined; the minimum number of doses that must be subsequently taken to return to pre-interruption drug levels is also established. Heterogeneity in inter-individual differences on drug-holiday length is explored using sensitivity analysis based on Latin Hypercube Sampling and Partial Rank Correlation Coefficient analysis. Extremely short drug holidays are acceptable, as long as they are followed by a period of strict adherence. Numerical simulations demonstrate that if the drug holiday exceeds these recommendations, the cost in virologic rebound is unacceptably high. These theoretical predictions are in line with clinical results and may also help form the basis of future clinical trials.

Dedication

To mom and dad, for teaching me that no goal is too high when you aim with care and confidence. You are my heroes.

Acknowledgements

First and foremost, I would like to express my deepest thanks to my supervisor Dr. Stacey Smith? for her continuous guidance and encouragement throughout the last two years. Since introducing me to the field of mathematical biology during the first semester of my undergraduate degree, you have taught me so much about the field, perseverance in the face of challenges, and how to become a better writer (namely, how to properly use en dash). For these things, I am truly grateful.

I would also like to thank my parents, Art and Diane, and my sister Cara, for always believing in me and supporting my dreams; I wouldn't be where I am today without your endless support and love. To Jérémie, your unwavering encouragement and patience has made all the difference.

I am also extremely grateful to my examiners Dr. Lucy Campbell and Dr. Diane Guignard for their valuable feedback and comments, which have led to significant improvement of my thesis.

Finally, I would like to extend my appreciation to all the professors and staff in the Department of Mathematics and Statistics who have taught and inspired me along my journey.

Contents

Introduction

The current armamentarium for Human Immunodeficiency Virus 1 (HIV-1) infection has proven remarkably effective in decreasing both morbidity and mortality rates of patients with HIV-1 [1]. When successful, it can reduce viral load to below viral detection limit, improve immune system function, and prevent progression to late-stage HIV infection, Acquired Immunodeficiency Syndrome (AIDS). However, significant pill burden, complex dosing schedules and several dietary restrictions can make strict adherence to antiretroviral therapy(ART) regimens difficult [2]. Given the high replication and mutation rates of the virus [3, 4], suboptimal adherence can rapidly compromise therapeutic response and facilitate the emergence of drug-resistant strains of the virus [5]. The World Health Organization's (WHO's) 2019 drug-resistance surveillance report [6] found that between 21% and 97% of those receiving ART harboured resistance to one or more commercially available antiretroviral drugs. Moreover, an estimated 16% of the AIDS-related deaths are directly attributable to drug resistance; this number is projected to increase to 25% before 2030 [7]. Despite its criticality, the relationship between therapy adherence and the emergence of drug resistance remains widely unknown. It is thus necessary to quantify the degree of adherence required to maintain virologic suppression; specifically, how many doses of medication can be missed before treatment is adversely affected and drug resistance arises.

While numerous mathematical models have investigated the in-host effects of HIV-1 drug resistance [8, 9, 10], the use of impulsive differential equations to model drug concentration dynamics is relatively new [5, 11, 12]. Impulsive differential equations allow short-term dynamics to be approximated by an instantaneous shock or jump, concentrating the analysis on the slower, between-shock dynamics [13, 14, 15]. Impulsive differential equations have been used to determine necessary conditions for the emergence of drug resistance in monotherapy to nucleoside reverse transcriptase inhibitors (NRTIs), non-nucleoside reverse transcriptase inhibitors (NNRTIs), protease inhibitors (PIs) and fusion inhibitors (FIs) [2, 11, 16]; however, these models do not adequately describe the action of multi-class ART.

The multi-step HIV-1 replication cycle provides several opportunities for therapeutic intervention, each of which is targeted by a different drug class. Combining HIV-1 drug classes allows for a more complete viral suppression and limits the emergence of drug resistance during chronic viral infection. However, since each class has

a unique genetic barrier to resistance, interacts differently with $CD4^+$ T cells and affects the pharmacokinetics of the other drugs in the combination, modelling the combination of different drug classes presents several unique challenges. For certain drug classes, multiple mutations are required to cause decreased drug susceptibility, whereas others require just a single mutation [17]. The number of mutations necessary to confer resistance contributes to the genetic barrier to resistance of the antiretroviral and is unique for each class. [17]. Selection of a mutant not only depends on the associated fitness effect, but on drug levels, which will vary with the dosage amount, drug half-life and dosing interval. Here, our modelling approach allows us integrate these factors into the model.

Our model considers two strains of HIV: the wild-type strain, which dominates in the absence of drugs, and a mutant strain, which is a less efficient competitor but has a higher resistance to antiretroviral drugs. Since antiretroviral drugs reduce viral fitness in a dose-dependent manner, drug levels determine the viral tropism of each strain and are thus divided into three regions: low drug levels will not affect either strain; intermediate drug levels will control the wild-type strain alone; high drug levels will control both strains. The following research questions are addressed: a) how many doses can a strongly adherent patient miss before resistance emerges? b) How many subsequent doses must be taken to return to pre-interruption drug levels? c) How do different patterns of adherence affect treatment outcome? The individual pharmacokinetics effects of each drug in all WHO-approved regimens are considered.

Chapter 1

Impulsive Differential Equations

Several evolutionary processes can be characterized by short perturbations in the system that imply a change in state. These short-term perturbations can be considered as having acted instantaneously; that is, in the form of impulses, since their length is negligible in comparison to the duration of the process as a whole. Differential equations involving impulsive effects — impulsive differential equations — serve as a natural description of such processes. They are often used in mathematical modelling to simplify complicated hybrid models. Impulsive differential equations have a host of applications to many fields in the natural sciences. In biology, examples include systems that undergo a sudden change of state like blood flow through the heart, periodic vaccination strategies or the introduction of medication into the system.

1.1 Description of systems with impulses

The information in this section is a summary of the books [13, 14, 15].

Let $\Omega \subset \mathbb{R}^n$ be the phase space of a given evolutionary process. Assume that the law of evolution of the process is described by

$$\frac{dx}{dt} = f(t, x) \tag{1.1.1}$$

where $t \in \mathbb{R}^+$, $x : \mathbb{R}^+ \times \Omega \subset \Omega$, and $f : \mathbb{R}^+ \times \Omega \to \mathbb{R}^n$.

Denote

i) $P_t \in \mathbb{R}^+ \times \Omega$ as the point that describes the state of the given process at time t.

ii) $M(t)$, $N(t) \subset \Omega$ for all $t \in \mathbb{R}^+$, and consider the operator $A(t) : M(t) \to N(t)$, for all $t \in \mathbb{R}^+$.

The solution of (1.1.1) is given by $x(t) = x(t, t_0, x_0)$ for some given (t_0, x_0).

The evolutionary process then behaves as follows: The point $P_t = (t, x(t))$ moves from its initial position $P_{t_0} = (t_0, x_0)$ along the curve $(t, x) : t \geq t_0, x = x(t)$ until the time $\tau_1 > t_0$ at which it meets the set $M(t)$. At time τ_1, the operator $A(t)$ instantaneously moves the point from $P_{\tau_1} = (\tau_1, x(\tau_1))$ to $P_{\tau_1^+} = (\tau_1, x_1^+) \in N(\tau_1)$, where $x_1^+ = A(\tau_1)x(\tau_1)$. After this, the point continues along the solution curve of (1.1.1), which is now given by $(t, x(\tau_1), x_1^+)$. When the point again meets the set $M(t)$, at time τ_2, the process will repeat as long as the solution to (1.1.1) exists. The set of relations i) and ii) characterizing the evolutionary process will be called an impulsive differential equation, and the moments τ_k at which the point P_t meets the set M_t are called impulses. The function $x(t)$ is called the solution of the impulsive differential equation and is assumed to be left continuous at the moments of impulse $\tau_k, k \in \mathbb{Z}$.

Define $I : \mathbb{R} \times \Omega \to \Omega$, by the relation

$$A(t) : M(t) \to N(t), (t, x) \to (t, x + I(t, x)),$$

where (t, x) is the mapping of the solution before the impulse, $\lim_{t \to \tau_k^-} x(t) \equiv x(\tau_k^-)$, to after the impulse effect, $\lim_{t \to \tau_k^+} x(t) \equiv x(\tau_k^+)$. Then $\Delta x(\tau_k) = I(\tau_k^-, x(\tau_k^-))$, where $\Delta x(\tau_k) = x(\tau_k^+) - x(\tau_k^-)$.

1.2 Classes of differential equations

There are three main classes of impulsive differential equations:

Class 1: Equations with state-dependent moments of the impulse effect.
The equations of this class are written as follows:

$$\begin{aligned} \frac{dx}{dt} &= f(t, x), \quad t \neq \tau_k(x), \\ \Delta x &= I_k(x), \quad t = \tau_k(x), \end{aligned} \tag{1.2.1}$$

where $\tau_k : \Omega \to \mathbb{R}$ and $\tau_k < \tau_{k+1} (k \in K \subset \mathbb{Z}, x \in \Omega)$. The impulsive effect occurs when the mapping point (t, x) meets some hyperspace σ_k of the equation $t = \tau_k(x)$.

Class 2: Equations with fixed moments of the impulsive effect.

These are equations of the form

$$\begin{aligned} \frac{dx}{dt} &= f(t,x), \quad t \neq \tau_k, \\ \Delta x &= I_k(x), \quad t = \tau_k. \end{aligned} \tag{1.2.2}$$

The moments of impulse effect are predetermined and are assumed to be monotonic and unbounded. That is, $\tau_k < \tau_{k+1}$, for all $k \in \mathbb{Z}$ and $\tau_k \to \infty$ as $k \to \infty$.

For $t \in (\tau_k, \tau_{k+1}]$, the solution $x(t)$ of (1.2.2) satisfies the equation (1.1.1), and for $t = \tau_k$ satisfies the recurrence relation $x(\tau_k^+) = x(\tau_k^-) + I_k(x(\tau_k^-))$. The model presented in Chapter 3.3 employs the use of Class 2 impulsive differential equations.

Class 3: Autonomous impulsive equations.
These equations are of the form

$$\begin{aligned} \frac{dx}{dt} &= f(t,x), \quad x \notin \sigma, \\ \Delta x &= I_k(x), \quad x \in \sigma, \end{aligned} \tag{1.2.3}$$

where σ is an $(n-1)$-dimensional manifold contained within $\Omega \subset \mathbb{R}^n$. The instants of impulsive effect occur when the point $x(t)$ of the phase space meets the manifold σ.

1.3 Existence and uniqueness of solutions

Class 1: State-Dependent Moments of Impulse Effect

Let $\Omega \subset \mathbb{R}^n$ be an open set. Suppose that the functions $\tau_k : \Omega \to \mathbb{R}$ are continuous in Ω for all $k \in \mathbb{Z}$ and are such that

$$\tau_k(x) < \tau_{k+1}(x), \qquad \lim_{k \to \pm\infty} \tau_k(x) = \pm\infty,$$

where $x \in \Omega$. Let $f : \mathbb{R} \times \Omega \to \mathbb{R}^n$, $I_k : \Omega \to \mathbb{R}$, $(t_0, x_0) \in \mathbb{R} \times \Omega$ and $\alpha < \beta$. Consider the impulsive differential equation

$$\begin{aligned} \frac{dx}{dt} &= f(t,x), \quad t \neq \tau_k, \\ \Delta x &= I_k(x), \quad t = \tau_k, \end{aligned} \tag{1.3.1}$$

with initial condition

$$x(t_0^+) = x_0. \tag{1.3.2}$$

Definition 1.3.1. *The function $\varphi : (\alpha, \beta) \to \mathbb{R}^n$ is said to be a* solution *of (1.3.1) on (α, β) if:*

1. $(t, \varphi(t)) \in \mathbb{R} \times \Omega$ *for* $t \in (\alpha, \beta)$*;*

2. *for* $t \in (\alpha, \beta)$, $t \neq \tau_k(\varphi(t))$, $k \in \mathbb{Z}$, *the funtion* $\varphi(t)$ *is differentiable and* $\frac{d\varphi}{dt}(t) = f(t, \varphi(t))$*;*

3. *the function* $\varphi(t)$ *is left continuous in* (α, β) *and if* $t \in (\alpha, \beta)$, $t = \tau_k(\varphi(t))$ *and* $t \neq \beta$, *then* $\varphi(t^+) = \varphi(t) + I_k(\varphi(t))$ *and, for each* $j \in \mathbb{Z}$ *and some* $\delta > 0$, $s \neq \tau_j(\varphi(s))$ *for* $t < s < t + \delta$.

Definition 1.3.2. *Each solution* $\varphi(t)$ *of (1.3.1) that is defined in an interval* (t_0, β) *and satisfies condition (1.3.2),* $\varphi(t^+) = x_0$ *is said to be a* solution of the initial-value problem (1.3.1)–(1.3.2).

For $t_0 \neq \tau_k(x_0)$, for all $k \in \mathbb{Z}$, the existence and uniqueness of the initial-value problem (1.3.1)–(1.3.2) is dependent only on the function f. If the function f is continuous in a neighbourhood of the point (t_0, x_0), then there exists a solution $x(t)$ to (1.3.1) with initial condition (1.3.2). Furthermore, if f is Lipshitz continuous around the point (t_0, x_0) then the solution is unique.

If for some $k \in \mathbb{Z}$, $t_0 = \tau_k(x_0)$, then additional requirements need to be imposed on f in order to guarantee any general existence theory for the initial-value problem (1.3.1)–(1.3.2), and to assert the validity of the condition

$$t \neq \tau_k(x(t)) \tag{1.3.3}$$

for $t \in (t_0, \beta)$ and $k \in \mathbb{Z}$. Such conditions are defined in the following theorem.

Theorem 1.3.3. *Assume that the following conditions hold:*

1. *The function* $f : \mathbb{R} \times \Omega \to \mathbb{R}^n$*is continuous for* $t \neq \tau_k$, $k \in \mathbb{Z}$.

2. *For any* $(t, x) \in \mathbb{R} \times \Omega$, *there exists a locally integrable function* g *such that in a small neighbourhood of* (t, x)

$$|f(s, y)| \leq g(s). \tag{1.3.4}$$

3. *For all* $k \in \mathbb{Z}$, *the condition* $t_1 = \tau_k(x_1)$ *implies the existence of some* $\delta > 0$ *such that* $t \neq \tau_k(x)$ *for all* $0 < t - t_1 < \delta$ *and* $|x - x_1| < \delta$.

Then, for all $(t_0, x_0) \in \mathbb{R} \times \Omega$, *there exists a solution* $x : (t_0, \beta) \to \mathbb{R}^n$ *of the initial-value problem (1.3.1)–(1.3.2) for some* $\beta > t_0$.

Class 2: Fixed Moments of Impulse Effect

Let $f : \mathbb{R} \times \Omega \to \mathbb{R}^n$, $I_k : \Omega \to \mathbb{R}$, $(t_0, x_0) \in \mathbb{R} \times \Omega$ and $\alpha < \beta$. Consider the impulsive differential equation

$$\begin{aligned} \frac{dx}{dt} &= f(t,x), \quad t \neq \tau_k, \\ \Delta x &= I_k(x), \quad t = \tau_k, \end{aligned} \tag{1.3.5}$$

where the moments of impulse effect are predetermined and

$$\tau_k(x) < \tau_{k+1}, \qquad \lim_{k\to\pm\infty} \tau_k(x) = \pm\infty \qquad (x \in \Omega).$$

Theorem 1.3.4. *Let the function $f : \mathbb{R}\times\Omega \to \mathbb{R}^n$ be continuous in the sets $(\tau_k, \tau_{k+1}]\times \Omega$, $k \in \mathbb{Z}$, and, for each $k \in \mathbb{Z}$ and $x \in \Omega$, suppose that there exists a finite limit of $f(t, y)$ as $(t, y) \to (\tau_k, x)$, $t > \tau_k$. Then, for each $(t_0, x_0) \in \mathbb{R} \times \Omega$, there exists $\beta > t_0$ and a solution $x : (t_0, \beta) \to \mathbb{R}^n$ of (1.3.5) with initial condition (1.3.2). Moreover, if the function f is locally Lipschitz continuous with respect to $x \in \Omega$, then this solution is unique.*

Theorem 1.3.5. *Assume that the following conditions hold:*

1. *The function $f : \mathbb{R} \times \Omega \to \mathbb{R}^n$ is continuous in the sets $(\tau_k, \tau_{k+1}] \times \Omega$, $k \in \mathbb{Z}$, and, for each $k \in \mathbb{Z}$ and $x \in \Omega$, there exists the finite limit of $f(t, y)$ as $(t, y) \to (\tau_k, x)$, $t > \tau_k$.*
2. *The function $\varphi : (\alpha, \beta) \to \mathbb{R}^n$ is a solution of (1.3.5).*

Then the solution $\varphi(t)$ is continuable to the right of β if and only if the limit

$$\lim_{t\to\beta^-} \varphi(t) = \eta \tag{1.3.6}$$

exists and one of the following conditions is fulfilled:

1. *$\beta \neq \tau_k$ for each $k \in \mathbb{Z}$ and $\eta \in \Omega$;*
2. *$\beta = \tau_k$ for some $k \in \mathbb{Z}$ and $\eta + I_k(\eta) \in \Omega$.*

Theorem 1.3.6. *Let the following conditions hold:*

1. *Condition 1 of Theorem 1.3.5 is satisfied.*
2. *The function f is locally Lipschitz continuous with respect to $x \in \Omega$.*
3. *$\eta + I_k(\eta) \in \Omega$ for all $k \in \mathbb{Z}$ and $\eta \in \Omega$.*

Then, for any $(t_0, x_0) \in \mathbb{R} \times \Omega$, there exists a unique solution of (1.3.5) with initial condition (1.3.2) that is defined in an interval of the form (t_0, ω) and is not continuous to the right of ω.

Definition 1.3.7. *Let Theorem 1.3.6 be satisfied and let $(t_0, x_0) \in \mathbb{R} \times \Omega$. Define $J^+(t_0, x_0)$ to be the* maximal interval *of the form (t_0, ω) in which $x(t;, t_0, x_0)$is defined.*

Theorem 1.3.8. *Let the following conditions hold:*

1. *Conditions 1, 2 and 3 of Theorem 1.3.6 are satisfied.*
2. *$\varphi(t)$ is a solution of the initial-value problem (1.3.5)–(1.3.2).*
3. *there exists a compact $Q \subset \Omega$ such that $\varphi(t) \in Q$ for $t \in J^+(t_0, x_0)$.*

Then $J^+(t_0, x_0) = (t_0, +\infty)$.

Let $\varphi : (\alpha, \omega) \to \mathbb{R}^n$ be a solution of 1.3.5 and consider the continuability of this solution to the left of α.

If $\alpha \neq \tau_k$, $k \in \mathbb{Z}$, then the problem of continuability to the left of α is solved as it is with ordinary differential equations. In this case, such an extension is possible if and only if the limit

$$\lim_{t \to \alpha^+} \varphi(t) = \eta \tag{1.3.7}$$

exists and $\eta \in \Omega$.

If $\alpha = \tau_k$ for some $k \in \mathbb{Z}$, then the solution $\varphi(t)$ will be continuable to the left of τ_k when the limit (1.3.7) exists, $\eta \in \Omega$, and the equation $x + I_k(x) = \eta$ has a unique solution for $x_k \in \Omega$. In thin s case, call $\psi(t)$ the extension of $\varphi(t)$ for $t \in (\tau_{k-1}, \tau_k]$, which coincides with the solution of the initial-value problem

$$\begin{aligned} \frac{d\psi}{dt} &= f(t, \psi), \quad \tau_{k-1} < t \leq \tau_k, \\ \phi(\tau_k) &= x_k. \end{aligned}$$

If the solution $\varphi(t)$ can be continued up to τ_{k-1}, then the above procedure is repeated. Under the conditions of Theorem 1.3.6, for each $(t_0, x_0) \in \Omega$, there exists a unique solution $x(t; t_0, x_0)$ of the initial-value problem (1.3.5)–(1.3.2); this solution is defined in an interval of the form (α, ω) and is not continuable to the left of α or to the right of ω. Denote $J(t_0, x_0)$ the maximal interval of the solution and set $J^+ = J^+(t_0, x_0) = [t_0, b)$ and $J^- = J^-(t_0, x_0) = (\alpha, t_0]$. Then the solution $x(t; t_0, x_0)$ of the initial-value problem (1.3.5)–(1.3.2) satisfies

$$x(t) = \begin{cases} x_0 + \int_{t_0}^{t} f(s, x(s))ds + \sum_{t_0 < \tau_k \leq t} I_k(x(\tau_k)) & \text{for } \ t \in J^+, \\ x_0 + \int_{t_0}^{t} f(s, x(s))ds - \sum_{t < \tau_k \leq t_0} I_k(x(\tau_k)) & \text{for } \ t \in J^-. \end{cases}$$

Chapter 2

Pathogenesis of HIV-1 Infection

HIV remains one of the world's most serious public health challenges. At the end of 2019, there were between 38.0 and 44.5 million people worldwide living with HIV. Globally, there have been improvements in the HIV detection and treatment cascade: 81% of those infected knew their status, and 67% were accessing antiretroviral therapy [18]. These advances, as well as an increased access to antiretroviral therapy, are reflected in the fact that almost 59% of those living with HIV had suppressed viral loads in 2019 [18]. However, there was also an increase of 1.7 million new infections, which is more than three times higher than the global goal of reducing new infections to fewer than 500,000 [19]. Since the beginning of the HIV epidemic, between 24.8 and 42.2 million people have died from AIDS-related illnesses [19].

Significant progress has been achieved towards the global goal of ending the AIDS epidemic by 2030. Several countries with diverse ranges of geographic and economic backgrounds are on track to achieve the 90-90-90 objective (90% of all people living with HIV know their HIV status, 90% of all people with diagnosed HIV infection receive sustained antiretroviral therapy, and 90% of all people receiving antiretroviral therapy have viral suppression) [18]. Switzerland has already succeeded in surpassing the viral suppression target, while Eswatini has surpassed all three targets. This proves that bold targets can be met when they are matched with sufficient financial resources, political will and community engagement. These successes are relevant to not only re-shaping the response to HIV in other countries, but are also vital lessons for the world as it mobilizes against the current COVID-19 pandemic.

However, in despite of these successes and advances in the scientific understanding of HIV prevention, pathogenesis and treatment, a significant number of people in

vulnerable populations still do not have reliable access to HIV services. This is especially true in Southern and Eastern African regions where an estimated two thirds of the population is living with HIV [19]. Globally, there has been unequal progress in reducing new HIV infections, increasing access to treatment, and ending AIDS-related deaths. Global targets of reducing new HIV infections and AIDS-related deaths to fewer than 500,000 by 2020 were both missed [18]. This collective failure comes at an unacceptably high price: from 2015 to 2020, there were 3.5 million more HIV infections and 820,000 more AIDS-related deaths than if the world was on track to meet its 2020 targets [18].

2.1 HIV-1 morphology

HIV-1 is classified as a retrovirus and belongs to the family of lentiviruses [20]. Mature HIV-1 virions are roughly spherical and have a diameter of 100–145 nm [21]. Viral particles contain two copies of positive-sense single-stranded RNA that codes for the virus's nine genes: *gag, pol, vif, vpr, rev, tat, vpu, env* and *nef* [20]. These RNA strands are enclosed by a conical capsid, which consists of 2000 copies of the core antigen p24 [21]. Surrounding the capsid is the matrix protein p17. The protein p17 is anchored to the inside of the viral envelope and ensures the integrity of the virion [22]. The matrix is, in turn, enclosed by the viral lipoprotein envelope (HIV-1 Env), which is comprised of a lipid bilayer [22]. HIV-1 Env contains 72 glycoproteins complexes that are integrated into the lipid membrane and two external glycoproteins: a cap made from glycoprotein gp120, and a stem comprised of glycoprotein gp41 that anchors it to the viral envelope. An HIV-1 virion contains all enzymatic components that are necessary for replication: reverse transcriptase p66/p51, integrase p32 and protease p11 [22].

2.2 Organization of HIV-1 genome

Like most replication competent retroviruses, HIV-1 has three structural genes: *gag, pol* and *env* [22]. It also contains two essential regulatory genes, *tat* and *ref*, as well as four auxiliary regulatory genes, *nef, vpr, vif* and *vpu*. The structural scheme of the genome is 5'-end long terminal repeat (LTR), *gag, pol, vif, vpr, rev, tat, vpu, env, nef* and then the 3'-end LTR [22]. The LTR regions of the HIV-1 virus are 643 base pairs in length and are identical. They function as the end parts of the viral genome that are connected to the host DNA during integration, but they do not encode for viral proteins [22].

The three genes, *gag*, *pol*, and *env*, contain all information needed to make the structural proteins for new virus particles [23]. The *gag* and *env* genes code for the

nucleocapsid and the glycoproteins of the viral membrane; the *pol* gene codes for the viral enzymes reverse transcriptase (RT), Ribonuclease-H (RNase-H), integrase (IN) and protease (PR) [23].

Both *tat* and *rev* stimulate the transcription of integrated viral DNA into RNA, promote RNA elongation, and aid in the transportation of RNA from the nucleus to the cytoplasm, which is essential for translation to occur [23].

In the past, *nef, vif, vpr* and *vpu* were classified as accessory genes, as they are not absolutely required for replication *in vitro*. However, they represent critical virulence factors *in vivo* [23].

A full summary of primary protein products and the processed protein products coded by each HIV-1 gene is found in Table 2.1. Broadly, antiretroviral therapy works by inhibiting the function of a specific protein by-product processed by the HIV-1 genes. The individual mechanisms of action of each class are outlined in Subsection 2.3.5.

Table 2.1: Proteins encoded by the HIV-1 genome. The HIV-1 genome contains nine genes that encode fifteen viral proteins.

Class	Gene name	Primary protein product	Processed protein products
Viral structural proteins	*gag*	Gag polyprotein	MA, CA, SP1, NC, SP2, P6
	pol	Pol polyprotien	RT, RNAse H, IN, PR
	env	gp160	gp120, gp41
Regulatory proteins	*tat*	Tat	–
	rev	Rev	–
Auxilitary regulatroy proteins	*nef*	Nef	–
	vpr	Vpr	–
	vif	Vif	–
	vpu	Vpu	–

2.3 HIV-1 replication cycle

Understanding HIV-1 immunopathogenesis has profound implications for viral tropism, transmission and pathogenesis. It is also a major prerequisite for improving existing HIV-1 therapeutic interventions and in the development of new immunotherapeutics or prophylactic vaccines.

2.3.1 Attachment and fusion

First, the HIV-1 virus requires entry into targeted cells. This occurs when nascent virions encounter cells with the appropriate receptor structures [24]. Such cells include $CD4^+$ T cells, macrophages and dendritic cells [3].

To gain entry, the HIV-1 virus uses its cell-protein envelope (Env), comprised of glycoproteins gp120 and gp41 [24]. The cell-surface attachment glycoprotein, gp120, first binds with high affinity to the primary cellular receptor $CD4^+$ [25]. This induces a conformational change in gp120, which forms the coreceptor-binding site [25]. The two possible chemokine coreceptors are CCR5 and CXCR4 [25]. Strains of HIV-1 can be broadly classified into one of three strains based on coreceptor binding: the R5 HIV-1 strain uses the CCR5 coreceptor, X4 HIV-1 uses the CXCR4 coreceptor, while the R5X4 HIV-1 strain uses both CCR5 and CXCR4 [24]. HIV-1 is usually R5-tropic during the early stages of infection but may subsequently switch to X4-tropic or dual-tropic [24].

Coreceptor binding activates a cascade of further conformational changes that causes gp120 to dissociate from gp41 [25]. This allows gp41 fusion peptides to be inserted into the host cell membrane, and that triggers the core of gp41 to fold into a six-helix coiled-coil [26]. This structure drives the fusion of the viral envelope and cell membrane [26]. The viral genome and the reverse transcriptase protein then enter the host cell, setting the stage for reverse transcription [24].

2.3.2 Reverse transcription and integration

Reverse transcriptase (RT) is an enzyme used to synthesize linear double-stranded DNA from a single-stranded RNA template, a process termed reverse transcription [3]. This process is extremely error-prone, producing 0.34 mutations per cycle [27]; the resulting mutations may cause drug resistance or allow the virus to evade the body's immune system response.

Shortly after viral capsid enters the cytoplasm of the host cell, RT liberates the single-stranded RNA genome [28]. Reverse transcription is initiated when Lys3 transfer RNA (tRNA) hybridizes to a complementary part of the RNA genome called the primer-binding site (PBS) [28]. RT has two active sites: a polymerase site and an RNAse H site. At the polymerase site, RT begins to synthesize a single DNA strand by adding host nucleotides onto the PBS, using the RNA strand as a template. This forms an RNA/DNA complex. At the RNAse H site, RT then cleaves the majority of viral RNA from the RNA/DNA complex, leaving only a small purine-rich sequence that is resistant to RNase H cleavage [29]. This sequence serves as the primer for the initiation of the second DNA strand. When the tRNA primer is removed, the primer from the second strand hybridizes with the PBS from the first stand to form a complementary double-stranded DNA (cDNA) copy of the original RNA genome [28].

The virus-encoded integrase p36 protein mediates integration of the cDNA into the host DNA [30]. After the cDNA is transcribed, it stably associates with integrase p36 [31]. The integrase dimer processes the cDNA by cleaving it at each 3'-end, preparing it for integration into host DNA [32]. This pre-integration complex is then translocated into the nucleus of the host cell, where it enters through one of the nuclear pore complexes [33]. The strand transfer reaction is initiated as p36 catalyzes the cDNAs free 3' hydroxyl to attack the phosphodiester backbone of the host DNA. The reaction leads to a separation in the bonds of the host DNA, thereby allowing the joining of the cDNA 3' hydroxyl group with host DNA 5' phosphate group [33]. The integrated cDNA is referred to as the provirus, or proviral DNA strand.

2.3.3 Transcription

Following integration, the cDNA can either be transcribed, leading to new virions, or lie dormant without viral gene and protein expression [34]. Latent infection occurs in resting memory T cells and dormant macrophages. HIV latency is a major barrier to achieving a cure of the infection as it will evade the host immune response and remains unaffected by therapeutic interventions [34].

Transcription is regulated by the 5' long-terminal-repeat (LTR) viral promoter as well as the regulatory proteins Tat and Rev [34]. The LTR region of the integrated viral DNA also contains three tandem binding sites for a variety of host transcription factors and a transactivation-responsive region (TAR) [35]. Tat recognizes and binds to the TAR, a positive transcription elongation factor and other host cellular cofactors, which stimulates transcription elongation [35]. This produces new full-length strands of RNA; some of these RNA strands then undergo RNA splicing to produce mature messenger RNAs (mRNAs), while others function as new copies of the virus genome [36]. The mRNAs are exported from the nucleus into the cytoplasm, where they can produce the structural proteins Gag and Env [35]. Gag proteins bind to copies of the viral RNA genome to package them into new virus particles, whereas Env forms the cell-protein envelope [36].

2.3.4 Assembly and budding

HIV-1 virion morphogenesis is divided into three stages that facilitate the conversion of an immature, non-infectious particle into a mature infectious virion. These include assembly, wherein the virion is packaged along with its essential replication components; budding, wherein the virion leaves the host cell, taking with it part of the plasma membrane of the host cell; and maturation, wherein the virion undergoes a series of structural changes that allow it to become infectious [37].These three stages are largely mediated by the Gag polyprotein and its proteolytic protein products,

which function as the major structural proteins of the virus [38].

An infectious HIV-1 particle requires two copies of the genomic viral RNA, cellular tRNA, the viral envelope (Env polyprotein), the Gag (p55) polyprotein as well as three viral enzymes packaged as domains within the Gag-Pol polyprotein: protease, reverse transcriptase and integrase [37]. The Env polyprotein first moves through the endoplasmic reticulum towards the Golgi apparatus, where it is then cleaved into gp41 and gp120, the two HIV-1 envelope glycoproteins. After being transported to the plasma membrane of the host cell, gp41 anchors gp120 to the membrane of the infected cell [37]. This anchoring becomes more secure once Gag, which has also bound to the RNA that was exported from the nucleus, associates to the inner plasma membrane [38]. The virus utilizes the host's endosomal sorting complexes required for transport (ESCRT) pathway to terminate Gag polymerization and facilitate virion budding from the host [37].

The budded virion, although fully assembled, is non-infectious as the Gag polyprotein still needs to be cleaved in order to produce the matrix, capsid and nucleocapsid proteins [38]. This cleavage is mediated by protease and can be inhibited by protease inhibitor antiretroviral drug class. The various structural components then assemble to produce a mature HIV-1 virion. Only a mature virion is then able to infect another $CD4^+$ T cell [37].

2.3.5 Antiretroviral mechanism of action

There are currently six major classes of antiretroviral drugs: fusion inhibitors (FIs), chemokine coreceptor antagonists (consisting of two subclasses: CCR5 antagonists and CXCR4 antagonists), nucleoside analogue reverse transcriptase inhibitors (NRTIs), nonnucleoside reverse transcriptase inhibitors (NNRTIs), integrase inhibitors (INSTIs) and protease inhibitors (PIs). Their individual mechanisms of action inform modelling choices made in Section 3.2.

Fusion inhibitors act extracellularly to prevent HIV-1 from entering the target cell. By competitively binding to the protein gp41, FIs prevent the conformational folding of gp41 required for fusion to occur [39].

Chemokine coreceptor antagonists also prevent the entry of HIV-1 into target cells by binding with either the CCR5 or CXCR4 co-receptors on the surface of $CD4^+$ T cells. By doing so, they prevent a required step in viral entry. Contrary to other antiretroviral drug classes which act on viral enzymes, co-receptor antagonists bind to human proteins [40].

NRTIs are chemical nucleotide base analogues that function as chain-terminators during the extension of the DNA chain during reverse transcription. While NRTIs permit correct base-pairing and become incorporated into the proviral DNA chain, an important hydroxyl group required for the addition of the following nucleotide is replaced with a non-reactive chemical group. As a consequence, natural nucleotides

can no longer be added. This results in chain termination, so a full-length copy of viral DNA is not produced [41].

NNRTIs also inhibit the synthesis of viral DNA. Instead of being added to the DNA chain as a false nucleotide, the NNRTIs target the reverse transcriptase enzyme. NNRTIs bind to the active ezymatic pocket of the RT enzyme, which prevents the molecule from converting the viral RNA to DNA [42].

INSTIs bind through competitive inhibition to the viral integrase. This causes functional impairment of this enzyme by interfering with the formation of covalent bonds with host DNA. This prevents incorporation of HIV-1 into the host genome [43].

PIs are chemicals that, through competitive inhibition, inhibit the action of the protease enzyme. By binding to the active site of protease, they prevent the proteolytic cleavage of the Gag and Gag-Pol polyproteins [44]. As these polyproteins contain vital structural and enzymatic components of a mature HIV-1 virion, new viral particles are produced, but they are non-infectious [45].

Since infected $CD4^+$ T cells have already integrated the viral genome in the host DNA, absoption of FIs, NRTIs, and NNRTIs have no effect in disrupting the replication cycle. Thus, the only possible fate for these cells is cell death. On the other hand, PIs disrupt the maturation step, and thereby still have an effect on infected $CD4^+$ T cells. This is reflected in the model presented in Section 3.3.

Chapter 3

The Mathematical Model

3.1 Modelling drug therapy

This model considers two strains of HIV-1: the wild-type strain, which dominates in the absence of drugs, and a mutant strain, which is a less efficient competitor but has a higher resistance to antiretroviral drugs. Since antiretroviral drugs reduce viral fitness in a dose-dependent manner, drug concentration determines the relative fitness of each strain. Both reverse transcriptase inhibiting drugs, NRTIs and NNRTIs, are denoted by RTI: as their mechanisms of action are similar, they would be modelled in the same way.

To model the effects of mutations on drug efficacy, we consider the dose-effect curve illustrated in Figure 3.1. The solid line represents the dose-effect curve for the wild-type virus, whereas the dashed line shows the same curve for a mutant drug-resistant strain with 10-fold resistance. Here, drug resistance implies an increase in the half-maximal inhibitory concentration IC_{50} of the drug, the concentration of drug required for 50% inhibition *in vitro*. The y-axis, or antiviral effect, is the probability that a given $CD4^+$ T cell absorbs sufficiently high quantities of the drug to prevent viral replication. Thus, the antiretroviral drug effect can be divided into three regions: Region 1 (low drug levels), Region 2 (intermediate drug levels) and Region 3 (high drug levels): low drug levels will not affect either strain, intermediate drug levels will control the wild-type strain alone, and high drug levels will control both strains. Therefore, our model of HIV-1 dynamics consists of three distinct systems, depending on both the RTI and PI drug concentration. Let R, P denote the concentration of RTIs and PIs, respectively; R_1, P_1 denote the threshold drug value concentrations that

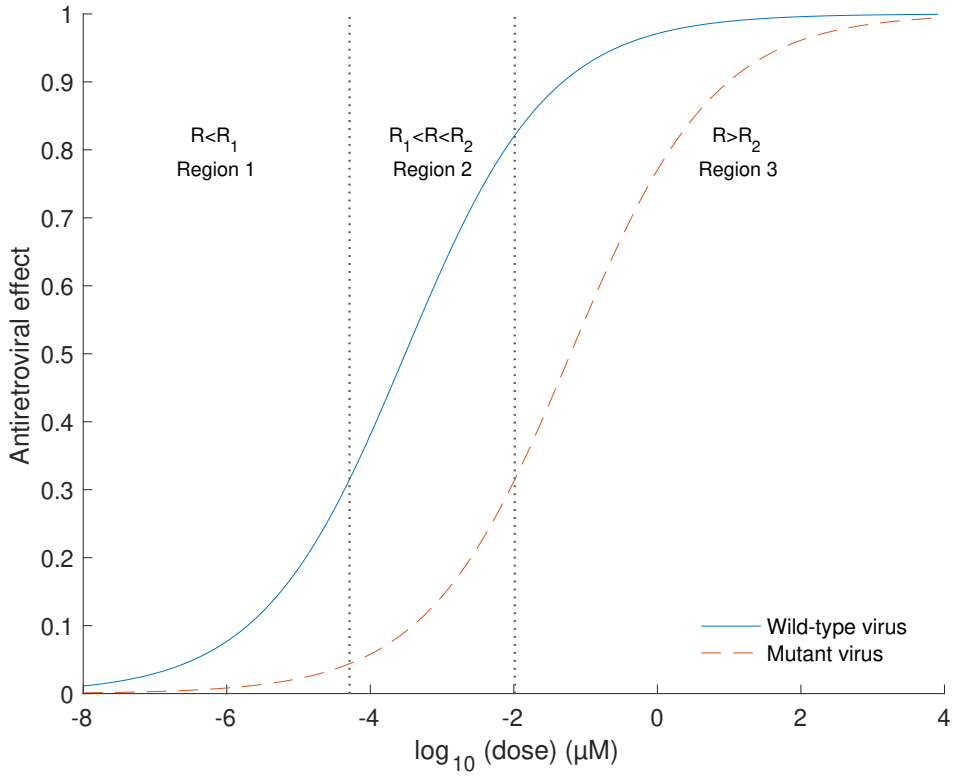

Figure 3.1: Dose-effect curves for the wild-type (solid curve) and 10-fold resistant (dashed curve) viral strains. Note that the x-axis is on a logarithmic scale. When drug concentration is less than the Region 1 threshold, the probability that a $CD4^+$ T cell absorbs sufficient drug to block infection is negligible for all strains. Between the thresholds for Regions 1 and 2, the drug has a non-negligible probability of blocking the wild-type strain alone. For drug concentrations exceeding the Region 2 threshold, the drug has a non-negligible probability of blocking both the wild-type and resistant strains. The IC_{50} value used in this example is for Lamivudine.

separates Regions 1 and 2 for the RTI and PI, respectively; and R_2, P_2 denote the threshold drug values that separate Regions 2 and 3 for the RTI and PI, respectively.

3.2 State variables

The mathematical model uses three state variables to describe the HIV-1 virus. The variables V_I, V_Y and V_N denote the concentration of wild-type, mutant and non-infectious virus, respectively. Eighteen state variables are used to describe the $CD4^+$ T cells in a variety of stages of infection and with varying drug concentrations. At any given time, a $CD4^+$ T cell may come into contact with a virion of the wild-type strain of the virus, a virion of the mutant strain of the virus or the antiretroviral drug. Drug concentration in this model determines the relative fitness of the wild-type virus and a resistant mutant; depending on the quantity and class of antiretroviral drug absorbed, a $CD4^+$ T cell may subsequently become immune to neither, one or both strains of the virus. The $CD4^+$ T cells can thus be classified as follows:

Region 1: Initially, there are three types of cells: susceptible $CD4^+$ T cells, denoted T_S; cells infected by wild-type virus, denoted T_I; and cells infected by the mutant virus, denoted T_Y.

Region 2: As antiretroviral drugs are introduced into the system, cells are transformed. T_{RS} describes susceptible cells that have absorbed an intermediate amount of RTIs. These cells may come into contact with either the wild-type or the mutant strain of the virus or the drug. An intermediate amount of RTI is sufficient to block the wild-type strain but is not high enough to prevent infection of the mutant strain. Thus, if the cell comes into contact with a wild-type virion, it cannot become infected, so this has no consequence for the cell. However, if the cell comes into contact with the mutant virus, it will become infected with the mutant strain. This type of cell is denoted T_{RY}. The variable T_{PS} denotes susceptible $CD4^+$ cells that have an intermediate level of PIs, whereas T_{PI} and T_{PY} denote wild-type-infected and mutant-infected cells, respectively, that also have an intermediate level of drug. Note that cells with an intermediate amount of PI may subsequently be infected by the wild-type strain, but this cell will only produce non-infectious virions. Intermediate concentration of PIs is not sufficient to inhibit the mutant strain. T_{RPS} denotes susceptible cells that have absorbed an intermediate amount of both RTIs and PIs. Since the RTI only blocks subsequent infection of the wild-type strain, this cell can still be infected by the mutant strain to become T_{RPY}.

Region 3: High drug levels in the system gives eight new types of cells. Susceptible cells that have absorbed a high level of RTIs are denoted by T_{RRS}. In this region, the level of drug is sufficiently high to prevent infection of both strains of the virus.

These cells can also absorb PIs to become T_{RRPS}. T_{PPS} denotes susceptible cells inhibited with a high level of PI, while T_{PPI} and T_{PPY} denotes wild-type-infected and mutant-infected cells, respectively, inhibited by a high level of PI. Susceptible cells inhibited by a high level of PIs can also absorb RTIs to become T_{RPPS}. Note that while the amount of RTIs is adequately high to block the wild-type strain, it is not high enough to block the mutant strain. Thus, this cell will become T_{RPPY} when it comes into contact with a mutant virion. T_{RRPPS} denotes susceptible cells with high levels of both classes of drugs.

Note that here we are considering drug levels to be in Region 3 when at least one, if not both, of the RTIs and PI are in Region 3. We also consider drug levels to be in Region 2, when at least one, if not both, of the RTIs and PI are in Region 2. The principal impetus for combination therapy is that since multiple drugs act on different viral targets, have different mechanisms and are processed differently by the body, taking them together will decrease the likelihood that resistance will develop. Each drug can thus be at the optimal dose to reduce intolerable side effects, while still having an adequate antiretroviral effect. Consider the possibility that either the RTIs or PI are in Region 2 (or Region 1), while the other is in Region 3. Here, the antiretroviral effect of the drug in Region 3 is still high enough to prevent viral replication. Due to this, the wild-type and mutant strains are both controlled, and it would be unlikely for drug resistance to emerge. Thus, this scenario behaves as a subset of Region 3. Similarly, if either the RTIs or PI are in Region 1, while the other is in Region 2, drug concentration of the drug in Region 2 is still high enough to control the wild-type strain. So, the mutant still has the competitive advantage. Hence, this behaves as a subset of Region 2.

All parameter descriptions, ranges and sample values used in simulations are summarized in Table 3.1, whereas all state variables and their initial values used in simulations are summarized in Table 3.2.

3.3 Mathematical model

While differential equations are often used to describe the dynamics of many biological phenomena, in some instances, there are moments in time when the system experiences an abrupt change of state. When the perturbations are negligible in duration compared to the time between impulses, these perturbations can be approximated by an instantaneous change in state, in the form of impulses [15].

Here, the impulsive effect occurs in the RTI drug concentrations if the dose is taken at the prescribed dosing time $t = t_k$; if a dose does not occur, no dose can be taken until time t_{k+1}, at which point the same decision of whether or not a dose is to be taken is applied [2]. Similarly, an impulse in the PI drug concentrations occurs at

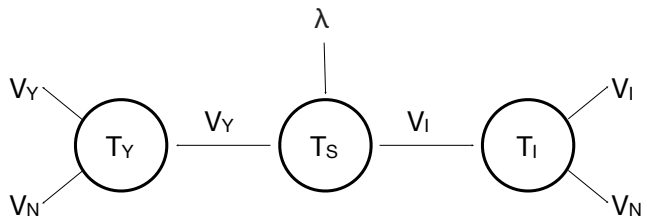

Figure 3.2: The model for Region 1. T_S, T_I and T_Y denote the susceptible, infected with wild-type strain and infected with mutant strain T cells, respectively. V_I and V_Y are the wild-type and mutant strain virions, respectively. V_N denotes non-infectious virions. λ is the rate of new T cells produced. In Region 1, drug levels are too low to block viral replication of either the wild-type or mutant virus.

$t = s_n$. While it is possible that $t_k = s_n$, this might not always be the case, depending on the drugs in the regimen.

The dynamics of the CD4$^+$ T cells and virus can be described by the following system of ordinary differential equations:

$$\begin{aligned}
\frac{dT_S}{dt} &= \lambda - r_I T_S V_I - r_Y T_S V_Y - \alpha_P r_P P^i T_S + m_P T_{PS} - \alpha_R r_R R^i T_S \\
&\quad + m_R T_{RS} - d_S T_S \\
\frac{dT_I}{dt} &= r_I T_S V_I - \alpha_P r_P P^i T_I + m_P T_{PI} - d_I T_I \\
\frac{dT_Y}{dt} &= r_Y T_S V_Y - \alpha_P r_P P^i T_Y + m_R T_{RY} + m_P T_{PY} - d_I T_Y \\
\frac{dT_{RS}}{dt} &= \alpha_R r_R R^i T_S - m_R T_{RS} - r_Y T_{RS} V_Y - \alpha_P r_P P^i T_{RS} + m_P T_{RPS} \\
&\quad - \beta_R r_{RR} R^i T_{RS} + m_{RR} T_{RRS} - d_S T_{RS} \\
\frac{dT_{RY}}{dt} &= r_Y T_{RS} V_Y - \alpha_P r_P P^i T_{RY} - m_R T_{RY} + m_P T_{RPY} - d_I T_{RY} \\
\frac{dT_{PS}}{dt} &= \alpha_P r_P P^i T_S - m_P T_{PS} - \alpha_R r_R R^i T_{PS} + m_R T_{RPS} - r_I T_{PS} V_I - r_Y T_{PS} V_Y \\
&\quad - \beta_P r_{PP} P^i T_{PS} + m_{PP} T_{PPS} - d_S T_{PS}
\end{aligned} \tag{3.3.1}$$

$$
\begin{aligned}
\frac{dT_{PI}}{dt} &= r_I T_{PS} V_I + \alpha_P r_P P^i T_I - m_P T_{PI} - \beta_P r_{PP} P^i T_{PI} + m_{PP} T_{PPI} - d_I T_{PI} \\
\frac{dT_{PY}}{dt} &= r_Y T_{PS} V_Y + \alpha_P r_P P^i T_Y - m_P T_{PY} + m_R T_{RPY} \\
&\quad - \beta_P r_{PP} P^i T_{PY} + m_{PP} T_{PPY} - d_I T_{PY} \\
\frac{dT_{RPS}}{dt} &= \alpha_R r_R R^i T_{PS} - m_R T_{RPS} + \alpha_P r_P P^i T_{RS} - m_P T_{RPS} - r_Y T_{RPS} V_Y \\
&\quad - \beta_P r_{PP} P^i T_{RPS} + m_{PP} T_{RPPS} - \beta_R r_{RR} R^i T_{RPS} + m_{RR} T_{RRPS} - d_S T_{RPS} \\
\frac{dT_{RPY}}{dt} &= r_Y T_{RPS} V_Y + \alpha_P r_P P^i T_{RY} - m_P T_{RPY} - m_R T_{RPY} \\
&\quad - \beta_P r_{PP} P^i T_{RPY} + m_{PP} T_{RPPY} - d_I T_{RPY} \\
\frac{dT_{RRS}}{dt} &= -\alpha_P r_P P^i T_{RRS} + m_P T_{RRPS} + \beta_R r_R R R^i T_{RS} - m_{RR} T_{RRS} - d_S T_{RRS} \\
\frac{dT_{PPS}}{dt} &= \beta_P r_{PP} P^i T_{PS} - m_{PP} T_{PPS} - r_Y T_{PPS} V_Y - r_I T_{PPS} V_I - \alpha_R r_R R^i T_{PPS} \\
&\quad + m_R T_{RPPS} - d_S T_{PPS} \\
\frac{dT_{PPI}}{dt} &= r_I T_{PPS} V_I + \beta_P r_{PP} P^i T_{PI} - m_{PP} T_{PPI} - d_I T_{PPI} \\
\frac{dT_{PPY}}{dt} &= r_Y T_{PPS} V_Y + \beta_P r_{PP} P^i T_{PY} - m_{PP} T_{PPY} + m_R T_{RPPY} - d_I T_{PPY} \\
\frac{dT_{RRPS}}{dt} &= \alpha_P r_P P^i T_{RRS} - m_P T_{RRPS} - \beta_P r_{PP} P^i T_{RRPS} + m_{PP} T_{RRPPS} \\
&\quad + \beta_R r_{RR} R^i T_{RPS} - m_{RR} T_{RRPS} - d_S T_{RRPS} \\
\frac{dT_{RPPS}}{dt} &= \alpha_R r_R R^i T_{PPS} - m_R T_{RPPS} - \beta_R r_{RR} R^i T_{RPPS} + m_{RR} T_{RRPPS} \\
&\quad - r_Y T_{RPPS} V_Y + \beta_P r_{PP} P^i T_{RPS} - m_{PP} T_{RPPS} - d_S T_{RPPS} \\
\frac{dT_{RPPY}}{dt} &= r_Y T_{RPPS} V_Y - m_R T_{RPPY} + \beta_P r_{PP} P^i T_{RPY} \\
&\quad - m_{PP} T_{RPPY} - d_I T_{RPPY} \\
\frac{dT_{RRPPS}}{dt} &= \beta_P r_{PP} P^i T_{RRPS} - m_{PP} T_{RRPPS} \\
&\quad + \beta_R r_{RR} R^i T_{RPPS} - m_{RR} T_{RRPPS} - d_S T_{RRPPS} \\
\frac{dV_N}{dt} &= \eta_I (1-\omega)(T_I + T_Y + T_{PY}) + \eta_I (T_{PI} + T_{PPI} + T_{PPY}) - d_V V_N \\
\frac{dV_I}{dt} &= \eta_I \omega T_I - r_I (T_S + T_{PS} + T_{PPS}) - d_V V_I \\
\frac{dV_Y}{dt} &= \eta_I \omega (T_Y + T_{PY}) - r_Y (T_S + T_{RS} + T_{PS} + T_{RPS} + T_{PPS} + T_{RPPS}) - d_V V_Y
\end{aligned}
\tag{3.3.2}
$$

for times $t \neq t_k$ or $t \neq s_n$ (see impulsive conditions below). This model varies between the three regions outlined in Section 3.2 by altering $\alpha_R, \beta_R, \alpha_P$ and β_P in the following way:

$$\alpha_R = \begin{cases} 0 \text{ if } R < R_1 \\ 1 \text{ if } R > R_1, \end{cases} \qquad \alpha_P = \begin{cases} 0 \text{ if } P < P_1 \\ 1 \text{ if } P > P_1, \end{cases}$$

and

$$\beta_R = \begin{cases} 0 \text{ if } R < R_2 \\ 1 \text{ if } R > R_2, \end{cases} \qquad \beta_P = \begin{cases} 0 \text{ if } P < P_2 \\ 1 \text{ if } P > P_2. \end{cases}$$

Here, t is the time in days, n_I is the number of virions produced per day, while ω is the proportion of these virions produced that are infectious. r_I and r_Y are the infection rates of CD4$^+$ T cells with wild-type or mutant virus, respectively. The constant λ describes the rate at which new susceptible CD4$^+$ T cells are produced. The death rates for the virus, susceptible and infected cells are denoted by d_V, d_S and d_I, respectively. r_R and r_{RR} describe the rates at which RTIs inhibit infection of the CD4$^+$ T cells when drug concentrations are intermediate and high whereas r_P and r_{PP} describes the rates at which the PI inhibits viral budding infectious virions when drug concentrations are intermediate and high. The rates m_R and m_{RR} denote the clearance rate of the RTIs from an intermediate and highly inhibited cell, respectively; the rates m_P and m_{PP} denote the clearance rate of the PIs from an intermediate and highly inhibited cell, respectively. λ, as well as all death and infection rates are assumed to be positive. We assume that $0 \leq \omega \leq 1$. As the wild-type strain is a more efficient competitor, we also assume that the infection rate of the wild-type strain is higher than that of the mutant strain; that is, $r_I > r_Y$. To analyse the model, we consider three subsystems corresponding to each region of drug concentration. Consider Region 1, where $\alpha_R = \alpha_P = 0$ and $\beta_R = \beta_P = 0$. In this case, $\frac{dT_{RRPSS}}{dt}$ is negative, which means that T_{RRPPS} decays to zero. As a consequence, all other T cell states except T_S, T_I, T_Y, decay to zero. Thus, the subsystem in this region only includes the following T cell states: T_S, T_I and T_Y. Similarly, consider Region 2, where $\alpha_R = \alpha_P = 1$ and $\beta_R = \beta_P = 0$. Again, $\frac{dT_{RRPSS}}{dt}$ is negative, meaning that T_{RRPPS} decays to zero. This consequently forces all of the T cell states in system (3.3.1)–(3.3.2), except the first ten, to decay to zero. Thus, the subsystem in this region only includes the following T cell states: T_S, T_I, T_Y,T_{RS}, T_{RY}, T_{PS},T_{PI},T_{PY}, T_{RPS} and T_{RPY}. Thus, for $t \neq t_k$ or $t \neq s_n$, we have the following three subregions of system (3.3.1)–(3.3.2).

For $P < P_1$ and $R < R_1$ (Region 1), the dynamics of the CD4$^+$ T cells and virions are given by

$$\begin{aligned}
\frac{dT_S}{dt} &= \lambda - r_I T_S V_I - r_Y T_S V_Y - d_S T_S \\
\frac{dT_I}{dt} &= r_I T_S V_I - d_I T_I \\
\frac{dT_Y}{dt} &= r_Y T_S V_Y - d_I T_Y \\
\frac{dV_N}{dt} &= \eta_I(1-\omega)(T_I + T_Y) - d_V V_N \\
\frac{dV_I}{dt} &= \eta_I \omega T_I - r_I T_S V_I - d_V V_I \\
\frac{dV_Y}{dt} &= \eta_I \omega T_Y - r_Y T_S V_Y - d_V V_Y.
\end{aligned} \tag{3.3.5}$$

For $P_1 < P < P_2$ and $R_1 < R < R_2$ (Region 2), the dynamics of the CD4$^+$ T cells and virions are given by

$$\begin{aligned}
\frac{dT_S}{dt} &= \lambda - r_I T_S V_I - r_Y T_S V_Y - r_P P^i T_S + m_P T_{PS} - r_R R^i T_S + m_R T_{RS} - d_S T_S \\
\frac{dT_I}{dt} &= r_I T_S V_I - r_P P^i T_I + m_P T_{PI} - d_I T_I \\
\frac{dT_Y}{dt} &= r_Y T_S V_Y - r_P P^i T_Y + m_R T_{RY} + m_P T_{PY} - d_I T_Y \\
\frac{dT_{RS}}{dt} &= r_R R^i T_S - m_R T_{RS} - r_P P^i T_{RS} + m_P T_{RPS} - r_Y T_{RS} V_Y - d_S T_{RS} \\
\frac{dT_{RY}}{dt} &= r_Y T_{RS} V_Y - r_P P^i T_{RY} - m_R T_{RY} + m_P T_{RPY} - d_I T_{RY} \\
\frac{dT_{PS}}{dt} &= r_P P^i T_S - m_P T_{PS} - r_R R^i T_S + m_R T_{RPS} - r_I T_{PS} V_I - r_Y T_{PS} V_Y - d_S T_{PS} \\
\frac{dT_{PI}}{dt} &= r_P P^i T_I - m_P T_{PI} + r_I T_{PS} V_I - d_I T_{PI} \\
\frac{dT_{PY}}{dt} &= r_P P^i T_Y - m_P T_{PY} + r_Y T_{PS} V_Y + m_R T_{RPY} - d_I T_{PY} \\
\frac{dT_{RPS}}{dt} &= r_R R^i T_{PS} - m_R T_{RPS} + r_P P^i T_{RS} - m_P T_{RPS} - r_Y T_{RPS} V_Y - d_S T_{RPS} \\
\frac{dT_{RPY}}{dt} &= r_P P^i T_{RY} - m_P T_{RPY} - m_R T_{RPY} + r_Y T_{RPS} V_Y - d_I T_{RPY} \\
\frac{dV_N}{dt} &= \eta_I(1-\omega)(T_I + T_Y + T_{PY}) + \eta_I T_{PI} - d_V V_N \\
\frac{dV_I}{dt} &= \eta_I \omega T_I - r_I T_S V_I - r_I T_{PS} V_I - d_V V_I \\
\frac{dV_Y}{dt} &= \eta_I \omega (T_Y + T_{PY}) - r_Y T_S V_Y - r_Y T_{PS} V_Y - r_Y T_{RS} V_Y - r_Y T_{RPS} V_Y - d_V V_Y.
\end{aligned} \tag{3.3.6}$$

For $P > P_2$ and $R > R_2$ (Region 3), the dynamics of the CD4$^+$ T cells and virions are given by

$$\begin{aligned}
\frac{dT_S}{dt} &= \lambda - r_I T_S V_I - r_Y T_S V_Y - r_P P^i T_S + m_P T_{PS} - r_R R^i T_S + m_R T_{RS} - d_S T_S \\
\frac{dT_I}{dt} &= r_I T_S V_I - r_P P^i T_I + m_P T_{PI} - d_I T_I \\
\frac{dT_Y}{dt} &= r_Y T_S V_Y - r_P P^i T_Y + m_R T_{RY} + m_P T_{PY} - d_I T_Y \\
\frac{dT_{RS}}{dt} &= r_R R^i T_S - m_R T_{RS} - r_Y T_{RS} V_Y - r_P P^i T_{RS} + m_P T_{RPS} - r_{RR} R^i T_{RS} \\
&\quad + m_{RR} T_{RRS} - d_S T_{RS} \\
\frac{dT_{RY}}{dt} &= r_Y T_{RS} V_Y - r_P P^i T_{RY} - m_R T_{RY} + m_P T_{RPY} - d_I T_{RY} \\
\frac{dT_{PS}}{dt} &= r_P P^i T_S - m_P T_{PS} - r_I T_{PS} V_I - r_Y T_{PS} V_Y - r_R R^i T_{PS} + m_R T_{RPS} \\
&\quad - r_{PP} P^i T_{PS} + m_{PP} T_{PPS} - d_S T_{PS} \\
\frac{dT_{PI}}{dt} &= r_I T_{PS} V_I + r_P P^i T_I - m_P T_{PI} - r_{PP} P^i T_{PI} + m_{PP} T_{PPI} - d_I T_{PI} \\
\frac{dT_{PY}}{dt} &= r_Y T_{PS} V_Y + r_P P^i T_Y - m_P T_{PY} + m_R T_{RPY} - r_{PP} P^i T_{PY} + m_{PP} T_{PPY} \\
&\quad - d_I T_{PY} \\
\frac{dT_{RPS}}{dt} &= r_R R^i T_{PS} - m_R T_{RPS} + r_P P^i T_{RS} - m_P T_{RPS} - r_Y T_{RPS} V_Y - r_{PP} P^i T_{RPS} \\
&\quad + m_{PP} T_{RPPS} - r_{RR} R^i T_{RPS} + m_{PP} T_{RPPS} - d_S T_{RPS} \\
\frac{dT_{RPY}}{dt} &= r_Y T_{RPS} V_Y + r_P P^i T_{RY} - m_P T_{RPY} - m_R T_{RPY} - r_{PP} P^i T_{RPY} \\
&\quad + m_{PP} T_{RPPY} - d_I T_{RPY} \\
\frac{dT_{RRS}}{dt} &= -r_P P^i T_{RRS} - m_P T_{RRPS} + r_{RR} R^i T_{RS} - m_{RR} T_{RRS} - d_S T_{RRS} \\
\frac{dT_{PPS}}{dt} &= r_{PP} P^i T_{PS} - m_{PP} T_{PPS} - r_Y T_{PPS} V_Y - r_I T_{PPS} V_I - r_R R^i T_{PPS} \\
&\quad + m_R T_{RPPS} - d_S T_{PPS} \\
\frac{dT_{PPI}}{dt} &= r_I T_{PPS} V_I + r_{PP} P^i T_{PI} - m_{PP} T_{PPI} - d_I T_{PPI} \\
\frac{dT_{PPY}}{dt} &= r_Y T_{PPS} V_Y + r_{PP} P^i T_{PY} - m_{PP} T_{PPY} + m_R T_{RPPY} - d_I T_{PPY} \\
\frac{dT_{RRPS}}{dt} &= r_P P^i T_{RRS} - m_P T_{RRPS} - r_{PP} P^i T_{RRPS} + m_{PP} T_{RRPPS} + r_{RR} R^i T_{RPS} \\
&\quad - m_{RR} T_{RRPS} - d_S T_{RRPS}
\end{aligned}$$

$$\begin{aligned}
\frac{dT_{RPPS}}{dt} &= r_R R^i T_{PPS} - m_R T_{RPPS} - r_{RR} R^i T_{RPPS} + m_{RR} T_{RRPPS} - r_Y T_{RPPS} V_Y \\
&\quad + r_{PP} P^i T_{RPS} - m_{PP} T_{RPPS} - d_S T_{RPPS} \\
\frac{dT_{RPPY}}{dt} &= r_Y T_{RPPS} V_Y - m_R T_{RPPY} + r_{PP} P^i T_{RPY} - m_{PP} T_{RPPY} - d_I T_{RPPY} \\
\frac{dT_{RRPPS}}{dt} &= r_{PP} P^i T_{RRPS} - m_{PP} T_{RRPPS} + r_{RR} R^i T_{RPPS} - m_{RR} T_{RRPPS} - d_S T_{RRPPS} \\
\frac{dV_N}{dt} &= \eta_I (1-\omega)(T_I + T_Y + T_{PY}) + \eta_I (T_{PI} + T_{PPI} + T_{PPY}) - d_V V_N \\
\frac{dV_I}{dt} &= \eta_I \omega T_I - r_I (T_S + T_{PS} + T_{PPS}) - d_V V_I \\
\frac{dV_Y}{dt} &= \eta_I \omega (T_Y + T_{PY}) - r_Y (T_S + T_{RS} + T_{PS} + T_{RPS} + T_{PPS} + T_{RPPS}) - d_V V_Y .
\end{aligned} \tag{3.3.8}$$

Let $R(t)$ and $P(t)$ denote the RTI and PI drug concentrations, as well as their active metabolites, respectively. The dynamics of the drugs are modelled using impulsive differential equations:

$$\begin{aligned}
\frac{dR}{dt} &= -d_R R, \quad t \neq t_k, \\
\frac{dP}{dt} &= -d_P P, \quad t \neq s_n,
\end{aligned}$$

with impulse conditions at $t = t_k, s_n$,

$$\Delta R = \begin{cases} R^i & \text{if a dose is taken,} \\ 0 & \text{if no dose is taken,} \end{cases}$$

and

$$\Delta P = \begin{cases} P^i & \text{if a dose is taken,} \\ 0 & \text{if no dose is taken.} \end{cases}$$

Here, d_R, d_P are the decay rates of the drug, given by the formula

$$d_R = d_P = 24 \log(2)/T_{1/2},$$

where $T_{1/2}$ is the intracellular half-life of the specific antiretroviral. Half-lives of each antiretroviral drug can be found in Table 5.2. R^i and P^i are the dosage amounts of the RTI and PI, respectively; we assume that $R(0) = P(0) = 0$. Note that, by definition of an impulsive effect, we have a recursion relation at the moments of impulse, given by

$$R(t_k^+) = R(t_k^-) + R^i, \tag{3.3.11}$$

$$P(s_n^+) = P(s_n^-) + P^i, \tag{3.3.12}$$

assuming a dose has been taken at times t_k and s_n. Here, the use of impulsive differential equations implies that the antiretroviral takes effect immediately.

Table 3.1: Range of parameters

Parameter	Description	Range	Sample Value	Reference
n_I	Number of virions produced by a susceptible CD4$^+$ T cell	10^2–10^4	1000 day^{-1}	[12,16,46]
ω	Proportion of infectious virions produced	0–1	0.7	[12,16,46]
λ	Production rate of the CD4$^+$ T cells	100–250	180 cells μL^{-1} day^{-1}	[12]
r_I	Infection rate of CD4$^+$ T cells with wild-type virus	0.001–0.1	0.01 day^{-1}	[9, 12]
r_Y	Infection rate of CD4$^+$ T cells with mutant virus	0.0003–0.03	0.0032 day^{-1}	[16]
d_S	Death rate for the susceptible CD4$^+$ T cells	0.002–0.2	0.02 day^{-1}	[9, 12, 16, 46]
d_V	Death rate of the HIV-1 virus	1–5	3 day^{-1}	[16,46,47]
d_I	Death rate for the infected CD4$^+$ T cells	0.05–1	0.5 day^{-1}	[9, 12, 16, 47]
r_R	Rate at which drug inhibits CD4$^+$ T cells when RTI concentrations are intermediate	30–50	40 μM^{-1}day^{-1}	[16]
r_P	Rate at which drug inhibits CD4$^+$ T cells when PI concentrations are intermediate	30–50	40 μM^{-1}day^{-1}	[48]
r_{RR}	Rate at which drug inhibits CD4$^+$ T cells when RTI concentrations are high	8–13	10.4 μM^{-1}day^{-1}	[16]
r_{PP}	Rate at which drug inhibits CD4$^+$ T cells when PI concentrations are high	8–13	10.4 μM^{-1}day^{-1}	[48]
m_R	Clearance rate of the RTI from an intermediate inhibited cell	1–4	24log(2)/6.2 day^{-1}	[16]
m_P	Clearance rate of the PI from an intermediate inhibited cell	1–4	24log(2)/6.2 day^{-1}	[48]
m_{RR}	Clearance rate of the RTI from an highly inhibited cell	1–4	24log(2)/6.2 day^{-1}	[16]
m_{PP}	Clearance rate of the PI from an highly inhibited cell	1–4	24log(2)/6.2 day^{-1}	[48]
d_R	RTI clearance rate	1–4	24log(2)/$T_{1/2}$ day^{-1}	[16]
d_P	PI clearance rate	1–4	24log(2)/$T_{1/2}$ day^{-1}	[48]

Table 3.2: State variables and initial conditions

State Variable	Description	Initial Value
V_I	Wild-type virions	500 virus μM^{-1}day^{-1}
V_Y	Mutant virions	5x10^{-5} virus μM^{-1}day^{-1}
V_N	Non-infectious virions	0 virus μM^{-1}day^{-1}
T_S	Susceptible CD4$^+$ cells	1000 cells μM^{-1}day^{-1}
T_I	CD4$^+$ T cells infected with the wild-type virus	0 cells μM^{-1}day^{-1}
T_Y	CD4$^+$ T cells infected with the mutant virus	0 cells μM^{-1}day^{-1}
T_{RS}	Susceptible CD4$^+$ T cells with an intermediate level of RTI	0 cells μM^{-1}day^{-1}
T_{RY}	CD4$^+$ T cells infected with the mutant virus with an intermediate level of RTI	0 cells μM^{-1}day^{-1}
T_{PS}	Susceptible CD4$^+$ T cells with an intermediate level of PI	0 cells μM^{-1}day^{-1}
T_{PI}	CD4$^+$ T cells infected with the wild-type virus with an intermediate level of PI	0 cells μM^{-1}day^{-1}
T_{PY}	CD4$^+$ T cells infected with the mutant virus with an intermediate level of PI	0 cells μM^{-1}day^{-1}
T_{RPS}	Susceptible CD4$^+$ T cells with an intermediate level of both RTI and PI	0 cells μM^{-1}day^{-1}
T_{RPS}	CD4$^+$ T cells infected with the mutant strain with an intermediate level of both RTI and PI	0 cells μM^{-1}day^{-1}
T_{RPY}	Susceptible CD4$^+$ T cells with high level of RTI	0 cells μM^{-1}day^{-1}
T_{PPS}	Susceptible CD4$^+$ T cells with high level of PI	0 cells μM^{-1}day^{-1}
T_{PPI}	CD4$^+$ T cells infected with the wild-type virus with a high level of PI	0 cells μM^{-1}day^{-1}
T_{PPY}	CD4$^+$ T cells infected with the mutant virus with a high level of PI	0 cells μM^{-1}day^{-1}
T_{RRPS}	Susceptible CD4$^+$ T cells virus with a high level of RTI and intermediate levels of PI	0 cells μM^{-1}day^{-1}
T_{RPPS}	Susceptible CD4$^+$ T cells virus with a high level of PI and intermediate levels of RTI	0 cells μM^{-1}day^{-1}
T_{RPPY}	CD4$^+$ T cells virus infected with the mutant strain with a high level of PI and intermediate levels of RTI	0 cells μM^{-1}day^{-1}
T_{RRPPS}	Susceptible CD4$^+$ T cells virus with a high level of both RTI and PI	0 cells μM^{-1}day^{-1}

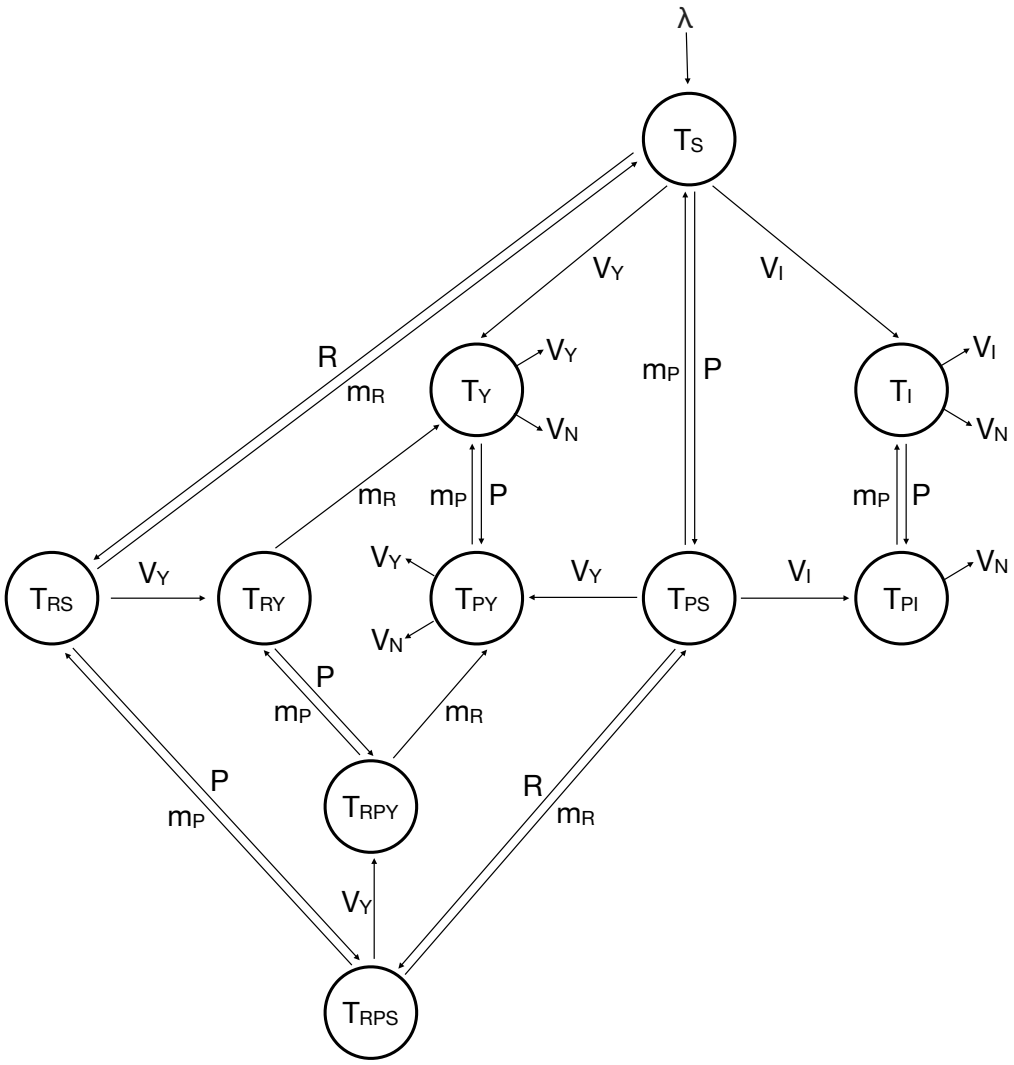

Figure 3.3: The model for Region 2. T_{RS} and T_{RY} are the susceptible and mutant-infected CD$^+$ T cells. Cells inhibited with intermediate RTI levels are immune to the wild-type virus while they remain inhibited but can be infected by the mutant strain. The variable T_{PS} denotes susceptible CD4$^+$ cells that have an intermediate level of PIs, whereas T_{PI} and T_{PY} denote wild-type-infected and mutant-infected cells, respectively, that have an intermediate level of drug. T_{RPS} denotes susceptible cells that have absorbed an intermediate amount of both RTIs and PIs. Since the RTI only blocks infection of the wild strain, this cell can still be infected by the mutant strain to become T_{RPY}. In Region 2, there is not enough drug in the T cells to inhibit the mutant strain from producing infectious virions, but the wild-type strain can be controlled, meaning it will only produce non-infectious virions.

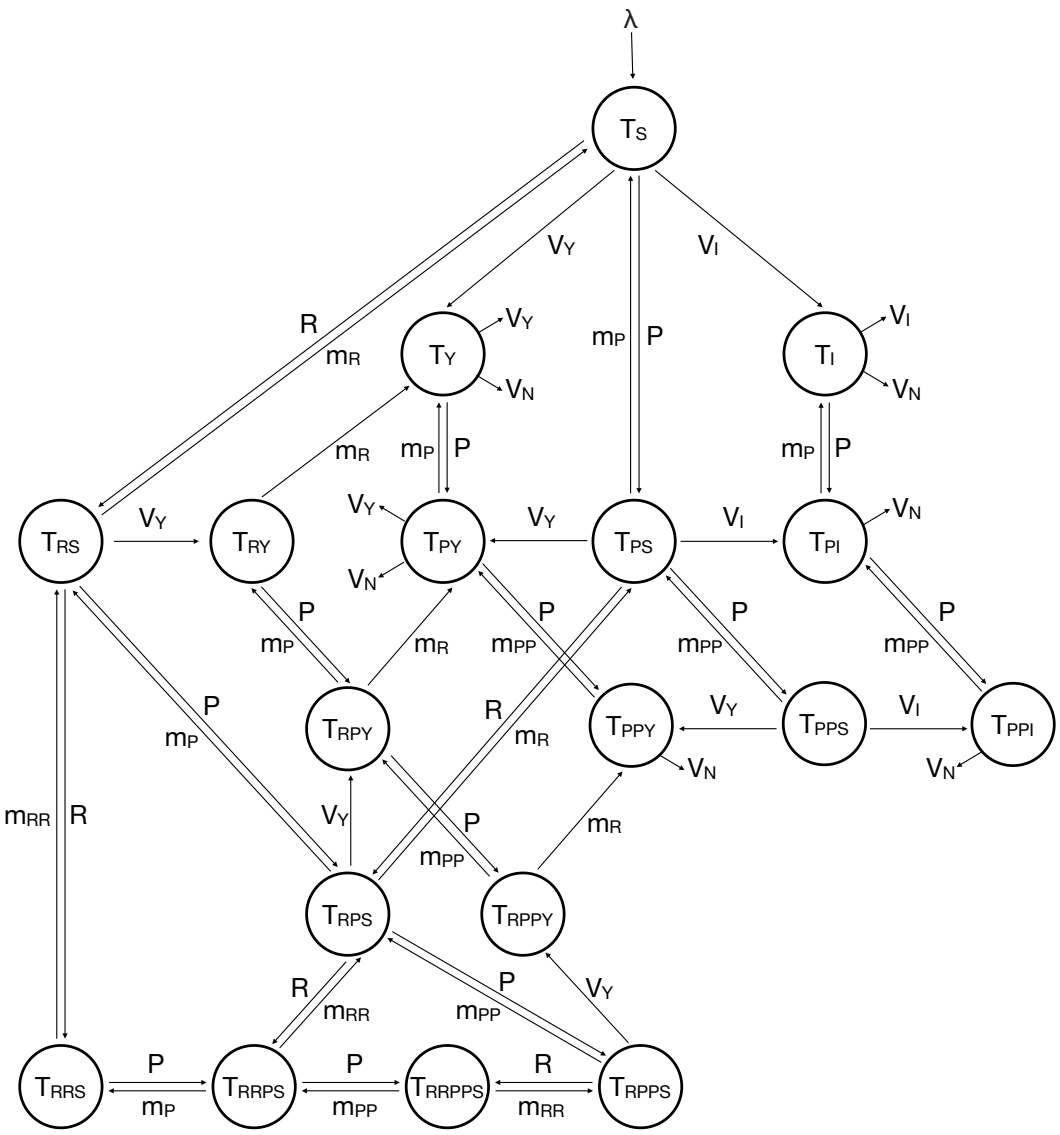

Figure 3.4: The model for Region 3. Susceptible cells that have absorbed a high level of RTIs are denoted by T_{RRS}. T_{PPS}, T_{PPI} and T_{PPY} are susceptible, wild-type and mutant-type infected cells, respectively, inhibited by a high level of PI. Susceptible cells inhibited by a high level of RTI can absorb PIs to become T_{RPPS}; similarly, susceptible cells inhibited by a high level of PI can absorb PIs to become T_{RPPS}. These cells may become infected with the mutant strain to become T_{RPPY}. T_{RRPPS} denotes susceptible cells with high levels of both classes of drugs. In Region 3, the level of drug is sufficiently high to prevent infection of both strains of the virus.

Chapter 4

Asymptotic Behaviour

4.1 Mathematical methods

The following subsections outline the mathematical tools needed to analyse the model. It is a summary of the following sources: [49, 50, 51, 52].

4.1.1 Next-generation method

The basic reproductive ratio, R_0, is a key epidemiologic metric used to describe the transmissibility of an infectious agent. Generally, R_0 gives the expected number of secondary individuals produced by a single individual in their lifetime. However, the interpretation of 'secondary' can depend on the context in which it is being applied. In ecology, R_0 represents the mean lifetime reproductive success of a typical member of the species. In epidemiology, R_0 gives the mean the number of individuals infected by a single infected individual during their infectious period, in a population where all individuals are susceptible to infection. For in-host dynamics, R_0 represents the number of newly infected cells produced by one infected cell during its lifetime, assuming all other cells are susceptible.

R_0 is not a biological constant for a pathogen, as it can be affected by numerous biological, sociobehavioral and environmental factors that govern disease transmission. For any given infectious agent, the scientific literature may present several different values of R_0, as it is dependent on both model structure and assumptions from which it is being calculated, as well as the method being used to calculate it. Often, R_0 is most useful when seen as a threshold: an outbreak is expected to con-

tinue when $R_0 > 1$ and will be cleared when $R_0 < 1$. In an endemic infection, it can be used to inform public health policies by determining which control measures, and at what magnitude, would be most effective in reducing R_0 below one. In a deterministic model, there are several methods for calculating R_0, one of which is the next-generation method.

This method was first introduced by Diekmann et al. [53] and is a general method of deriving R_0 when the population is divided into discrete, disjoint compartments and there are multiple classes of infectives.

Assume there are n compartments, of which m are infected. Define the vector $\bar{x} = x_i$, for $i = 1, ..., n$ to be the number of individuals in the ith compartment. Then the model is given by

$$\frac{dx_i}{dt} = F_i(\bar{x}) - V_i(\bar{x}) = F_i(\bar{x}) - (V_i^-(\bar{x}) - V_i^+(\bar{x})) \tag{4.1.1}$$

where $F_i(\bar{x})$ is the rate of new infections in compartment i, $V_i^-(\bar{x})$ is the rate of transfer of individuals into compartment i by all other means, and $V_i^+(\bar{x})$ is the rate of transfer of individuals out of compartment i. Note that F_i should only include infections that are newly arising, and not terms describing the transfer of infectious individuals from one infected compartment to another. Here, F_i must be non-negative and V_i must be a non-singular M-matrix. The next generation operator, FV^{-1}, can be formed from the matrices of partial derivatives of F_i and V_i:

$$F = \frac{dF_i(x_0)}{dx_j}, V = \frac{dV_i^-(x_0)}{dx_j}, \tag{4.1.2}$$

where $i, j = 1, ..., m$ and x_0 is the disease-free equilibrium. Then spectral radius of the matrix FV^{-1} defines R_0.

4.1.2 Latin hypercube sampling

Latin hypercube sampling (LHS) is a statistical method in which a near-random sample of parameter values is generated. The LHS method is a type of stratified Monte Carlo sampling and gives an unbiased estimate of the average model output. In comparison to other random sampling procedures, it requires a smaller number of samples to achieve the same level of accuracy. When paired with Partial Rank Correlation Coefficient (PRCC) analysis, it is an efficient tool used to explore the entire parameter space of a mathematical model. PRCC analysis is a robust measure of the nonlinear but monotonic relationship between an input parameter and the outcome measure. The goal of the LHS/PRCC procedure is to identify and rank which of the model's parameters contribute to prediction imprecision. The magnitude of a PRCC value indicates the level of uncertainty an LHS parameter contributes to the outcome measure. PRCC values are between -1 and 1; significant values are

considered to be those where $|x| > 0.5$. The closer a value is to -1 or $+1$, the more strongly the LHS parameter influences the outcome measure

With the mathematical model of interest, suppose there are n uncertain parameters, v_i, $1 \leq i \leq n$. The LHS/PRCC procedure can be applied to a wide variety of mathematical models, including those with continuous or discrete features. After deciding on the sample size of the analysis, K, the parameter space is then defined by K dimensions. The following inequality must be satisfied: $K > (4/3)n$. The following steps detail the LHS/PRCC procedure:

1. Specify a probability density function (pdf) for each of the uncertain parameters. Each pdf describes the range of possible values of the parameter and determines the relative likelihood of each value within it. Each pdf is chosen by observing the distribution of a plot of available data. It may be left or right skewed, triangular, uniform, etc. Note that when the data distribution is not available, a uniform distribution should be used as the default.

2. Each pdf is then split into K equiprobable non-overlapping intervals and is randomly sampled once. This results in the sampled values reflecting the shape of the particular pdf. Since each parameter is sampled independently, they are uncorrelated. Once complete, each of the n uncertain parameters will have K values. The sampled values are then stores in a $K \times n$ Latin Hypercube (LH) matrix. Each column is random and is not arranged in any particular way.

3. The outcome measure is then generated for each row of the LH matrix, resulting in an updated LH matrix of the size $K \times (n + 1)$.

4. Next, verify that a monotonic relationship exists between each outcome variable chosen and the LHS parameters.

5. The updated LH matrix is then ranked using a sort routine. The ranking is done by assigning the smallest a value of 1, the next smallest a value of 2 etc.

6. For a given parameter, two multiple linear regression models are found: the first represents the ranked parameter in terms of the other ranked parameters and the second represents the ranked parameter in terms of the other ranked parameter values. The residuals from these two models can be used to calculate a Spearman correlation coefficient. This gives the PRCC value of the given parameter. Note that when the regression is performed on the raw LHS sample values, a Pearson correlation coefficient would be obtained.

4.1.3 Routh–Hurwitz conditions

The Routh–Hurwitz criterion gives the necessary and sufficient condition for all of the roots of a characteristic polynomial with real coefficients to have negative real

parts. Consider the characteristic polynomial

$$P(\mu) = \mu^n + a_1\mu^{n-1} + ... + a_{n-1}\mu + a_n,$$

where the coefficients a_i are real constants, $i = 1, ..., n$. Then these coefficients a_i define the $n \times n$ Hurwitz matrices:

$$H_1 = \begin{bmatrix} a_1 \end{bmatrix}, \quad H_2 = \begin{bmatrix} a_1 & 1 \\ a_3 & a_2 \end{bmatrix}, \quad H_3 = \begin{bmatrix} a_1 & 1 & 0 \\ a_3 & a_2 & a_1 \\ a_5 & a_4 & a_3 \end{bmatrix},$$

$$H_n = \begin{bmatrix} a_1 & 1 & 0 & 0 & \dots & 0 \\ a_3 & a_2 & a_1 & 1 & \dots & 0 \\ a_5 & a_4 & a_3 & a_2 & \dots & 0 \\ \vdots & \vdots & \vdots & \vdots & \dots & \vdots \\ 0 & 0 & 0 & 0 & \dots & a_n \end{bmatrix}$$

where $a_j = 0$ if $j > n$. Then all the roots of $P(\mu)$ are negative or have negative real parts if *all* Hurwitz matrices satisfy

$$\det(H_j) > 0, \quad j = 1, 2, 3, ..., n$$

For $n = 2$, the Routh-Hurwitz conditions simplify to $a_1, a_2 > 0$. To see this, consider the characteristic polynomial:

$$P(\mu) = \mu^n + a_1\mu + a_2.$$

The eigenvalues then satisfy

$$\mu = \frac{-a_1 \pm \sqrt{a_1^2 - 4a_2}}{2}.$$

First, suppose both roots are negative or have negative real parts. Then it follows that $a_1 > 0$. If the roots are real, then $0 < a_1^2 - 4a_2 < a_1$, which implies $a_2 > 0$. If the roots are complex, then $0 < a_1^2 < 4a_2$, which also implies $a_2 > 0$. To prove the converse, assume both $a_1, a_2 > 0$. Then it easily follows that if the roots are real, then they are both negative, and if the roots are complex, then they both have negative real part.
For $n = 3$, the criterion simplifies to $a_1, a_3 > 0$ and $a_1a_2 > a_3$. For $n = 4$, the criterion simplifies to $a_1, a_3, a_4 > 0$ and $a_1a_2a_3 > a_3^2 + a_1^2a_4$.

4.2 Region 1

In order to interpret system (3.3.1)–(3.3.2), we investigate the behaviour in each region separately. We fix the drug concentration as a constant in order to approximate the

effect of the impulsive periodic orbit. Region 1 is not affected by drug concentration, but the analysis of Regions 2 and 3 uses R^* and P^* as the representative drug-level values for RTIs and PIs, respectively.

In Region 1, the disease-free equilibrium is given by

$$(T_S, T_I, T_Y, V_N, V_I, V_Y) = \left(\frac{\lambda}{d_S}, 0, 0, 0, 0, 0\right).$$

The next-generation method [53, 54] is used to derive the basic reproductive number for Region 1, $R_{0,1}$. The next-generation matrices are:

$$F = \begin{bmatrix} 0 & 0 & r_I\overline{T}_S & 0 \\ 0 & 0 & 0 & r_Y\overline{T}_S \\ 0 & 0 & 0 & 0 \\ 0 & 0 & 0 & 0 \end{bmatrix} \tag{4.2.2}$$

$$V = \begin{bmatrix} d_I & 0 & 0 & 0 \\ 0 & d_I & 0 & 0 \\ -n_I\omega & 0 & d_V + r_I\overline{T}_S & 0 \\ 0 & -n_I\omega & 0 & d_V + r_Y\overline{T}_S \end{bmatrix}. \tag{4.2.3}$$

Here, we have that F is non-negative, it remains to show that V is a nonsingular M-matrix. By definition, if V is a real, square matrix with negative off-diagonal elements, then V is a M-matrix if all roots of its characteristic polynomial are positive. As the roots of V are $d_V + r_I\overline{T}_S, d_V + \overline{T}_S, d_I$ and d_I and all parameters are greater than 0, each characteristic root of V is positive. So,V is an M-matrix. Furthermore, since the $\det(V) = d_I^2(d_V + r_I\overline{T}_S)(d_V + \overline{T}_S) > 0$, V is non-singular. $R_{0,1}$ is then the spectral radius of the FV^{-1} matrix. Thus,

$$\begin{aligned} R_{0,1} &= \max\{R_{0,1,I}, R_{0,1,Y}\} \\ &= \max\left\{\frac{n_I r_I \omega\lambda}{d_I(d_V d_S + r_I\lambda)}, \frac{n_I r_Y \omega\lambda}{d_I(d_V d_S + r_Y\lambda)}\right\}. \end{aligned}$$

So, $R_{0,1,I} > R_{0,1,Y}$ under the assumption that $r_I > r_Y$: the mutant strain is less infectious than the wild-type strain.

The disease-free equilibrium is locally asymptotically stable in Region 1 if $R_{0,1} < 1$ and unstable if $R_{0,1} > 1$. The Jacobian matrix for Region 1 is

$$J = \begin{bmatrix} -r_I V_I - r_Y V_Y - d_S & 0 & 0 & 0 & -r_I T_S & -r_Y T_S \\ r_I V_I & -d_I & 0 & 0 & r_I T_S & 0 \\ r_Y V_Y & 0 & -d_I & 0 & 0 & r_Y T_S \\ 0 & n_I(1-\omega) & n_I(1-\omega) & -d_V & 0 & 0 \\ -r_I V_I & n_I\omega & 0 & 0 & -r_I T_S - d_V & 0 \\ -r_Y V_Y & 0 & n_I\omega & 0 & 0 & -r_Y T_S - d_I \end{bmatrix}.$$

For the disease-free equilibrium, $\overline{V}_I = 0 = \overline{V}_Y$ and $\overline{T}_S = \frac{\lambda}{d_S}$. So, the characteristic polynomial is

$$\begin{aligned} 0 = &\det(J(\overline{T}_S, \overline{T}_I, \overline{T}_Y, \overline{V}_N, \overline{T}_I, \overline{T}_Y) - \mu I_6) \\ &= (-d_S - \mu)(-d_V - \mu)(\mu^2 + a_1\mu + a_2)(\mu^2 + b_1\mu + b_2), \end{aligned}$$

where

$$\begin{aligned} a_1 &= d_V + r_I\overline{T}_S + d_I \\ a_2 &= d_I d_V + d_I r_Y \overline{T}_S + n_I\omega r_Y \overline{T}_S \\ b_1 &= d_V + r_Y\overline{T}_S + d_I \\ b_2 &= d_I d_V + d_I r_I \overline{T}_S - n_I\omega r_I \overline{T}_S \\ &= \frac{d_I d_S d_V + r_I\lambda}{d_S}(1 - R_{0,1,I}). \end{aligned}$$

We have $a_i, b_1 > 0$ for $i = 1, 2$, while $b_2 > 0$ if and only if $R_{0,1,I} < 1$. By the Routh–Hurwitz criterion [51,52], all the eigenvalues of the Jacobian matrix have negative real parts. Since $r_I > r_Y$, we have $0 < R_{0,1,Y} < R_{0,1,I}$, and so the disease-free equilibrium is locally asymptotically stable when $R_{0,1} < 1$ and unstable when $R_{0,1} > 1$.
The endemic equilibria are computed by setting the right hand side of equations 3.3.5 equal to zero, with $V_I \neq 0$ for the wild-type equilibrium and $V_Y \neq 0$ for the mutant equilibrium and both $V_I \neq 0$, $V_Y \neq 0$ for the interior equilibrium. The wild-type endemic equilibrium is given by

$$(T_S, T_I, T_Y, V_N, V_I, V_Y) = (\overline{T}_S, \overline{T}_I, 0, \overline{V}_N, \overline{V}_I, 0),$$

where

$$\begin{aligned} \overline{T}_S &= \frac{-d_I d_V}{r_I(d_I - n_I\omega)} \\ \overline{T}_I &= \frac{d_I d_S d_V + \lambda r_I(d_I - n_I\omega)}{d_I r_I(d_I - n_I\omega)} \\ \overline{V}_N &= \frac{n_I(1-\omega)(d_I d_S d_V + \lambda r_I(d_I - n_I\omega))}{d_I d_V r_I(d_I - n_I\omega)} \\ \overline{V}_I &= -\frac{d_I d_S d_V + \lambda r_I(d_I - n_I\omega)}{d_I d_V r_I} \\ &= \frac{d_S d_V + r_I\lambda}{r_I d_V}(R_{0,1,I} - 1). \end{aligned}$$

Note that the wild-type equilibria is only biologically relevant and hence only exists for $R_{0,1,I} > 1$. The characteristic polynomial of the Jacobian evaluated at the wild-type equilibrium is

$$\begin{aligned} 0 = &\det(J(\overline{T}_S, \overline{T}_I, \overline{T}_Y, \overline{V}_N, \overline{T}_I, \overline{T}_Y) - \mu I_6) \\ &= (-d_V - \mu)(\mu^3 + a_1\mu^2 + a_2\mu + a_3)(\mu^2 + b_1\mu + b_2), \end{aligned}$$

where

$$\begin{aligned} a_1 &= r_I\overline{V}_I + r_I\overline{T}_S + d_S + d_V + d_I \\ a_2 &= d_I(r_I\overline{V}_I + d_S) + d_S(d_V + r_I\overline{T}_S) - d_V r_I\overline{V}_I \\ a_3 &= d_I(d_S d_V + r_I\lambda)(R_{0,1,I} - 1) \\ b_1 &= r_Y\overline{T}_S + d_V + d_I \\ b_2 &= \frac{d_I d_V(r_I - r_Y)}{r_I}. \end{aligned}$$

Here, $a_1 > 0$. When $R_{0,1,I} < 1$, we have $a_3 > 0$ and $a_1 a_2 > a_3$. So, all roots of the cubic polynomial have negative real parts when $R_{0,1,I} < 1$. Furthermore, we have $b_1 > 0$, and since the infection rate of the wild-type strain is higher than that of the mutant strain, that is, $r_I > r_Y$, we have $b_2 > 0$. So, the Jacobian has all eigenvalues with negative real parts by the Routh-Hurwitz conditions [51,52]. Thus, the wild-type equilibrium is locally asymptotically stable when it exists.

The mutant endemic equilibrium is given by

$$(T_S, T_I, T_Y, V_N, V_I, V_Y) = (\overline{T}_S, 0, \overline{T}_Y, \overline{V}_N, 0, \overline{V}_Y),$$

where

$$\begin{aligned} \overline{T}_S &= \frac{-d_I d_V}{r_Y(d_I - n_I\omega} \\ \overline{T}_Y &= \frac{d_I d_S d_V + \lambda r_Y(d_I - n_I\omega)}{d_I r_Y(d_I - n_I\omega)} \\ \overline{V}_N &= \frac{n_I(1-\omega)(d_I d_S d_V + \lambda r_Y(d_I - n_I\omega))}{d_I d_V r_Y(d_I - n_I\omega)} \\ \overline{V}_Y &= -\frac{d_I d_S d_V + \lambda r_Y(d_I - n_I\omega)}{d_I d_V r_Y} \\ &= \frac{d_S d_V + r_Y\lambda}{r_Y d_V}(R_{0,1,Y} - 1). \end{aligned}$$

Note that the mutant equilibria is only biologically relevant and hence only exists for $R_{0,1,Y} > 1$. The characteristic polynomial of the Jacobian evaluated at the mutant equilibrium is

$$0 = \det(J(\overline{T}_S, \overline{T}_I, \overline{T}_Y, \overline{V}_N, \overline{T}_I, \overline{T}_Y) - \mu I_6)$$

$$= (-d_V - \mu)(\mu^3 + a_1\mu^2 + a_2\mu + a_3)(\mu^2 + b_1\mu + b_2),$$

where

$$\begin{aligned}
a_1 &= r_Y\overline{V}_Y + r_Y\overline{T}_S + d_S + d_V + d_I \\
a_2 &= d_I(r_Y\overline{V}_Y + d_S) + d_S(d_V + r_Y\overline{T}_S) - d_V r_Y\overline{V}_Y \\
a_3 &= d_I(d_S d_V + r_Y\lambda)(R_{0,1,Y} - 1) \\
b_1 &= r_Y\overline{T}_S + d_V + d_I \\
b_2 &= \frac{d_I d_V(r_Y - r_I)}{r_Y}.
\end{aligned}$$

Note that the characteristic polynomial for the mutant equilibrium is the same as the wild-type equilibrium, with r_I and $\overline{V}_I$ interchanged with r_Y and $\overline{V}_Y$, respectively. However, since $r_Y - r_I < 0$, this means that $b_2 < 0$. So, by the Routh-Hurwitz stability criterion [51, 52], the Jacobian matrix has at least one positive eigenvalue. Thus, the mutant equilibrium is unstable when it exists.

The interior equilibrium exists only when $r_I = r_Y$, which is not biologically realistic. Indeed, for an interior equilibrium, we have $V_I \neq 0$ and $V_Y \neq 0$. Setting system (3.3.5) equal to zero, from the second and third equations, we have

$$\begin{aligned}
T_I &= \frac{r_I}{d_I}T_S V_I, \\
T_Y &= \frac{r_Y}{d_I}T_S V_Y.
\end{aligned}$$

Substituting T_I into the fifth equation, we have

$$r_I T_S V_I \frac{n_I\omega - d_I}{d_I} - d_V V_I = 0,$$

which implies

$$T_S = \frac{d_V d_I}{r_I(n_I\omega - d_I)},$$

since $V_I \neq 0$.

Similarly, substituting T_Y into the sixth equation, we have

$$T_S = \frac{d_V d_I}{r_Y(n_I\omega - d_I)},$$

since $V_Y \neq 0$. This implies $r_I = r_Y$.

4.3 Region 2

As drug concentration affects the outcome of the system in this case, we let $\overline{X}$ denote the equilibrium solutions not affected by the drug dynamics (as in Region 1) and denote X^* as those that are affected by the drug dynamics (as in Regions 2 and 3). We fix R^*, P^* to be constants such that $R_1 < R^* < R_2$ and $P_1 < P^* < P_2$, where R_1, P_1 and R_2, P_2 are the Region 1 and Region 2 thresholds, respectively. Then we have

$$\begin{aligned}&(T_S, T_I, T_Y, T_{RS}, T_{RY}, T_{PS}, T_{PI}, T_{PY}, T_{RPS}, T_{RPY}, V_N, V_I, V_Y, R, P)\\ &= (T_S^*, 0, 0, T_{RS}^*, 0, T_{PS}^*, 0, 0, T_{RPS}^*, 0, 0, 0, 0, R^*, P^*),\end{aligned}$$

where

$$\begin{aligned}T_S^* &= \frac{\lambda((d_S+m_R)(d_S+m_P)(d_S+m_P+m_R)+r_R R^*(d_S+m_R)(d_S+m_P)}{a}\\ &\quad+\frac{r_R R^*(d_S r_P P^*+)r_P P^*(d_S+m_R)(d_S+m_P)}{a}\\ T_{RS}^* &= \frac{R^*\lambda r_R((d_S+m_P)^2+d_S m_R+m_P m_R+R^* d_S r_R+P^* m_P r_P+R^* m_P r_R)}{a}\\ T_{PS}^* &= \frac{P^*\lambda r_P((d_S+m_R)^2+d_S m_P+m_P m_R+P^* d_S r_P+P^* m_R r_P+R^* m_R r_R)}{a}\\ T_{RPS}^* &= \frac{P^* R^*\lambda r_P r_R(2d_S+m_P+m_R+P^* r_P+R^* r_R)}{a},\end{aligned}$$

with

$$a = d_S(d_S+m_R+R^* r_R)(d_S+m_P+P^* r_P)(d_S+m_P+m_R+P^* r_P+R^* r_R).$$

The next-generation matrix is given by the matrices F and $V = [V_1|V_2]$:

$$F = \begin{bmatrix}0&0&0&0&0&0&r_I T_S^*&0\\0&0&0&0&0&0&0&r_Y T_S^*\\0&0&0&0&0&0&0&r_Y T_{RS}^*\\0&0&0&0&0&0&r_I T_{PS}^*&0\\0&0&0&0&0&0&0&r_Y T_{PS}^*\\0&0&0&0&0&0&0&r_Y T_{RPS}^*\\0&0&0&0&0&0&0&0\\0&0&0&0&0&0&0&0\end{bmatrix}$$

$$V_1 = \begin{bmatrix}r_P P+d_I&0&0&-m_P&0\\0&r_P P+d_I&-m_R&0&-m_P\\0&0&m_R+r_P P+d_I&0&0\\-r_P P&0&0&m_P+d_I&0\\0&-r_P P&0&0&m_P+d_I\\0&0&-r_P P&0&0\\-n_I\omega&0&0&0&0\\0&-n_I\omega&0&0&-n_I\omega\end{bmatrix}$$

$$V_2 = \begin{bmatrix} 0 & 0 & 0 \\ 0 & 0 & 0 \\ -m_P & 0 & 0 \\ 0 & 0 & 0 \\ -m_R & 0 & 0 \\ m_R + m_P + d_I & 0 & 0 \\ 0 & r_I(T_S^* + T_{PS}^*) + d_V & 0 \\ 0 & 0 & r_Y(T_S^* + T_{PS}^* + T_{RS}^* + T_{RPS}^*) + d_V \end{bmatrix}.$$

Here, F is non-negative and V can be shown to be a non-singular M-matrix using similar methods as in Region 1. The basic reproductive number in Region 2, $R_{0,2}$, is computed as before using the next-generation method and is given by

$$R_{0,2} = \max\left\{R_{0,2,I}, R_{0,2,Y}\right\},$$

where

$$\begin{aligned} R_{0,2,I} &= \frac{n_I \omega r_I (m_P(T_S^* + T_{PS}^*) + d_I T_S^*)}{d_I(d_I + r_P P^* + m_P)(d_V + r_I(T_S^* + T_{PS}^*))} \\ R_{0,2,Y} &= \frac{n_I \omega r_Y (T_S^* + T_{PS}^*)}{d_I(d_V + r_Y(T_S^* + T_{RS}^* + T_{PS}^* + T_{RPS}^*))} \\ &\quad + \frac{n_I \omega m_R r_Y (T_{RS}^* + T_{RPS}^*)}{d_I(d_I + m_R)(d_V + r_Y(T_S^* + T_{RS}^* + T_{PS}^* + T_{RPS}^*))}. \end{aligned}$$

The Jacobian for Region 2 is $J = [J_1|J_2|J_3|J_4]$

$$J_1 = \begin{bmatrix} -r_I V_I - r_Y V_Y - r_R R - r_P P - d_S & 0 & 0 \\ r_I V_I & -r_P P - d_I & 0 \\ r_Y V_Y & 0 & -r_P P - d_I \\ r_R R & 0 & 0 \\ 0 & 0 & 0 \\ r_P P & 0 & 0 \\ 0 & r_P P & 0 \\ 0 & 0 & r_P P \\ 0 & 0 & 0 \\ 0 & 0 & 0 \\ 0 & n_I(1-\omega) & n_I(1-\omega) \\ -r_I V_I & n_I \omega & 0 \\ -r_Y V_Y & 0 & n_I \omega \\ 0 & 0 & 0 \\ 0 & 0 & 0 \end{bmatrix}$$

$$J_2 = \begin{bmatrix} m_R & 0 & m_P \\ 0 & 0 & 0 \\ 0 & m_R & 0 \\ -m_R - r_P P - r_Y V_Y - d_S & 0 & 0 \\ r_Y V_Y & -m_R - r_P P - d_I & 0 \\ 0 & 0 & -m_P - r_R R - r_I V_I - r_Y V_Y - d_I \\ 0 & 0 & r_I V_I \\ 0 & 0 & r_Y V_Y \\ r_P P & 0 & r_R R \\ 0 & r_P P & 0 \\ 0 & 0 & 0 \\ 0 & 0 & r_I V_I \\ -r_Y V_Y & 0 & r_Y V_Y \\ 0 & 0 & 0 \\ 0 & 0 & 0 \end{bmatrix}$$

$$J_3 = \begin{bmatrix} 0 & 0 & 0 & 0 & 0 \\ m_P & 0 & 0 & 0 & 0 \\ 0 & m_P & 0 & 0 & 0 \\ 0 & 0 & m_P & 0 & 0 \\ 0 & 0 & 0 & m_P & 0 \\ 0 & 0 & m_R & 0 & 0 \\ -m_P - d_I & 0 & 0 & 0 & 0 \\ 0 & -m_P - d_I & 0 & m_R & 0 \\ 0 & 0 & -m_R - m_P - r_Y V_Y - d_S & 0 & 0 \\ 0 & 0 & r_Y V_Y & -m_R - m_P - d_I & 0 \\ n_I \omega & n_I(1-\omega) & 0 & 0 & -d_V \\ 0 & 0 & 0 & 0 & 0 \\ 0 & n_I \omega & -r_Y V_Y & 0 & 0 \\ 0 & 0 & 0 & 0 & 0 \\ 0 & 0 & 0 & 0 & 0 \end{bmatrix}$$

$$J_4 = \begin{bmatrix} -r_I T_S & -r_Y T_S & -r_R T_S & -r_P T_S \\ r_I T_S & 0 & 0 & -r_P T_I \\ 0 & r_Y T_S & 0 & -r_P T_I \\ 0 & -r_Y T_{RS} & r_R T_S & -r_P T_{RS} \\ 0 & r_Y T_{RS} & 0 & -r_P T_{RY} \\ -r_I T_{PS} & -r_Y T_{PS} & -r_R T_{PS} & r_P T_S \\ r_I T_{PS} & 0 & 0 & r_P T_I \\ 0 & r_Y T_{PS} & 0 & r_P T_Y \\ 0 & -r_Y T_{RPS} & r_R T_{PS} & r_P T_{RS} \\ 0 & r_Y T_{RPS} & 0 & r_P T_{RY} \\ 0 & 0 & 0 & 0 \\ -r_I(T_S + T_{PS}) - d_V & 0 & 0 & 0 \\ 0 & -r_Y(T_S + T_{RS} + T_{PS} + T_{RPS}) - d_V & 0 & 0 \\ 0 & 0 & -d_R & 0 \\ 0 & 0 & 0 & -d_P \end{bmatrix}.$$

For the disease-free equilibrium, $V_I^* = V_Y^* = 0$, so the characteristic polynomial is

$$\begin{aligned} 0 = {} & \det(J(T_S^*, T_I^*, T_Y^*, T_{RS}^*, T_{RY}^*, T_{PS}^*, T_{PI}^*, T_{PY}^*, T_{RPS}^*, T_{RPS}^*, T_{RPY}, V_N^*, V_I^*, V_Y^*, R^*, P^*) \\ & - \mu I_{15}) \\ = {} & (-d_V - \mu)(-d_R - \mu)(-d_P - \mu)(\mu^3 + a_1\mu^2 + a_2\mu + a_3) f_1(\mu) f_2(\mu), \end{aligned}$$

where

$$\begin{aligned} a_1 &= m_P + 2d_I + d_V + r_P P^* + r_I(T_S^* + T_{PS}^*) \\ a_2 &= (d_I + r_P P^*)(d_V + r_I T_S^* + r_I T_{PS}^*) + (m_P + d_I)(d_V + r_I T_S^* + r_I T_{PS}^* + d_I + r_P P^*) \\ &\quad - m_P r_P P^* - n_I \omega r_I T_S^* \\ a_3 &= d_I(d_I + r_P P^* + m_P)(d_V + r_I T_S^* + r_I T_{PS}^*)(1 - R_{0,2,I}) \end{aligned}$$

and $f_1(\mu) = \det[\gamma_1|\gamma_2]$ and $f_2(\mu) = \det[\gamma_3|\gamma_4]$, where

$$\gamma_1 = \begin{bmatrix} -r_P P^* - d_I - \mu & m_R & m_P \\ 0 & -m_R - r_P P^* - d_I - \mu & 0 \\ r_P P^* & 0 & -m_P - d_I - \mu \\ 0 & r_P P^* & 0 \\ n_I \omega & 0 & n_I \omega \end{bmatrix}$$

$$\gamma_2 = \begin{bmatrix} 0 & r_Y T_S^* \\ m_P & r_Y T_{RS}^* \\ m_R & r_Y T_{PS}^* \\ -m_R - m_P - d_I - \mu & r_Y T_{RPS}^* \\ 0 & -r_Y(T_S^* + T_{RS}^* + T_{PS}^* + T_{RPS}^*) - d_V - \mu \end{bmatrix}$$

$$\gamma_3 = \begin{bmatrix} -r_P P^* - r_R R^* - d_I - \mu & m_R \\ r_R R^* & -r_P P^* - m_R - d_I - \mu \\ r_P P^* & 0R \\ 0 & r_P P^* \end{bmatrix}$$

$$\gamma_4 = \begin{bmatrix} m_P & 0 \\ 0 & m_P \\ -r_R R^* - m_P - d_S - \mu & m_R \\ r_R R^* & -m_P - m_R - d_S - \mu \end{bmatrix}.$$

The cubic polynomial $\mu^3 + a_2\mu^2 + a_0\mu + a_0$ has $a_1, a_3 > 0$ in any case, and $a_1 a_2 - a_3 > 0$ if $R_{0,2,I} < 1$. By the Routh–Hurwitz stability criterion [51, 52], the roots of the third-order polynomial all have a negative real part when $R_{0,2,I} < 1$ and positive real part when $R_{0,2,I} > 1$. Note that $f_1(\mu)$ is of the following form:

$$f_1(\mu) = \begin{bmatrix} a & x & f & 0 & m \\ 0 & d & 0 & j & n \\ b & 0 & g & k & p \\ 0 & e & 0 & l & q \\ c & 0 & h & 0 & r \end{bmatrix}$$

, where $x = k, c = h, f = j, b = e, d = a - k$ and $l = g - k$. Thus, $f_1(\mu)$ can be written as:

$$f_1(\mu) = \det \begin{bmatrix} a & f & m \\ b & g & p \\ c & h & r \end{bmatrix} \det \begin{bmatrix} d & j \\ e & l \end{bmatrix} + S$$

where $S > 0$. Thus, the characteristic equation can be written as

$$f_1(\mu) = (\mu + b_1\mu + b_2)(\mu^3 + c_1\mu^2 + c_2\mu + c_3) + S \equiv \tilde{f}_1(\mu) + S,$$

where

$b_1 = 2d_I + 2m_R + m_P + r_P P^*$
$b_2 = (d_I + m_R)(d_I + m_R + m_P + r_P P^*)$
$c_1 = 2d_I + m_P + r_P P^* + r_Y(T_S^* + T_{RS}^* + T_{PS}^* + T_{RPS}^*)$
$c_2 = (d_I + r_Y(T_S^* + T_{RS}^* + T_{PS}^* + T_{RPS}^* + d_V)(2d_I + m_P + r_P P^*))$–$(d_I + n_I\omega(T_S^* + T_{PS}^*))$
$c_3 = (d_I + m_P + r_P P^*)(d_I r_Y(T_S^* + T_{RS}^* + T_{PS}^* + T_{RPS}^*) - n_I\omega(T_S^* + T_{RS}^*))$.

Since we have $b_{1,2} > 0$ and $c_1, c_3 > 0$ with $c_1 c_2 > c_3$, by the Routh–Hurwitz stability condition [51, 52], the roots of the second and third-order polynomial both have negative real parts. So, as S shifts the characteristic polynomial upward, since the real

parts of $\tilde{f}_1(\mu)$ are negative, then the real parts of $\tilde{f}$ must also be negative. Computing $f_2(\mu)$, we have

$$f_2(\mu) = \mu^4 + d_1\mu^3 + d_2\mu^2 + d_3\mu + d_4,$$

where

$$\begin{aligned}
d_1 &= 2(d_I + m_R + m_P + r_P P^* + r_R R^* + d_S) \\
d_2 &= (d_I + m_R + m_P + d_S + r_R R^* + r_P P^*)^2[d_I(m_R + 2m_P + r_R R^* + 2d_S) + \\
&\quad (m_R + r_R R^*)(m_P + r_P P^*) + d_S(m_R + 2r_P P^* + r_R R^*)] \\
d_3 &= (d_I + m_P + r_P P^* + d_S)(m_R + r_R R^*) \\
&\quad + 2(d_I m_P + d_I d_S + r_P P^* d_S)(d_I + m_R + m_P + r_P P^* + r_R R^* + d_S) \\
d_4 &= (d_I m_P + d_I d_S + r_P P^* d_S)[d_I(m_R + m_P + r_R R^* + d_S) \\
&\quad + (m_R + r_R R^*)(m_P + r_P P^* + m_R + r_R R^*) + d_S(m_R + r_P P^* + r_R R^*)].
\end{aligned}$$

We have $d_1, d_3, d_4 > 0$, with $d_1 d_2 d_3 > d_3^2 + d_1^2 d_4$. By the Routh–Hurwitz stability condition [51, 52], the roots of the fourth-order polynomial have negative real part. Thus, since Jacobian matrix has all eigenvalues with negative real part when $R_{0,2,I} < 1$, the disease-free equilibrium is locally asymptotically stable.

4.4 Region 3

In this region, $R^* > R_2$ and $P^* > P_2$. The disease-free equilibrium is

$$\begin{aligned}
&(T_S, T_I, T_Y, T_{RS}, T_{RY}, T_{PS}, T_{PI}, T_{PY}, T_{RPS}, T_{RPY}, T_{RRS}, T_{PPS}, T_{PPI}, \\
&T_{PPY}, T_{RRPS}, T_{RPPS}, T_{RPPY}, T_{RRPPS}, V_N, V_I, V_Y, R, P) \\
&= (T_S^*, 0, 0, T_{RS}^*, 0, T_{PS}^*, 0, 0, T_{RPS}^*, T_{RRS}^*, T_{PPS}^*, 0, 0, T_{RRPS}^*, T_{RPPS}^*, \\
&0, T_{RRPPS}^*, 0, 0, 0, R^*, P^*),
\end{aligned}$$

where

$$\begin{aligned}
T_S^* &= \frac{\lambda + m_P T_{PS}^* + m_R T_{RS}^*}{r_R R^* + r_P P^* + d_S} \\
T_{RS}^* &= \frac{r_R R^* T_S^* + m_P T_{RPS}^* + m_{RR} T_{RRS}^*}{m_R + r_P P^* + r_{RR} R^* + d_S} \\
T_{PS}^* &= \frac{r_P P^* T_S^* + m_R T_{RPS}^* + m_{PP} T_{PPS}^*}{m_P + r_R R^* + r_{PP} P^* + d_S} \\
T_{RPS}^* &= \frac{r_R R^* T_{PS}^* + r_P P^* T_{RS}^* + m_{RR} T_{RRPS}^* + m_{PP} T_{RPPS}^*}{m_R + m_P + r_{RR} R^* + r_{PP} P^* + d_S} \\
T_{RRS}^* &= \frac{r_{RR} R^* T_{RS}^* + m_P T_{RRPS}^*}{r_P P^* + m_{RR} + d_S}
\end{aligned}$$

$$
\begin{aligned}
T^*_{PPS} &= \frac{r_{PP}P^*T^*_{PS} + m_R T^*_{RPPS}}{r_R R^* + m_{PP} + d_S} \\
T^*_{RRPS} &= \frac{r_P P^* T^*_{RRS} + m_{PP} T^*_{RRPPS} + r_{RR} R^* T^*_{RPS}}{m_{RR} + m_P + r_{PP}P^* + d_S} \\
T^*_{RPPS} &= \frac{r_R R^* T^*_{PPS} + m_{RR} T^*_{RRPPS} + r_{PP} P^* T^*_{RPS}}{m_R + r_{RR}R^* + m_{PP} + d_S} \\
T^*_{RRPPS} &= \frac{r_{PP} R^* T^*_{RPPS} + r_{PP} P^* T^*_{RRPS}}{m_{RR} + m_{PP} + d_S}.
\end{aligned}
$$

The next-generation matrix is given by the matrices $F = [0_{11,11}|F_2]$ and $V = [V_1|V_2|V_3]$:

$$
F_2 = \begin{bmatrix}
r_I T^*_S & 0 \\
0 & r_Y T^*_S \\
0 & r_Y T^*_{RS} \\
r_I T^*_{PS} & 0 \\
0 & r_Y T^*_{PS} \\
0 & r_Y T^*_{RPS} \\
r_I T^*_{PPS} & 0 \\
0 & r_Y T^*_{PPS} \\
0 & r_Y T^*_{RPPS} \\
0 & 0 \\
0 & 0
\end{bmatrix}
$$

$$
V_1 = \begin{bmatrix}
r_P P - d_I & 0 & 0 & -m_P & 0 \\
0 & m_R + r_P P - d_I & -m_R & 0 & -m_P \\
0 & 0 & r_P P + d_I & 0 & 0 \\
-r_P P & 0 & 0 & m_P + r_{PP}P + d_I & 0 \\
0 & -r_P P & 0 & 0 & m_P + r_{PP}P + d_I \\
0 & 0 & -r_P P & 0 & 0 \\
0 & 0 & 0 & -r_{PP}P & 0 \\
0 & 0 & 0 & 0 & -r_{PP}P \\
0 & 0 & 0 & 0 & 0 \\
-n_I\omega & 0 & 0 & 0 & 0 \\
0 & -n_I\omega & 0 & 0 & -n_I\omega
\end{bmatrix}
$$

$$V_2 = \begin{bmatrix} 0 & 0 & 0 & 0 \\ 0 & 0 & 0 & 0 \\ -m_P & 0 & 0 & 0 \\ 0 & -m_{PP} & 0 & 0 \\ -m_R & 0 & -m_{PP} & 0 \\ m_R + m_P + r_{PP}P + d_I & 0 & 0 & -m_{PP} \\ 0 & m_{PP} + d_I & 0 & 0 \\ 0 & 0 & m_{PP} + d_I & -m_R \\ -r_{PP}P & 0 & 0 & m_R + m_{PP} + d_I \\ 0 & 0 & 0 & 0 \\ 0 & 0 & 0 & 0 \end{bmatrix}$$

$$V_3 = \begin{bmatrix} 0 & 0 \\ 0 & 0 \\ 0 & 0 \\ 0 & 0 \\ 0 & 0 \\ 0 & 0 \\ 0 & 0 \\ 0 & 0 \\ 0 & 0 \\ r_I(T_S^* + T_{PS}^* + T_{PPS}^*) + d_V & 0 \\ 0 & r_Y(T_S^* + T_{RS}^* + T_{PS}^* + T_{RPS}^* + T_{PPS}^* + T_{RPPS}^*) + d_V \end{bmatrix}.$$

Here, F is non-negative and V can be shown to be a non-singular M-matrix using similar methods as in Region 1. The basic reproductive number in Region 3, $R_{0,3}$, is computed using the next-generation method and is given by

$$R_{0,3} = \max\left\{R_{0,3,I}, R_{0,3,Y}\right\},$$

where

$$R_{0,3,I} = \frac{n_I \omega r_I (a + b + c)}{d_I e (d_V + r_I (T_S^* + T_{PS}^* + T_{PPS}^*))}$$
$$R_{0,3,Y} = \frac{n_I \omega r_Y (f + g)}{d_I h (d_V + r_Y (T_S^* + T_{RS}^* + T_{PS}^* + T_{RPS}^* + T_{PPS}^* + T_{RPPS}^*))},$$

with

$$a = T_S^* (d_I r_{PP} P^* + (d_I + m_P)(d_I + m_{PP}))$$
$$b = m_P T_{PS}^* (d_I + m_{PP})$$
$$c = m_P m_{PP} T_{PPS}^*$$

$$
\begin{aligned}
e &= (r_{PP}P^*(d_I + r_P P^*) + (d_I + m_{PP})(d_I + m_P + r_P P^*)) \\
f &= (d_I + r_P P^* + m_P)(m_P P(T_S^* + T_{PS}^* + T_{PPS}^*) + d_I(T_S^* + T_{PS}^*) + d_I r_P P^* T_S^*) \\
g &= r_Y(m_R(\delta_1 T_{RS}^* + \delta_2 T_{RPS}^* + \delta_3 T_{RPPS}^*) + m_{PP}\delta_3 T_{RPPS}^*) \times (j(d_I + m_R))^{-1} \\
h &= r_{PP}P^*(d_I + r_P P^*) + (d_I + m_{PP})(d_I + m_P + r_P P^*)
\end{aligned}
$$

and

$$
\begin{aligned}
j &= r_{PP}P^*(d_I + m_R + r_P P^*) + (d_I + m_R + m_{PP})(d_I + m_R + m_P + r_P P^*) \\
\delta_1 &= r_P P^*(4d_I(d_I + m_P + m_R) + m_{PP}(m_R + 2m_R^2) + P^* r_P(2d_I + m_{PP} + m_R) \\
&\quad + r_{PP}P^*(2d_I + m_P + m_R + P^* r_P)) + r_{PP}P^* d_I(d_I + 2m_P + m_R) \\
&\quad + (d_I + m_P)(2d_I + m_{PP} + m_R)(d_I + m_P + m_R) \\
\delta_2 &= m_{PP}\delta_1 + P^* d_I(r_P(d_I + m_R)(2(d_I + m_P) + m_R + r_P P^*) + m_R(m_{PP}m_R \\
&\quad + m_P(r_{PP} + m_P + m_R)) + 2r_{PP}r_P P^* m_{PP}) + d_I(d_I(d_I^2 + m_P^2) \\
&\quad + m_R(d_I + m_P)(2d_I + m_P) + m_R^2(d_I + m_{PP} + m_P)) \\
\delta_3 &= \delta_2 + P^* r_{PP} d_I((d_I + m_R)(2d_I + m_{PP} + m_P + m_R + P^*(r_{PP} + r_P)))
\end{aligned}
$$

The Jacobian for Region 3 is $J = [J_1|J_2|J_3|J_4|J_5|J_6|J_7|J_8|J_9|J_{10}]$, where

$$
J_1 = \begin{bmatrix}
-r_I V_I - r_Y V_Y - r_P P - r_R R - d_S & 0 & 0 \\
r_I V_I & -r_P P - d_I & 0 \\
r_Y V_Y & 0 & -r_P P - d_I \\
r_R R & 0 & 0 \\
0 & 0 & 0 \\
r_P P & 0 & 0 \\
0 & r_P P & 0 \\
0 & 0 & r_P P \\
0 & 0 & 0 \\
0 & 0 & 0 \\
0 & 0 & 0 \\
0 & 0 & 0 \\
0 & 0 & 0 \\
0 & 0 & 0 \\
0 & 0 & 0 \\
0 & 0 & 0 \\
0 & 0 & 0 \\
0 & n_I(1-\omega) & n_I(1-\omega) \\
-r_I V_I & n_I \omega & 0 \\
-r_Y V_Y & 0 & n_I \omega \\
0 & 0 & 0 \\
0 & 0 & 0
\end{bmatrix}
$$

$$J_2 = \begin{bmatrix} m_R & 0 \\ 0 & 0 \\ 0 & m_R \\ -r_Y V_Y - m_R - r_P P - r_{RR} R - d_S & 0 \\ r_Y V_I & -m_R - r_P P - d_I \\ 0 & 0 \\ 0 & 0 \\ 0 & 0 \\ r_P P & 0 \\ 0 & r_P P \\ r_{RR} R & 0 \\ 0 & 0 \\ 0 & 0 \\ 0 & 0 \\ 0 & 0 \\ 0 & 0 \\ 0 & 0 \\ 0 & 0 \\ 0 & 0 \\ 0 & 0 \\ -r_Y V_Y & 0 \\ 0 & 0 \\ 0 & 0 \end{bmatrix}$$

$$J_3 = \begin{bmatrix} m_P & 0 \\ 0 & m_P \\ 0 & 0 \\ 0 & 0 \\ 0 & 0 \\ -r_I V_I - r_Y V_Y - m_P - r_R R - r_{PP} P - d_S & 0 \\ r_I V_Y & -m_P - r_{PP} P - d_I \\ r_Y V_Y & 0 \\ r_R R & 0 \\ 0 & 0 \\ 0 & 0 \\ r_{PP} P 0 & 0 \\ 0 & r_{PP} P \\ 0 & 0 \\ 0 & 0 \\ 0 & 0 \\ 0 & 0 \\ 0 & 0 \\ 0 & n_I \omega \\ -r_I V_Y & 0 \\ -r_Y V_Y & 0 \\ 0 & 0 \\ 0 & 0 \end{bmatrix}$$

$$J_4 = \begin{bmatrix} 0 & 0 \\ 0 & 0 \\ m_P & 0 \\ 0 & m_P \\ 0 & 0 \\ 0 & m_R \\ 0 & 0 \\ -m_P - r_{PP}P - d_I & 0 \\ 0 & -r_Y V_Y - m_R - m_P - r_{PP}P - r_{RR}R - d_S \\ 0 & r_Y V_Y \\ 0 & 0 \\ 0 & 0 \\ 0 & 0 \\ 0 & r_{RR}R \\ 0 & r_{PP}P \\ 0 & 0 \\ 0 & 0 \\ n_I(1-\omega) & 0 \\ 0 & 0 \\ n_I\omega & -r_Y V_Y \\ 0 & 0 \\ 0 & 0 \end{bmatrix}$$

$$J_5 = \begin{bmatrix} 0 & 0 \\ 0 & 0 \\ 0 & 0 \\ 0 & m_{RR} \\ m_P & 0 \\ 0 & 0 \\ 0 & 0 \\ m_R & 0 \\ 0 & 0 \\ -m_P - m_R - r_{PP}P - d_I & 0 \\ 0 & -r_P P - m_{RR} - d_S \\ 0 & 0 \\ 0 & 0 \\ 0 & 0 \\ 0 & r_P P \\ 0 & 0 \\ r_{PP}P & 0 \\ 0 & 0 \\ 0 & 0 \\ 0 & 0 \\ 0 & 0 \\ 0 & 0 \\ 0 & 0 \end{bmatrix}$$

$$J_6 = \begin{bmatrix} 0 & 0 & 0 \\ 0 & 0 & 0 \\ 0 & 0 & 0 \\ 0 & 0 & 0 \\ 0 & 0 & 0 \\ m_{PP} & 0 & 0 \\ 0 & m_{PP} & 0 \\ 0 & 0 & m_{PP} \\ 0 & 0 & 0 \\ 0 & 0 & 0 \\ 0 & 0 & 0 \\ -r_I V_I - r_Y V_Y - m_{PP} - r_R R - d_S & 0 & 0 \\ r_I V_I & -m_{PP} - d_I & 0 \\ r_Y V_Y & 0 & -m_{PP} - d_I \\ 0 & 0 & 0 \\ r_R R & 0 & 0 \\ 0 & 0 & 0 \\ 0 & 0 & 0 \\ 0 & n_I \omega & n_I \omega \\ -r_I V_Y & 0 & 0 \\ -r_Y V_Y & 0 & 0 \\ 0 & 0 & 0 \\ 0 & 0 & 0 \end{bmatrix}$$

$$J_7 = \begin{bmatrix} 0 & 0 \\ 0 & 00 \\ 0 & 0 \\ 0 & 0 \\ 0 & 0 \\ 0 & 0 \\ 0 & 0 \\ 0 & 0 \\ m_{RR} & m_{PP} \\ 0 & 0 \\ m_P & 0 \\ 0 & m_R \\ 0 & 0 \\ 0 & 0 \\ -m_P - r_{PP}P - m_{RR} - d_S & 0 \\ 0 & -r_Y V_Y - m_R - r_{RR}R - m_{PP} - d_S \\ 0 & r_Y V_Y \\ r_{PP}P & r_{RR}R \\ 0 & 0 \\ 0 & 0 \\ 0 & -r_Y V_Y \\ 0 & 0 \\ 0 & 0 \end{bmatrix}$$

$$J_8 = \begin{bmatrix} 0 & 0 & 0 \\ 0 & 0 & 0 \\ 0 & 0 & 0 \\ 0 & 0 & 0 \\ 0 & 0 & 0 \\ 0 & 0 & 0 \\ 0 & 0 & 0 \\ 0 & 0 & 0 \\ 0 & 0 & 0 \\ m_{PP} & 0 & 0 \\ 0 & 0 & 0 \\ 0 & 0 & 0 \\ 0 & 0 & 0 \\ m_R & 0 & 0 \\ 0 & m_{PP} & 0 \\ 0 & m_{RR} & 0 \\ -m_R - m_{PP} - d_I & 0 & 0 \\ 0 & -m_{PP} - m_{RR} - d_S & 0 \\ 0 & 0 & d_V \\ 0 & 0 & 0 \\ 0 & 0 & 0 \\ 0 & 0 & 0 \\ 0 & 0 & 0 \end{bmatrix}$$

$$J_9 = \begin{bmatrix} -r_I T_S & -r_Y T_S \\ r_I T_S & 0 \\ 0 & r_Y T_S \\ 0 & -r_Y T_{RS} \\ 0 & r_Y T_{RS} \\ -r_I T_{PS} & r_Y T_{PS} \\ r_I T_{PS} & 0 \\ 0 & r_Y T_{PS} \\ 0 & -r_Y T_{RPS} \\ 0 & r_Y T_{RPS} \\ 0 & 0 \\ -r_I T_{PPS} & r_Y T_{PPS} \\ r_I T_{PPS} & 0 \\ 0 & r_Y T_{PPS} \\ 0 & 0 \\ 0 & -r_Y T_{RPPS} \\ 0 & r_Y T_{RPPS} \\ 0 & 0 \\ 0 & 0 \\ -r_I(T_S + T_{PS} + T_{PPS}) - d_V & 0 \\ 0 & -r_Y(T_S + T_{RS} + T_{PS} + T_{RPS} + T_{PPS} + T_{RPPS}) - d_V \\ 0 & 0 \\ 0 & 0 \end{bmatrix}$$

$$J_{10} = \begin{bmatrix} -r_R T_S & -r_P T_S \\ 0 & -r_P T_I \\ 0 & -r_P T_Y \\ r_R T_S - r_{PP} T_{RS} & -r_P T_{RS} \\ 0 & -r_P T_{RY} \\ -r_R T_{PS} & r_P T_{PS} - r_{PP} T_{PS} \\ 0 & r_P T_{PI} - r_{PP} T_{PI} \\ 0 & r_P T_{PY} - r_{PP} T_{PY} \\ r_R T_{PS} - r_{RR} T_{RPS} & r_P T_{RS} - r_{PP} T_{RPS} \\ 0 & r_P T_{RY} - r_{PP} T_{RPY} \\ r_{RR} T_{RS} & -r_P T_{RRS} \\ -r_{RR} T_{PPS} & r_{PP} T_{PS} \\ 0 & r_{PP} T_{PI} \\ 0 & r_{PP} T_{PY} \\ r_{RR} T_{RPS} & r_P T_{RPS} - r_{PP} T_{RRPS} \\ r_R T_{PPS} - r_{RR} T_{RPPS} & r_{PP} T_{RPS} \\ 0 & r_{PP} T_{RPY} \\ r_{RR} T_{RPPS} & r_{PP} T_{RRPS} \\ 0 & 0 \\ 0 & 0 \\ 0 & 0 \\ -d_R & 0 \\ 0 & -d_P \end{bmatrix}.$$

We now explore the conditions under which the disease-free equilibrium becomes stable. We consider a subset of Region 3 where both R^* and P^* are sufficiently large so that the disease-free equilibrium is asymptotically stable. This will be referred to as the region of viral elimination. Although RTI and PI drug levels will fluctuate over time between the upper and lower endpoints of their periodic orbit, we use R^* and P^* as the representative drug-level values for RTIs and PIs, respectively, so that the conditions of the Hartman–Grobman theorem [55] are satisfied.

Case 1: Taking first $R^* \to \infty$, we have

$$\begin{aligned} T_S^* &\to 0 \\ T_{RS}^* &\to 0 \\ T_{PS}^* &\to 0 \\ T_{RPS}^* &\to 0 \\ T_{RRS}^* &\to \frac{\lambda r_{RR}(P^* m_{RR} r_{RR} + P^* r_{PP} d_S + (d_S + m_P)(d_S + m_{RR} + m_{PP}))}{a} \\ &\quad - \frac{\lambda r_{PP} m_{RR}(d_S + m_P + P^* r_P)}{a} \end{aligned}$$

$$
\begin{aligned}
T^*_{PPS} &\to 0 \\
T^*_{RRPS} &\to \frac{P^*\lambda r_P(r_{RR}(d_S + m_{PP} + m_{RR}) - m_{RR}R^* r_{PP})}{a} \\
T^*_{RPPS} &\to 0 \\
T^*_{RRPPS} &\to \frac{\lambda P^{*2} r_P r_{PP} r_{RR}}{a},
\end{aligned}
$$

where

$$
\begin{aligned}
a = \; & r_{RR}(d_S(d_S + m_P)(d_S + m_{PP} + m_{RR}) + P^* r_P(d_S + m_{PP} + m_{RR})) \\
& - r_{PP}(d_S m_{RR}(d_S + m_P + r_{PP}P^*) + m_{RR}P^* r_P(d_S + r_{PP}P^*)) \\
& + r_{RR}r_{PP}(P^*(d_S(m_{RR} + P^* d_S r_P + d_S) + P^* m_{RR} r_P)).
\end{aligned}
$$

When $P^* \to \infty$, we have

$$
\begin{aligned}
T^*_S &\to 0 \\
T^*_{RS} &\to 0 \\
T^*_{PS} &\to 0 \\
T^*_{RPS} &\to 0 \\
T^*_{RRS} &\to 0 \\
T^*_{PPS} &\to 0 \\
T^*_{RRPS} &\to 0 \\
T^*_{RPPS} &\to 0 \\
T^*_{RRPPS} &\to \frac{\lambda r_{RR}}{d_S r_{RR} - m_{RR} r_{PP} + m_{RR} r_{RR}}.
\end{aligned}
$$

Case 2: Taking first $P^* \to \infty$, we have

$$
\begin{aligned}
T^*_S &\to 0 \\
T^*_{RS} &\to 0 \\
T^*_{PS} &\to 0 \\
T^*_{RPS} &\to 0 \\
T^*_{RRS} &\to 0 \\
T^*_{PPS} &\to \frac{\lambda((d_S + m_R)(d_S + m_{RR}) + R^*(d_S r_{RR} + m_{RR} r_{RR} - m_{RR} r_{PP}))}{b} \\
T^*_{RRPS} &\to 0 \\
T^*_{RPPS} &\to \frac{\lambda R^* r_R(d_S + m_{RR})}{b}
\end{aligned}
$$

$$T^*_{RRPPS} \to \frac{\lambda R^{*2} r_{PP} r_{RR}}{b},$$

where

$$\begin{aligned} b = \; & d_S((d_S + m_{RR})(d_S + m_R) + R^*(d_S(r_R + r_{RR}) + m_{RR}(r_R + r_{RR} - r_{PP}) + R^* r_R r_{RR})) \\ & + R^{*2} m_{RR} r_R (r_{RR} - r_{PP}). \end{aligned}$$

When $R^* \to \infty$, we have

$$\begin{aligned} T^*_S &\to 0 \\ T^*_{RS} &\to 0 \\ T^*_{PS} &\to 0 \\ T^*_{RPS} &\to 0 \\ T^*_{RRS} &\to 0 \\ T^*_{PPS} &\to 0 \\ T^*_{RRPS} &\to 0 \\ T^*_{RPPS} &\to 0 \\ T^*_{RRPPS} &\to \frac{\lambda r_{PP}}{d_S r_{RR} - m_{RR} r_{PP} + m_{RR} r_{RR}}. \end{aligned}$$

When both $R^*, P^* \to \infty$, $R_{0,3}$ defined by equation (4.4.3) will equal zero, meaning in the limit of $R^*, P^* \to \infty$, the basic reproductive number will be below unity. We will now show that the disease-free equilibrium is locally asymptotically stable in this region. Computing the Jacobian for Region 3 we have $V^*_I = V^*_Y = 0$, so

$$0 = \det(J - \mu I_{23}) = (-d_V - \mu)(-d_R - \mu)(-d_P - \mu) f_1(\mu) f_2(\mu) f_3(\mu)$$

where

$$f_1(\mu) = \det[\gamma_1 | \gamma_2 | \gamma_3]$$

with

$$\gamma_1 = \begin{bmatrix} -r_P P^* - d_I - \mu & m_R & m_P \\ 0 & -m_R - r_P P^* - d_I - \mu & 0 \\ r_P P^* & 0 & -m_P - r_{PP} P^* - d_I - \mu \\ 0 & r_P P^* & 0 \\ 0 & 0 & r_{PP} P^* \\ 0 & 0 & 0 \\ n_I \omega & 0 & n_I \omega \end{bmatrix}$$

$$\gamma_2 = \begin{bmatrix} 0 & 0 \\ m_P & 0 \\ m_R & m_{PP} \\ -m_P - m_R - r_{PP}P^* - d_I - \mu & 0 \\ 0 & -m_{PP} - d_I - \mu \\ r_{PP}P^* & 0 \\ 0 & 0 \end{bmatrix}$$

$$\gamma_3 = \begin{bmatrix} 0 & r_Y T_S^* \\ 0 & r_Y T_{RS}^* \\ 0 & r_Y T_{PS}^* \\ m_{PP} & r_Y T_{RPS}^* \\ m_R & r_Y T_{PPS}^* \\ -m_R - m_{PP} - d_I - \mu & r_Y T_{RPPS}^* \\ 0 & -r_Y(T_S^* + T_{RS}^* + T_{PS}^* + T_{RPS}^* + T_{PPS}^* + T_{RPPS}^*) - d_V - \mu \end{bmatrix}.$$

Computing $f_1(\mu)$ and taking $R^*, P^* \to \infty$, the seventh-order polynomial can be reduced to two third-order polynomials $(\mu^3 + a_1\mu^2 + a_2\mu + a_3)(\mu^3 + b_1\mu^2 + b_2\mu + b_3)$ where

$$\begin{aligned}
a_1 &= 3d_I + m_P + m_{PP} + P^*(r_P + r_{PP}) \\
a_2 &= 3d_I^2 + m_P m_{PP} + r_P P^*(m_{PP} + r_{PP}P^*) + 2d_I(m_P + m_{PP} + r_P P^* + r_{PP}P^*) \\
a_3 &= d_I(d_I + m_{PP})(d_I + m_P + r_{PP}P^*) + d_I(d_I + r_P P^*)r_{PP}P^* \\
b_1 &= 3d_I + m_P + m_{PP} + r_{PP}P^* + 3m_R + r_{PP}P^* \\
b_2 &= 3d_I^2 + m_P(m_{PP} + 2m_R) + m_R(2(m_{PP} + r_{PP}P^*) + 3m_R) + m_P r_P P^* \\
&\quad + r_{PP}P^* m_R(r_P P^*)^3 + 2d_I(m_P + m_{PP} + r_{PP}P^* + 3m_R + r_P P^*) \\
b_3 &= d_I(2m_P m_R + 2r_{PP}P^* m_R + m_{PP}(m_P + 2m_R + r_P P^*) + d_I(d_I + m_P + m_{PP} \\
&\quad + r_{PP}P^* + 3m_R + r_P P^*) + m_R(3m_R + 2r_P P^*)) + m_R(m_P(m_{PP} + m_R) \\
&\quad + (m_{PP} + r_{PP}P^* + m_R)(m_R + r_P P^*)).
\end{aligned}$$

The two third-order polynomials have the properties $a_1, a_3, b_1, b_3 > 0$, $a_1 a_2 - a_3 > 0$ and $b_1 b_2 - b_3 > 0$. So, by the Routh–Hurwitz stability criterion [51, 52], the roots of both polynomials have negative real part. Then,

$$f_2(\mu) = \det[\gamma_4 | \gamma_5]$$

where

$$\gamma_4 = \begin{bmatrix} -r_P P^* - d_I - \mu & m_P \\ r_P P^* & -m_P - r_{PP}P^* - d_I - \mu \\ 0 & r_{PP}P^* \\ n_I\omega & 0 \end{bmatrix}$$

$$\gamma_5 = \begin{bmatrix} 0 & r_I T_S^* \\ m_{PP} & r_I T_{PS}^* \\ -m_{PP} - d_I - \mu & r_I T_{PPS}^* \\ 0 & -r_I(T_S^* + T_{PS}^* + T_{PPS}^*) - d_V - \mu \end{bmatrix}.$$

Computing $f_2(\mu)$ and taking $R^*, P^* \to \infty$, the fourth-order characteristic polynomial can be reduced to a third-order polynomial $\mu^3 + c_1\mu^2 + c_2\mu + c_3$, where

$$\begin{aligned} c_1 &= 3d_I + r_P P^* + r_{PP} P^* + m_P + m_{PP} \\ c_2 &= d_I(3d_I + 2r_P P^* + 2r_{PP} P^* + 2m_P + 2m_{PP}) + m_P m_{PP} + r_P P^*(m_{PP} + r_{PP} P^*) \\ c_3 &= d_I(d_I + m_{PP})(d_I + r_P P^* + m_P) + d_I r_{PP} P^*(d_I + r_P P^*). \end{aligned}$$

The third-order polynomial has the properties $c_1, c_3 > 0$ and $c_1 c_2 - c_3 > 0$. Then, by the Routh–Hurwitz stability criterion [51, 52], the roots of the third-order polynomial all have negative real part. Then,

$$f_3(\mu) = \det[\gamma_6|\gamma_7|\gamma_8|\gamma_9|\gamma_{10}]$$

where

$$\gamma_6 = \begin{bmatrix} -r_P P^* - r_R R^* - d_S - \mu & m_R \\ r_R R^* & -m_R - r_P P^* - r_{RR} R^* - d_S - \mu \\ r_P P^* & 0 \\ 0 & r_P P^* \\ 0 & r_{RR} R^* \\ 0 & 0 \\ 0 & 0 \\ 0 & 0 \\ 0 & 0 \end{bmatrix}$$

$$\gamma_7 = \begin{bmatrix} m_P & 0 \\ 0 & m_P \\ -m_P - r_R R^* - r_{PP} P^* - d_S - \mu & m_R \\ r_R R^* & -m_R - m_P - r_{PP} P^* - r_{RR} R^* - d_S - \mu \\ 0 & 0 \\ r_{PP} P^* & 0 \\ 0 & r_{RR} R^* \\ 0 & r_{PP} P^* \\ 0 & 0 \end{bmatrix}$$

$$\gamma_8 = \begin{bmatrix} 0 & 0 \\ m_{RR} & 0 \\ 0 & m_{PP} \\ 0 & 0 \\ -r_P P^* - m_{RR} - d_S - \mu & 0 \\ 0 & -m_{PP} - r_R R^* - d_S - \mu \\ r_P P^* & 0 \\ 0 & r_R R^* \\ 0 & 0 \end{bmatrix}$$

$$\gamma_9 = \begin{bmatrix} 0 & 0 \\ 0 & 0 \\ 0 & 0 \\ m_{RR} & m_{PP} \\ m_P & 0 \\ 0 & m_R \\ -m_P - r_{PP} P^* - m_{RR} - d_S - \mu & 0 \\ 0 & -m_R - r_{RR} R^* - m_{PP} - d_S - \mu \\ r_{PP} P^* & r_{RR} R^* \end{bmatrix}$$

$$\gamma_{10} = \begin{bmatrix} 0 \\ 0 \\ 0 \\ 0 \\ 0 \\ 0 \\ m_{PP} \\ m_{RR} \\ -m_{PP} - m_{RR} - d_S - \mu \end{bmatrix}.$$

Due to the complexity of $f_3(\mu)$, we examine the sign of the largest root using the LHS/PRCC procedure detailed in 4.1. Here, we varied the parameters of $f_3(\mu)$ through the ranges given in Table 3.1 for 1000 runs. Figure 4.1 demonstrates that the value of the largest root largely sensitive to the death rate of susceptible cells, d_S, and is always negative for these ranges. The LHS of all remaining parameters not shown in Figure 4.1 are approximately uniformly scattered. Thus, the disease-free equilibrium is locally asymptotically stable in the region of viral elimination when $R^*, P^* \to \infty$.

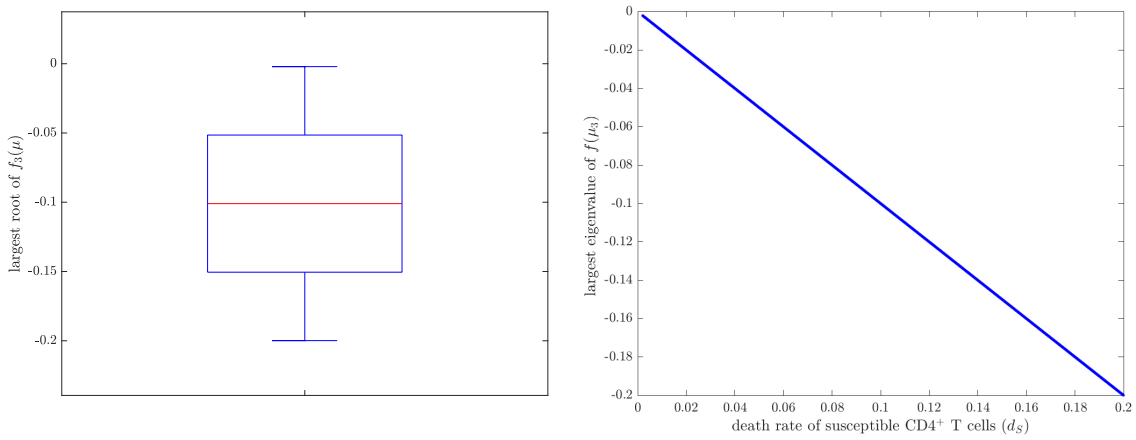

(a) (b)

Figure 4.1: a) Boxplot of LHS values for the largest root of $f_3(\mu)$.
b) The effect of the death rate of susceptible CD4$^+$ cells on the largest eigenvalue of $f_3(\mu)$.

Chapter 5

Determining the Number of Missable and Subsequent Doses

5.1 Region threshold values

To determine the Region 2 threshold, the time for resistance levels to reach a minimum was found. The drug concentration for both the RTIs and PI at this time were evaluated and used as the Region 2 threshold, R_2 and P_2, respectively. Note that, since $T_Y(0) = 0$ during the beginning stages of infection, we have

$$\begin{aligned}\frac{dV_Y}{dt} &= \eta_I\omega(T_Y + T_{PY}) - r_Y(T_S + T_{RS} + T_{PS} + T_{RPS} + T_{PPS} + T_{RPPS}) - d_V V_Y \\ &< 0. \end{aligned} \tag{5.1.1}$$

The resistant viral load is therefore initially decreasing. Since it will not decrease indefinitely, we define t^* to be the time at which viral load reaches a minimum. Thus, we define $R_2 = R(t^*)$ and $P_2 = P(t^*)$.

We define R_1 to be the drug concentration value such that

$$\frac{R_1}{R_1 + IC_{50}} = \frac{R_2}{R_2 + nIC_{50}},$$

where IC_{50} is the half maximal inhibitory concentration and n is the degree of n-fold resistance conferred by the mutation. In this thesis, we consider 10-fold resistance. Hence, $R_1 = 0.1R_2$.

5.2 Number of missable doses

Suppose that the drugs are given at fixed intervals. Let $\tau = t_{k+1} - t_k$ be the time period in between doses for the transcriptase inhibitor and $\phi = s_{n+1} - s_n$ be the time period in between doses for the protease inhibitor (for $k, n \geq 1$). We have

$$\begin{aligned} R(t) =& R(t_k^+)e^{-d_R(t-t_k)}, \ t_k < t \leq t_{k+1} \\ P(t) =& P(s_n^+)e^{-d_P(t-s_n)}, \ s_n < t \leq s_{n+1}. \end{aligned}$$

By definition of impulsive effect, we have the following recurrence relations at the moments of impulse:

$$\begin{aligned} R(t) =& R(t_k^+) + R^i, \ t = t_{k+1} \\ P(t) =& P(s_n^+) + P^i, \ t = s_{n+1}. \end{aligned}$$

From Smith and Wahl [12], for perfect adherence, the points $\frac{R^i e^{-d_R\tau}}{1-e^{-d_R\tau}}$ and $\frac{R^i}{1-e^{-d_R\tau}}$ define the endpoints of an impulsive periodic orbit in the reverse transcriptase drug levels, to which the endpoints of each cycle monotonically increase. Similarly, there is an impulsive periodic orbit in the protease inhibitor drug levels, defined by the endpoints $\frac{P^i e^{-d_P\phi}}{1-e^{-d_P\phi}}$ and $\frac{P^i}{1-e^{-d_P\phi}}$. Thus, under the assumption of perfect adherence, after the k^{th} dose, the reverse transcriptase drug levels satisfy

$$R(t_k^+) = \frac{R^i}{1 - e^{-d_R\tau}}.$$

Suppose that a drug holiday lasts for h successive doses, that is, both drugs are stopped for h doses. Then

$$R(t_{k+h}^-) = \frac{R^i e^{-hd_R\tau}}{1 - e^{-d_R\tau}}.$$

During this interruption, to avoid the emergence of drug-resistant mutations, drug concentrations must remain higher than the Region 2 threshold. Thus, we impose the condition that $R(t_{k+h}^-) > R_2$. So,

$$\frac{R^i e^{-hd_R\tau}}{1 - e^{-d_R\tau}} > R_2,$$

$$\implies e^{-hd_R\tau} > \frac{R_2(1 - e^{-d_R\tau})}{R^i}.$$

Since h and $\frac{R^i}{R_2(1-e^{-d_R\tau})}$ are both positive, the maximum number of missable doses satisfies

$$h < \frac{1}{d_R\tau} \ln\left[\frac{R^i}{R_2(1 - e^{-d_R\tau})}\right]. \tag{5.2.1}$$

Similarly, a protease inhibitor P which is taken for n doses in succession will satisfy

$$P(t_n^+) = \frac{P^i}{1 - e^{-d_P \phi}}.$$

After j missed doses, the condition required to avoid Region 2 is $P_2 < P(t_{n+j}^-)$, giving

$$\begin{aligned} P_2 &< \frac{P^i e^{-j d_P \phi}}{1 - e^{-d_P \phi}}, \\ j &< \frac{1}{d_P \phi} \ln \left[\frac{P^i}{P_2(1 - e^{-d_P \phi})} \right]. \end{aligned}$$

Resistance cannot emerge until *both* drugs are in their respective Region 2. However, both drugs may not be stopped at the same time. Reverse transcriptase inhibitors can be taken once, twice or three times a day, whereas protease inhibitors are only taken once or twice a day. Here, we are assuming that drugs are taken in sync, so that if one drug is taken once a day, and one is taken three times a day, then there will only be three distinct pill events, one of which will involve two drugs. Thus, results will depend on when the drug holiday actually begins. Let

$$h^* = \frac{1}{d_R \tau} \ln \left[\frac{R^i}{R_2(1 - e^{-d_R \tau})} \right]$$

and

$$j^* = \frac{1}{d_P \phi} \ln \left[\frac{P^i}{P_2(1 - e^{-d_P \phi})} \right].$$

We examine the following cases:

(i) If both drugs are taken at the same frequency, then the maximum length of a drug holiday is $\max\{h^*, j^*\}$.

(ii) If $\tau = 1$ and $\phi = 1/2$, there are two possibilities. If both drugs are stopped at the same time, then the maximal drug holiday would last for $\max\{h^*, j^*\}$. If the PI is stopped after the RTI, then the drug holiday could last for $\max\{h^* - \phi, j^*\}$.

(iii) When $\tau = 1/2$ and $\phi = 1$, we have two possibilities. If both drugs are stopped at the same time, then the longest a drug holiday could last is $\max\{h^*, j^*\}$. If the PI is stopped before the RTI, the maximal drug holiday is $\max\{h^*, j^* - \tau\}$.

Table 5.1: Lengths of maximal drug holiday. These cases describe the length of time for the second drug in the combination to reach its Region 2 threshold, depending on when each drug is stopped.

ϕ \ τ	1	$\frac{1}{2}$	$\frac{1}{3}$
1	$\max\{h^*, j^*\}$	$\max\{h^*, j^*\}$ or $\max\{h^*, j^* - \tau\}$	$\max\{h^*, j^*\}$ or $\max\{h^*, j^* - \tau\}$ or $\max\{h^*, j^* - 2\tau\}$
$\frac{1}{2}$	$\max\{h^*, j^*\}$ $\max\{h^* - \phi, j^*\}$	$\max\{h^*, j^*\}$	$\max\{h^*, j^*\}$ or $\max\{h^*, j^* - \tau\}$

(iv) If $\tau = 1/3$ and $\phi = 1$, there are three different possibilities. If both drugs are stopped at the same time, then the condition is $\max\{h^*, j^*\}$. If the RTI is taken once after stopping the PI, then the condition is $\max\{h^*, j^* - \tau\}$, whereas if the RTI was taken twice after stopping the PI, then the condition is $\max\{h^*, j^* - 2\tau\}$.

(v) For $\tau = 1/3$ and $\phi = 1/2$, there are two possibilities. If both drugs are stopped at the same time, then the longest a drug holiday could last is $\max\{h^*, j^*\}$. If the RTI is taken once after stopping the PI, then the condition is $\max\{h^*, j^* - \tau\}$.

These conditions are summarized in Table 5.1.

5.3 Number of subsequent doses

Following the h missed doses of the RTI, a subsequent q doses must be taken in succession to ensure that viral replication remains low. In order to return to a drug concentration approximating pre-interruption levels, we need

$$R(t^-_{k+h+q}) > \frac{R^i e^{-d_R \tau}}{1 - e^{-d_R \tau}} - \epsilon \tag{5.3.1}$$

for some required level of tolerance $\epsilon > 0$. Using impulsive theory:

$$R(t^+_{k+h}) = R^i + \frac{R^i e^{-h d_R \tau}}{1 - e^{-d_R \tau}}$$

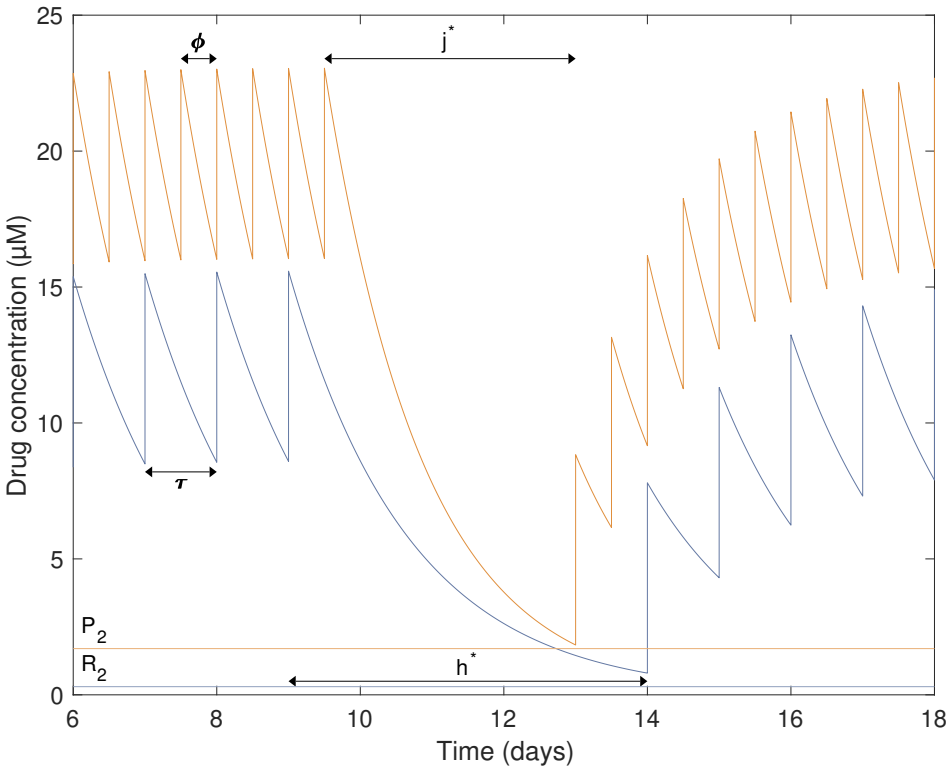

Figure 5.1: Illustrative example of Table 5.1. Here, $\tau = 1$ is the RTI dosing interval, and R_2 represents the Region 2 threshold of the RTI. Similarly, $\phi = \frac{1}{2}$ represents the PI dosing interval, and P_2 is the Region 2 threshold of the PI. h^* and j^* are the maximal number of doses able to be missed during a drug holiday for the RTI and PI, respectively. Since the PI is stopped after the RTI, the maximal drug holiday would last for $\max\{h^* - \phi, j^*\}$ doses.

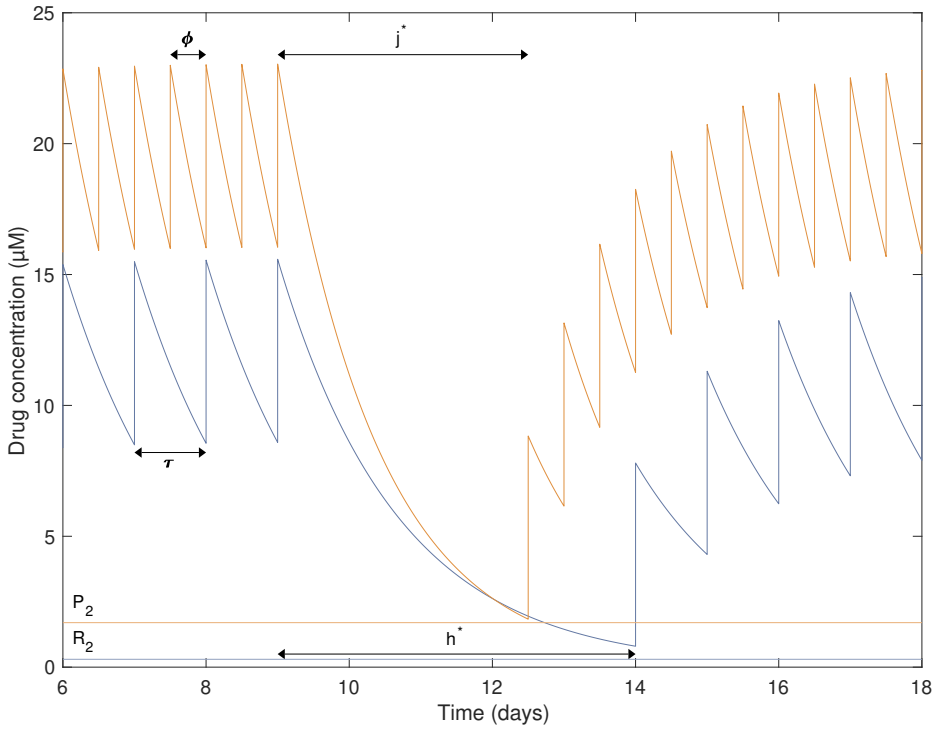

Figure 5.2: Another illustrative example of Table 5.1. Here, $\tau = 1$ is the RTI dosing interval, and R_2 represents the Region 2 threshold of the RTI. Similarly, $\phi = \frac{1}{2}$ represents the PI dosing interval, and P_2 is the Region 2 threshold of the PI. h^* and j^* are the maximal number of doses able to be missed during a drug holiday for the RTI and PI, respectively. Since both drugs are stopped at the same time, the maximal drug holiday would last for $\max\{h^*, j^*\}$ doses.

$$
\begin{aligned}
R(t^-_{k+h+1}) &= R^i e^{-d_R\tau}\left[1+\frac{e^{-hd_R\tau}}{1-e^{-d_R\tau}}\right]\\
R(t^+_{k+h+1}) &= R^i\left[1+e^{-d_R\tau}+\frac{e^{-(h+1)d_R\tau}}{1-e^{-d_R\tau}}\right]\\
R(t^-_{k+h+2}) &= R^i e^{-d_R\tau}\left[1+e^{-d_R\tau}+\frac{e^{-(h+1)d_R\tau}}{1-e^{-d_R\tau}}\right]\\
&\vdots\\
R(t^-_{k+h+q}) &= R^i e^{-d_R\tau}\left[1+\ldots+e^{-(q-1)d_R\tau}+\frac{e^{-(h+q-1)d_R\tau}}{1-e^{-d_R\tau}}\right]\\
&= R^i e^{-d_R\tau}\left[\frac{1-e^{-qd_R\tau}}{1-e^{-d_R\tau}}+\frac{e^{-(h+q-1)d_R\tau}}{1-e^{-d_R\tau}}\right].
\end{aligned}
$$

Hence,

$$
\begin{aligned}
R(t^-_{k+h+q})-\frac{R^i e^{-d_R\tau}}{1-e^{-d_R\tau}} &= \frac{R^i e^{-(q+1)d_R\tau}(e^{-(h-1)d_R\tau}-1)}{1-e^{-d_R\tau}} > -\epsilon\\
&\implies \frac{R^i e^{-(q+1)d_R\tau}(1-e^{-(h-1)d_R\tau})}{1-e^{-d_R\tau}} < \epsilon.
\end{aligned}
$$

Thus, from (5.3.1), the minimum number of doses to return to within ϵ of perfect adherence satisfies

$$
q > \frac{1}{d_R\tau}\ln\left[\frac{R^i(1-e^{-(h-1)d_R\tau})}{\epsilon(1-e^{-d_R\tau})}\right]-1. \tag{5.3.2}
$$

Following these q doses, a patient could safely begin another drug holiday, without the emergence of significant drug resistance. Analogously, the PI for which n doses were taken, j doses missed and then v subsequent doses with

$$
v > \frac{1}{d_P\tau}\ln\left[\frac{P^i(1-e^{-(j-1)d_P\phi})}{\epsilon(1-e^{-d_P\phi})}\right]-1 \tag{5.3.3}
$$

must be taken to return to within ϵ of perfect adherence. Hence the minimum number of days for which therapy must be resumed following a drug holiday satisfies

$$
\max\left\{\frac{1}{d_R\tau}\ln\left[\frac{R^i(1-e^{-(h-1)d_R\tau})}{\epsilon(1-e^{-d_R\tau})}\right]-1,\frac{1}{d_P\tau}\ln\left[\frac{P^i(1-e^{-(j-1)d_P\phi})}{\epsilon(1-e^{-d_P\phi})}\right]-1\right\}.
$$

5.4 Numerical results

5.4.1 Numerical methods

The software used to plot the figures in the following sections is MATLAB version 2020a. To solve the system of ordinary differential equations outlined in model (3.3.1),

ode45 was used, along with the initial conditions and sample parameter values outlined in Tables 3.1 and 3.2. The ode45 function implements the Dormand–Prince algorithm, which is an explicit Runge–Kutta method with an adaptive time step. It is a fifth-order method, with a fourth-order error companion method.

It has seven stages, but only uses six function evaluations per step because it employs the FSAL (First Same As Last) property: the first stage is evaluated at the same point as the last stage of the previous successful step. The coefficients of the remaining function evaluations were chosen to minimize the error of the fifth-order solution. The Butcher tableau is:

0							
1/5	1/5						
3/10	3/40	9/40					
4/5	44/45	−56/15	32/9				
8/9	19372/6561	−253602187	64448/6561	−212/729			
1	9017/3168	−355/33	46732/5247	49/176	−5103/18656		
1	35/384	0	500/1113	125/192	−2187/6784	11/84	
	35/384	0	500/1113	125/192	−2187/6784	11/84	0
	5179/57600	0	7571/16695	393/640	−92097/339200	187/2100	1/40

The first row of coefficients gives the fifth-order solution, whereas the second row gives an fourth-order solution; when subtracted from the first solution, it yields the error estimate. If this estimate is below the prescribed error tolerance, the step is successful. Otherwise, the step size is reduced and the process repeats.

5.4.2 Pharmacokinetic implications

The length of time that combination therapy can be halted for was calculated (see Table 5.3), as well as the subsequent schedule of doses that must be taken after such a holiday. The pharmacokinetic data used to calculate drug holiday length is summarized in Table 5.2. The exact length of the drug holiday depends on whether the NRTI and PI are stopped at the same time or asynchronously, as outlined in Table 5.1. Estimates are calculated for all triple-drug regimens recommended for use as first-line or second-line regimens in the World Health Organization's 2019 antiretroviral guidelines [56]. Note that only WHO-approved regimens that consist of NRTI and PI combinations are being considered in our numerical results; however, the model can also be used to study NNRTI and PI regimens or FI and PI regimens, as the mechanism of action of NRTIs, NNRTIs and FIs all function in similar ways. Table 5.1 assumes 10-fold resistance. The minimum value between h^* and j^* can be interpreted as the lower bound of the number of missable doses, as this is the length of time for the first drug in the regimen to reach its Region 2 threshold. After this, triple-drug therapy is reduced to dual therapy. These estimates were calculated

conservatively; for example, the number of missable doses for the co-formulation of Abacavir and Lamivudine (ABC+3TC) was 5.723 when taken in combination with both Darunavir boosted with ritonavir (DRV/r), while the number of subsequent doses was 14.401, so this translates to four missable and 15 subsequent doses.

Table 5.2: Summary of pharmacokinetic data for all FDA-approved reverse transcriptase inhibitors, and boosted protease inhibitors.

Class	Reverse Transcriptase Inhibitor	Dose amount R^i or P^i (μM)	Dosing interval τ (days^{-1})	Half-life $t_{1/2}$ (hours)	IC_{50} (μM)
NRTI	Abacavir (ABC)	10.12	2	21.0	0.0381
	Emtricitabine (FTC)	7.28	1	39.0	0.0079
	Lamivudine (3TC)	6.12	2	10.7	0.0298
	Tenofovir disoproxil fumarate (TDF)	1.18	1	60.0	0.0561
	Zidovudine (AZT)	4.34	2	8.5	0.1823
PI[1]	Atazanavir (ATV/r)	6.27	1	8.6	0.0150
	Darunavir (DRV/r)	13.49	2	15.0	0.0265
	Lopinavir (LPV/r)	15.58	2	9.9	0.0380

[1] Protease inhibitors are never taken without being boosted with one of the following pharmacokinetic enhancers: ritonavir(r) or cobistat (COBI).

To illustrate the effect of exceeding the recommendations in Table 5.3, consider a patient taking TDF+FTC+DRV/r. When taken concomitantly with DRV/r, TDF and FTC (co-formulated as Truvada) can be stopped for a maximum of five doses (corresponding to five days), while DRV/r can be stopped for a maximum of four doses (corresponding to four days). If both the NRTIs and the PI are all stopped at the same time, then the maximum length of a drug holiday is five days. Figures 5.3 and 5.4 demonstrate the effects of missing four and five doses, respectively. In both cases, the wild-type and mutant strains remain controlled. Even though DRV/r reaches its Region 2 threshold after 4 doses, the NRTI levels remain high enough

Table 5.3: Summary of results for all NRTI–PI drug combinations recommended by the World Health Organization's 2019 antiretroviral guidelines. The second column represents the number of doses the RTI can miss, whereas the penultimate column shows the number of doses that may be missed for the PI. The exact number of missable doses for each combination will depend on whether the drugs are stopped concomitantly or at different times. The final column shows the number of successive doses for which doses must be taken after the drug holiday, to be within a 1% tolerance of perfect adherence.

Regimen	h^*	j^*	Number of subsequent doses
ABC + 3TC + ATV/r [1]	2	1	14
ABC + 3TC + DRV/r [1]	5	5	15
ABC + 3TC + LPV/r [1]	2	2	14
AZT + 3TC + ATV/r [2]	2	2	7
AZT + 3TC + DRV/r [2]	3	5	14
AZT + 3TC + LPV/r [2]	3	2	9
TDF + 3TC + ATV/r [3]	2	2	5
TDF + 3TC + DRV/r [3]	2	5	14
TDF + 3TC + LPV/r [3]	2	3	9
TDF + FTC + ATV/r [4]	3	2	17
TDF + FTC + DRV/r [4]	5	4	18
TDF + FTC + LPV/r [4]	4	3	17

[1] ABC + 3TC are co-formulated as Epizcom, taken once daily
[2] AZT + 3TC are co-formulated as Combivir, taken twice daily
[3] TDF + 3TC are co-formulated as Cimduo, taken once daily
[4] TDF + FTC are co-formulated as Truvada, taken once daily.

to control viral load, even though the regimen has been reduced from triple to dual therapy. Figure 5.5 demonstrates the virologic cost of exceeding drug-holiday length recommendations. Here, as six doses were missed and both the NRTIs and the PI reach their Region 2 threshold, there is a spike in mutant virions. Since perfect adherence quickly resumes after the additional missed dose, the viral load is quickly eliminated.

The WHO strongly recommends that first-line ART for adults and adolescents should consist of two nucleoside/nucleotide reverse transcriptase inhibitors and a third agent from another drug class (an integrase strand transfer inhibitor (INSTI), protease inhibitor, or non-nucleoside reverse transcriptase inhibitor). The standard regimen for adults initiating ART includes two NRTIs, as well the INSTI, dolutegravir. A

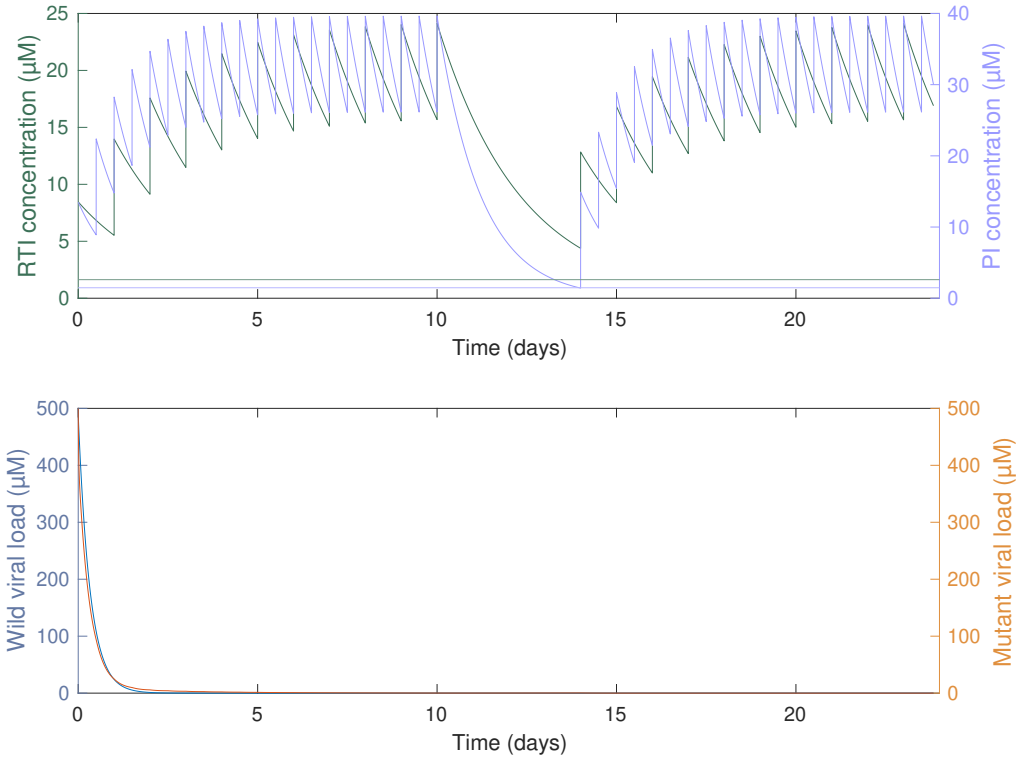

Figure 5.3: The regimen TDF + FTC + DRV/r when four doses are missed.

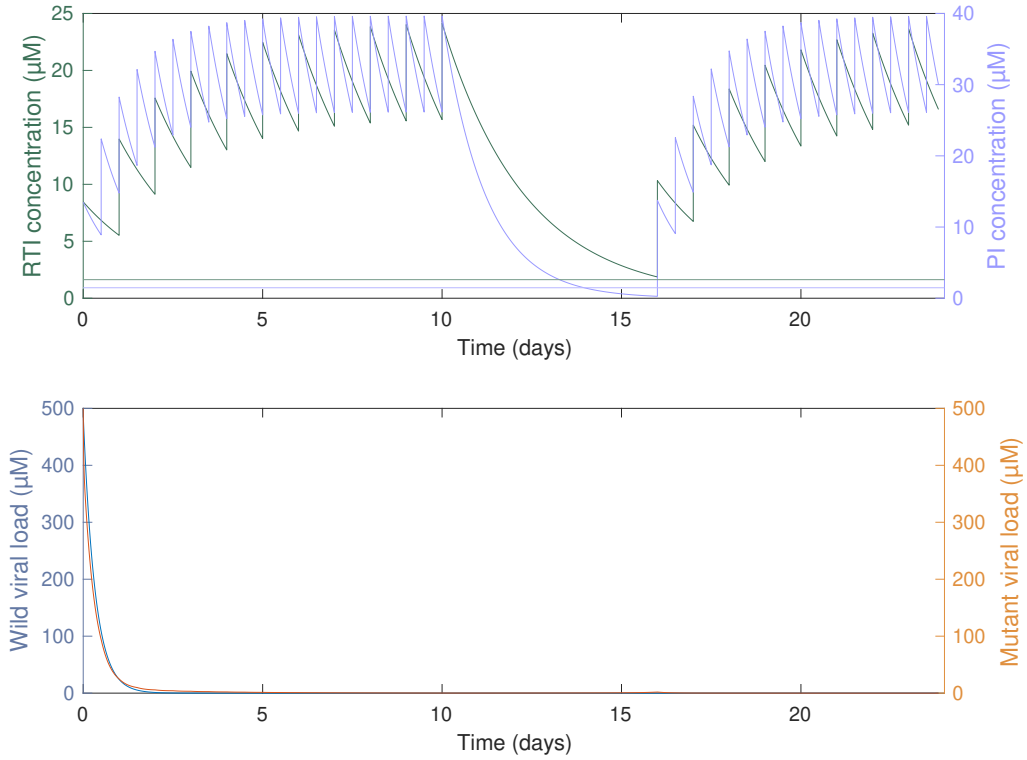

Figure 5.4: The regimen TDF + FTC + DRV/r when five doses are missed.

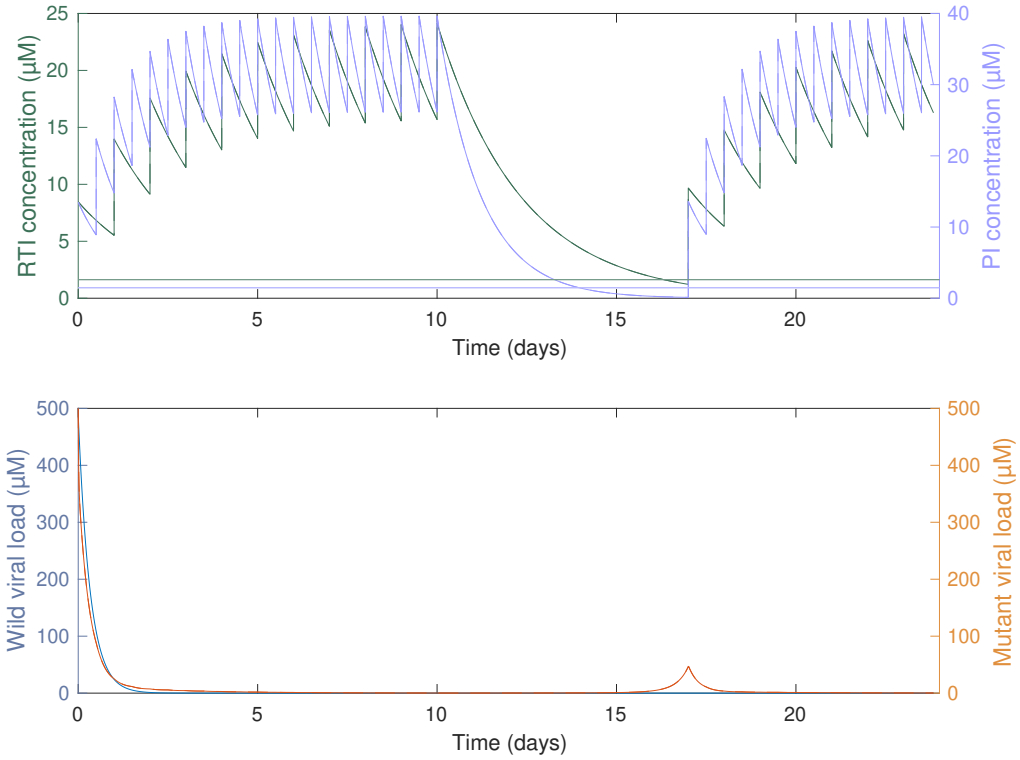

Figure 5.5: The regimen TDF + FTC + DRV/r when six doses are missed.

summary of all recommended regimens by population can be found in Table 5.4. If this preferred regimen is not available or suitable because of toxicities, drug–drug interactions, drug-resistance mutations or drug-procurement issues, then a boosted PI-regimen is preferred over the use of an NNRTI, especially in low-income countries. Currently, pre-treatment drug resistance (PDR) is largely being driven by the use of the NNRTIs efavirenz and nevirapine [6]. As individualized treatment plans based on genotypic resistance testing are not available in many low-income countries, NNRTI-based ART regimens are not recommended in countries with national estimates of PDR exceeding 10%. The 2019 antiretroviral drug-resistance report [6] by the WHO reported that PDR has already exceeded the 10% limit in 66% of the countries surveyed, and this number has been steadily trending higher in recent years. In the case of a failing first-line regimen (repeated HIV RNA values above 50 copies per mL), the preferred second-line regimen by population is summarized in Table 5.5.

5.5 Comparison with clinical results

A number of studies have attempted to characterize the safety of structured treatment interruptions (STIs), including two large-scale trials: the SMART trial and the Trivacan study. The SMART trial [57] examined episodic ART guided by the $CD4^+$ T cell count. The study protocol called for the deferral of therapy until $CD4^+$ T cell count decreased to less than 250 per cubic millimetre. Patient follow-ups that determined whether therapy should be resumed occurred every two months during the first year, and every four months in the second year. The Trivacan study [58] compared continuous ART to timed STIs consisting of two months off and four months on therapy. Both studies were halted prematurely after two years due to a significantly greater risk of opportunistic infections or deaths in those who were assigned to receive interrupted therapy. The Trivacan study also noted that the STIs led to an unacceptably high risk of selecting for a drug-resistant strain of the virus. However, it should be noted that these two trials involved lengthy periods of treatment interruption, of the order of months, whereas our results recommend significantly shorter periods of treatment interruption, of the order of days. Furthermore, our results predict significant increase in the drug-resistant strain if these periods are exceeded, which is consistent with the results from the majority of trials.

Recently, smaller studies looking at shorter treatment interruptions have shown encouraging results. The ANRS 162-4D trial [59] studied STIs in in virologically controlled HIV-1-infected adults. The study protocol consisted of following a given regimen for four consecutive days per week followed by a three-day drug interruption. Prior to the study, patients were taking either two NRTIs with a boosted PI or two NRTIs with an NNRTI and had undetectable viral loads for at least 12 months prior to the study. In the PI arm, there was an observed success rate of 93% of patients. The patients who experienced virologic failure were on ABC+ 3TC + ATV/r or ABC

+ 3TC + LPV/r. These results are in line with our findings: several regimens can tolerate 3 days off therapy; however, the two aforementioned regimens would not.

The FOTO [60] study (five-days-on, two-days-off treatment) also investigated a short-cycle treatment interruption strategy. Patients were on five consecutive days on treatment (typically Monday through Friday) followed by two days off treatment. In the PI-based arm, the 48 week as-treated analysis revealed that virologic suppression was maintained in 78% of patients. Participants adhered well and expressed a strong preference for the FOTO treatment schedule compared to continuous ART. These findings are pursuant to our results: all regimens studied here except for AZT+3TC+ATV/r and AZT+3TC+LPV/r, would tolerate two days off therapy. Continuous and affordable ART is a key factor in maintaining adherence: a FOTO treatment scheme would reduce the cost of antiretroviral therapy by 29%. In Canada, the price for first regimens is approximately $15 000 per year, with costs only increasing for second-line and pediatric regimens, and none of Canada's publicly funded drug plans provide universal coverage of all prescription drugs [61]. A FOTO treatment schedule would reduce costs to $10 650 per year, for a savings of $4350 per year.

5.6 Patterns of adherence

Maintaining strong adherence may be particularly difficult when the drug regimen has a complex dosing schedule or overwhelming side effects, as is often the case with ART. While long-term average adherence is typically a good indicator of long-term treatment prognosis, it should be noted that different patterns of adherence may result in different viral responses, even within the same adherence strata. To illustrate, suppose that a patient misses i doses among the last n. If the i doses were missed in succession, this could shift the balance in favour of one strain of the virus, compared to missing the same number of doses intermittently throughout the same period of time. A schematic representation of these two patterns is shown in Figure 5.6.

Several studies using the Medication Event Monitoring System demonstrated that consecutive interruptions may have increased levels of detectable HIV-RNA compared to the same number of intermittent missed doses [62, 63]. Both studies examined the relationship between patterns of adherence within varying adherence strata and concluded that sustained treatment interruptions more accurately predicted viral rebound than interspersed missed doses for patients following a PI-based ART regimen.

Since many patients are known to be between 70 and 80% adherent [2,64], Figures 5.7–5.9 show three randomly generated viral responses to a patient who is 75% adherent to the regimen 3TC+FTC+ATV/r. Here, both drugs were taken with perfect adherence until concentrations reached the upper endpoint of the impulsive periodic endpoint; thereafter, a dose was taken 75% percent of the time. We assume that a

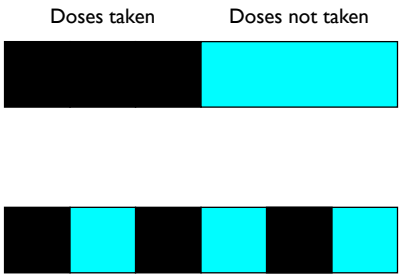

Figure 5.6: Two different drug-taking patterns with the same proportion of adherence: black represents drugs taken, while blue represents missed doses. The top figure depicts a pattern in which 50% of the doses are missed in succession. The bottom figure illustrates the same number of doses missed, but in an equally spaced, yet nonconsecutive manner.

patient misses both drugs if a dose is not taken. In Figure 5.7, a patient misses doses intermittently; however, neither drug is stopped long enough to reach its Region 2 threshold, so the viral load remains controlled. Although there is a spike in mutant virions, this is the best viral outcome of the three outcomes. In Figure 5.8, doses are missed consecutively, with good adherence before and after the missed doses. Since both drugs fall below their Region 2 threshold, there is a large spike in mutant virions that eventually dissipates as drug concentrations increase to pre-interruption levels. Figure 5.9 demonstrates the worst-case virologic response to 75% adherence: the doses are missed intermittently but drug levels also fall into Region 2 multiple times. This not only allows the mutant virus to dominate, but it remains difficult to control, even after adherence improves. This figure demonstrates not only the cost of exceeding the recommended drug holiday length, but also the importance of resuming therapy for the minimum number of subsequent doses outlined in Table 5.3.

To maintain complete viral suppression, adherence levels higher than 75% are required [65]. A recent study looking at the adherence level necessary for viral suppression varied according to the regimen type [65]. For PI-based ART, an average adherence of 87% was necessary for viral suppression; 75% and 78% adherence was required for INSTI-based and NNRTI-based regimens, respectively. This may explain the rapid viral rebound in Figures 5.7–5.9.

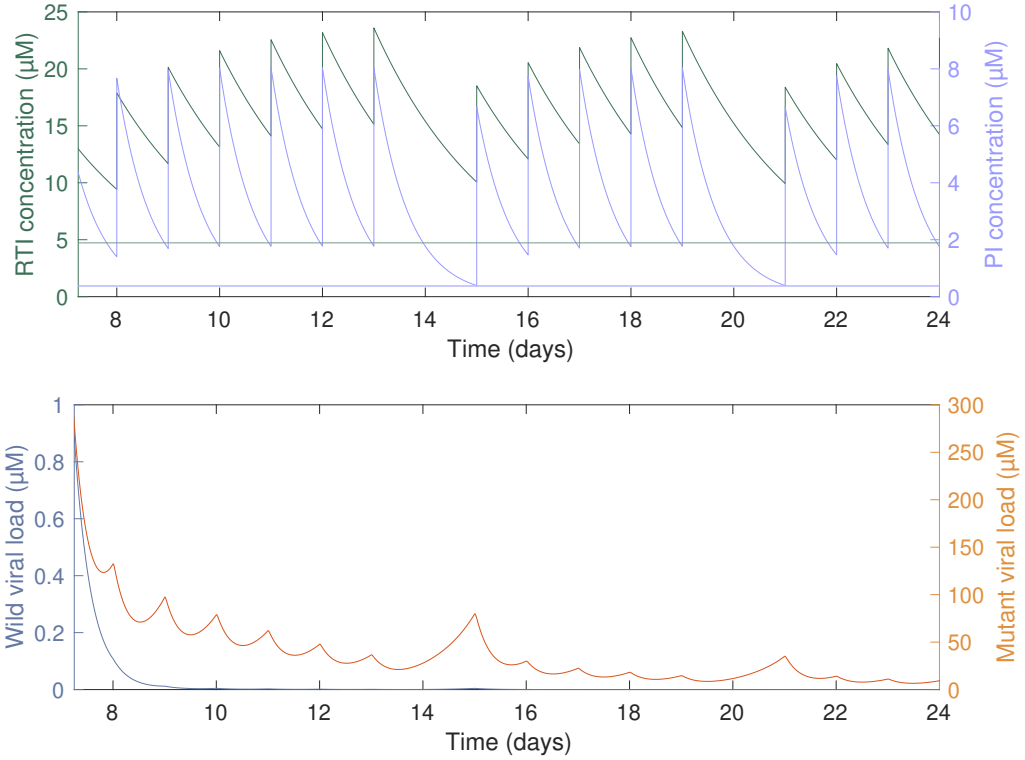

Figure 5.7: Randomly generated viral response to patient who is 75% adherent. Between days 1 and 6, doses were taken with perfect adherence. Days 7 to 24 are shown to illustrate one of the three possible viral responses. Here, the doses are missed intermittently. While there is a small increase in mutant virions, since both drugs never reach their Region 2 thresholds at the same time, the increase in mutant-virion concentration is negligible and quickly eliminated.

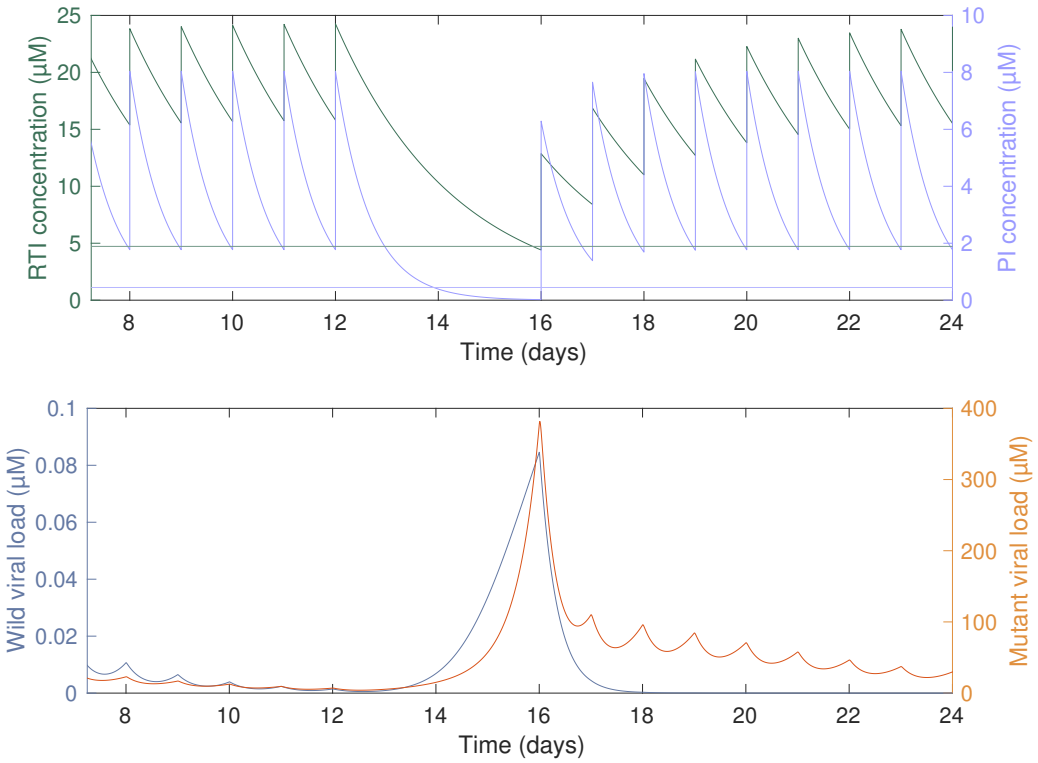

Figure 5.8: Randomly generated viral response to a patient 75% adherent. Between days 1 and 6, doses were taken with perfect adherence. Days 7 to 24 are shown to illustrate one of the three possible viral responses. Here, doses are missed consecutively. There is a spike in mutant virions but is quickly controlled over the following 10 days as perfect adherence is resumed.

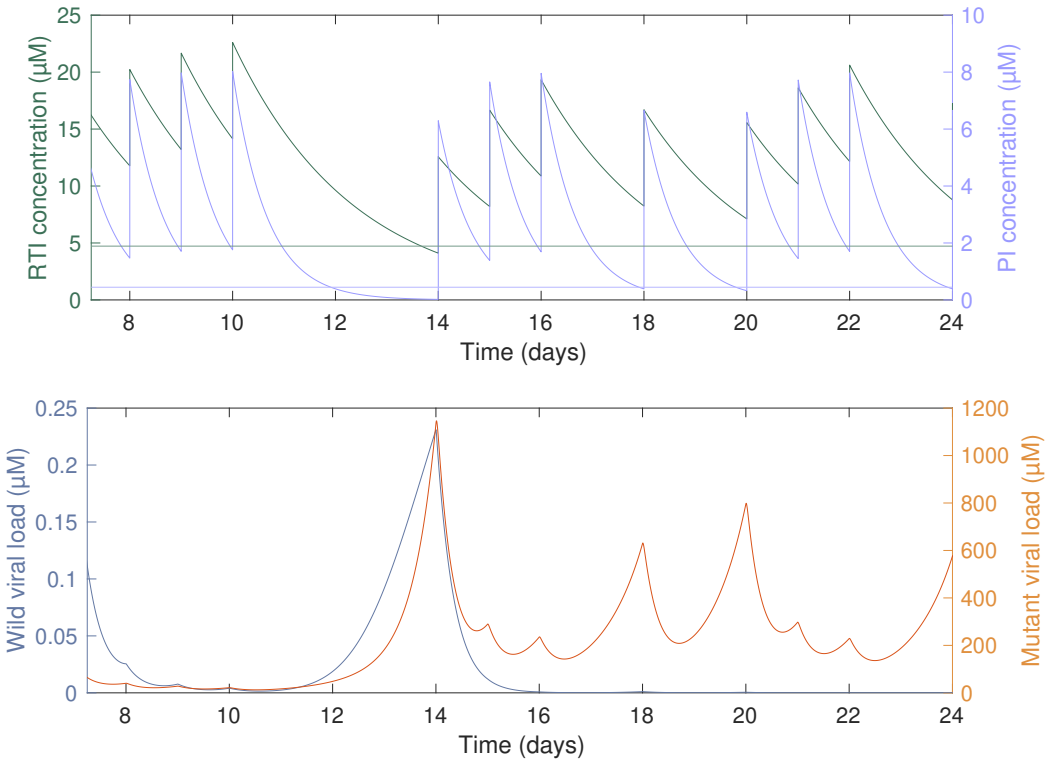

Figure 5.9: Randomly generated viral response to patient who is 75% adherent. Between days 1 and 6, doses were taken with perfect adherence. Days 7 to 24 are shown to illustrate one of the three possible viral responses. Here, doses are missed sporadically. Since both drugs reach their Region 2 threshold during the first block of missed doses, there is a large spike in mutant virions that is difficult to control.

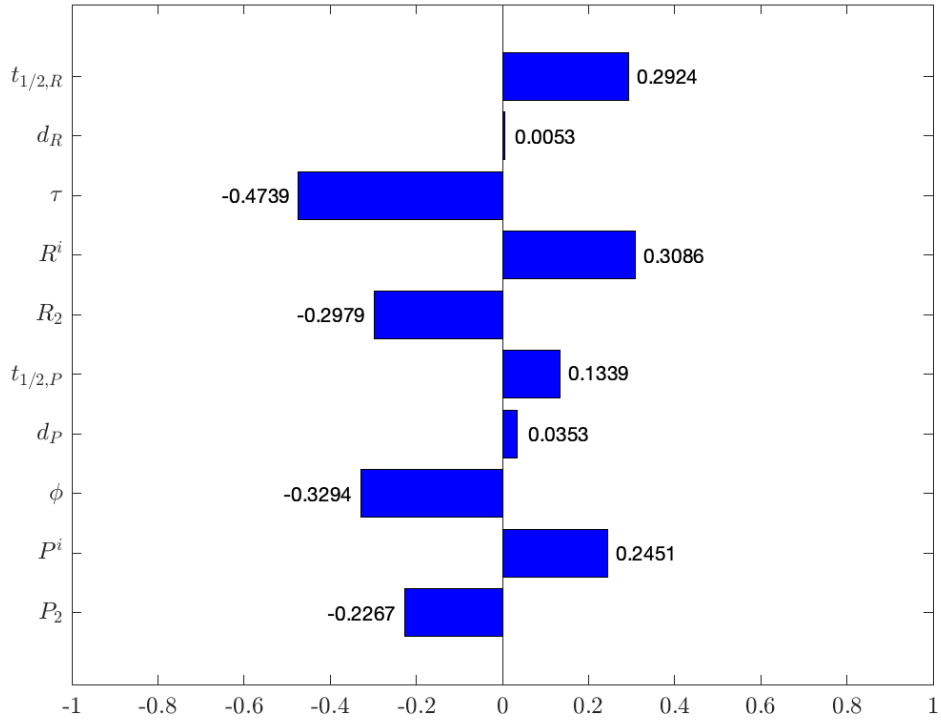

Figure 5.10: Partial rank correlation coefficients for the maximum number of missable doses for all parameters.

5.7 Sensitivity to variations

Heterogeneity in the response to different antiretroviral drugs can be attributed to metabolic, behavioural and immunologic differences among patients. To examine the effect of these differences, we explore the sensitivity of each parameter on the maximal number of missable doses and R_0 using LHS.

Figure 5.10 shows the PRCC sensitivity analysis on the number of missable doses for 1000 runs. All relevant parameters are varied against the maximum number of missable doses; here, we are assuming both drugs are stopped at the same time, so the number of missable doses is given by $\max\{h^*, j^*\}$. The range of uncertainty, units and references for all parameters can be found in Table 3.1.

The maximum number of missable doses is most sensitive to the time between doses, τ, ϕ. Figure 5.11 shows that decreasing the time between doses or decreasing the Region 2 thresholds will lower the maximum number of missable doses. However, as seen in Figure 5.10, longer drug half-lives $t_{1/2,R}$, $t_{1/2,P}$, as well as increasing drug

dosage amounts will slightly increase the length of drug holidays. Drug decay rates for the NRTI and PI do not have a large impact, and their LHS plots are approximately uniformly distributed.

Figures 5.12a, 5.13a and Figure 5.14 show the PRCC sensitivity analysis for Regions 1, 2 and 3, respectively. All relevant parameters are varied against the R_0 of each region for the ranges given in Table 3.1. PRCC and LHS analysis was performed using 1000 runs for $R_{0,1}$ and $R_{0,2}$, and 250 runs for $R_{0,3}$ (due to MATLAB memory constraints). In all three regions, R_0 is most sensitive to the number of infectious virions produced per day by an infected $CD4^+$ T cell, $n_I\omega$ and the death rate of infected $CD4^+$ T cells, d_I. The effects of $n_I\omega$ on R_0 can be seen in Figures 5.12b, 5.13c and 5.15a, whereas the effect of d_I can be seen in Figures 5.12c, 5.13c and 5.15b. In Region 3, $R_{0,3}$ is also sensitive to the death rate of the virus, d_V and $CD4^+$ T cell infection rate of the mutant virus, r_Y, as shown in Figures 5.15d and 5.15c. All other parameters not pictured in Figures 5.12, 5.13 and 5.15 are approximately uniformly distributed.

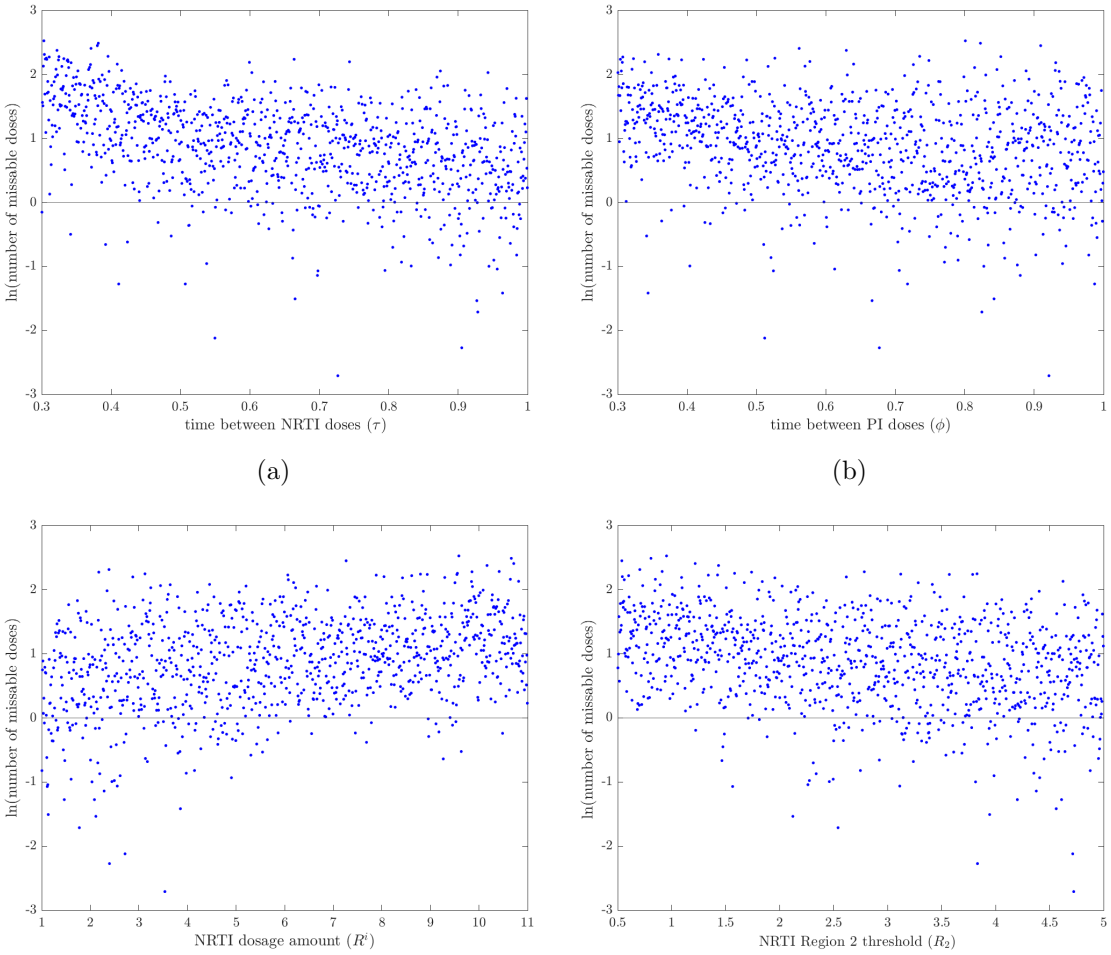

Figure 5.11: Sensitivity analysis for the maximal number of missable doses. (a) The effect of time between NRTI doses on the maximum number of missable doses. (b) The effect of time between PI doses on the maximum number of missable doses. (c) The effect of NTRI dosage amount on the maximum number of missable doses. (d) The effect of the NRTI Region 2 threshold on the maximum number of missable doses.

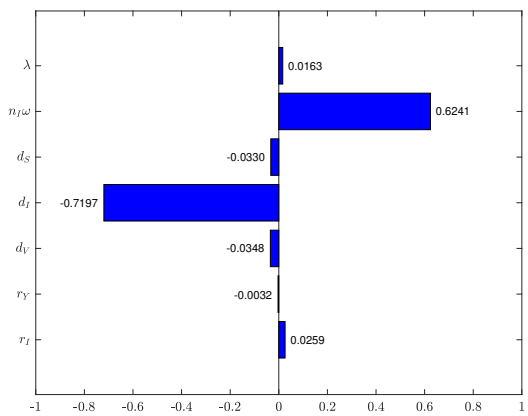

(a)

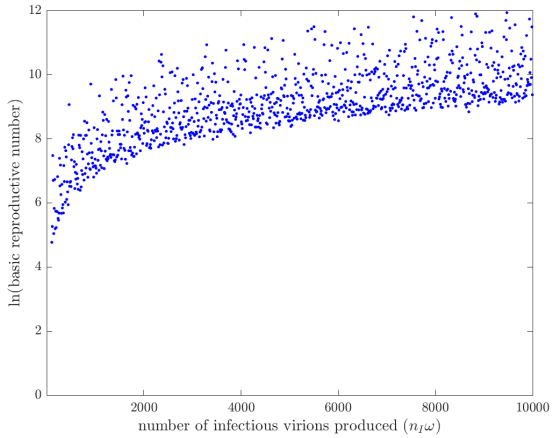

(b)

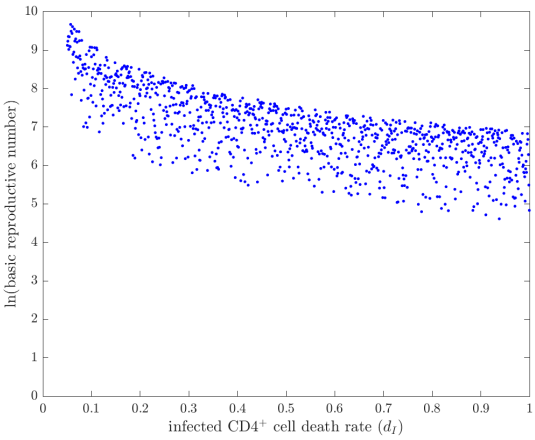

(c)

Figure 5.12: Sensitivity analysis for Region 1. (a) Partial rank correlation coefficients for $R_{0,1}$ for all parameters. (b) The effect of the number of infectious virions produced per day from an infected CD4$^+$ T cell on $R_{0,1}$. (c) The effect of the death rate of infected CD4$^+$ T cells on $R_{0,1}$.

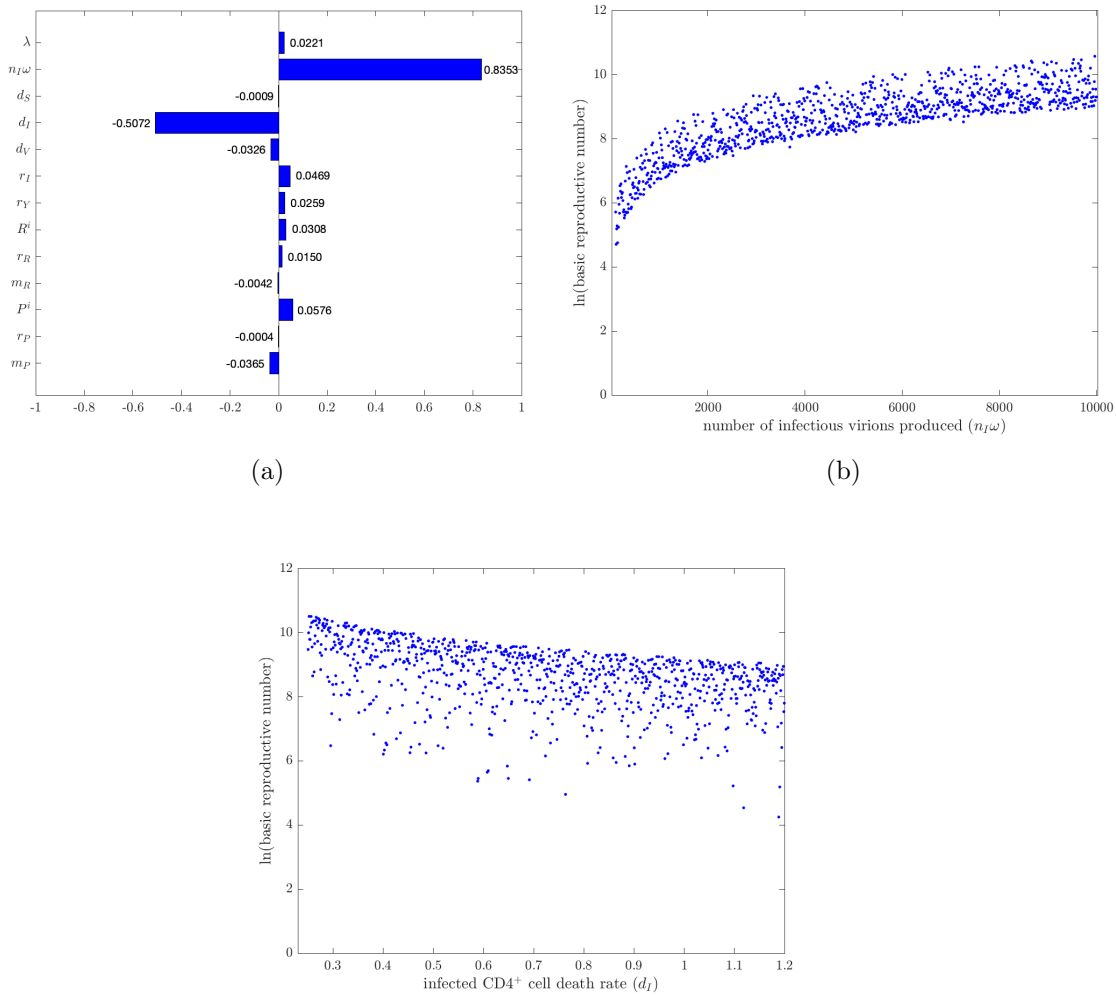

Figure 5.13: Sensitivity analysis for Region 2. (a) Partial rank correlation coefficients for $R_{0,2}$ for all parameters. (b) The effect of the number of infectious virions produced per day from an infected CD4$^+$ T cell on $R_{0,2}$. (c) The effect of the death rate of infected CD4$^+$ T cells on $R_{0,2}$.

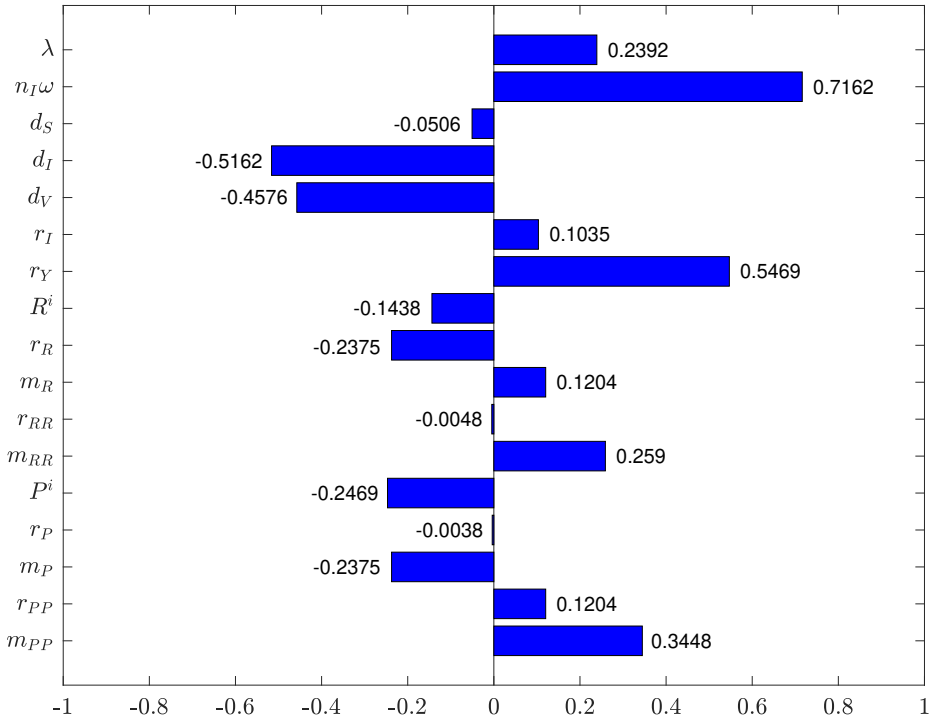

Figure 5.14: Partial rank correlation coefficients for $R_{0,3}$ for all parameters.

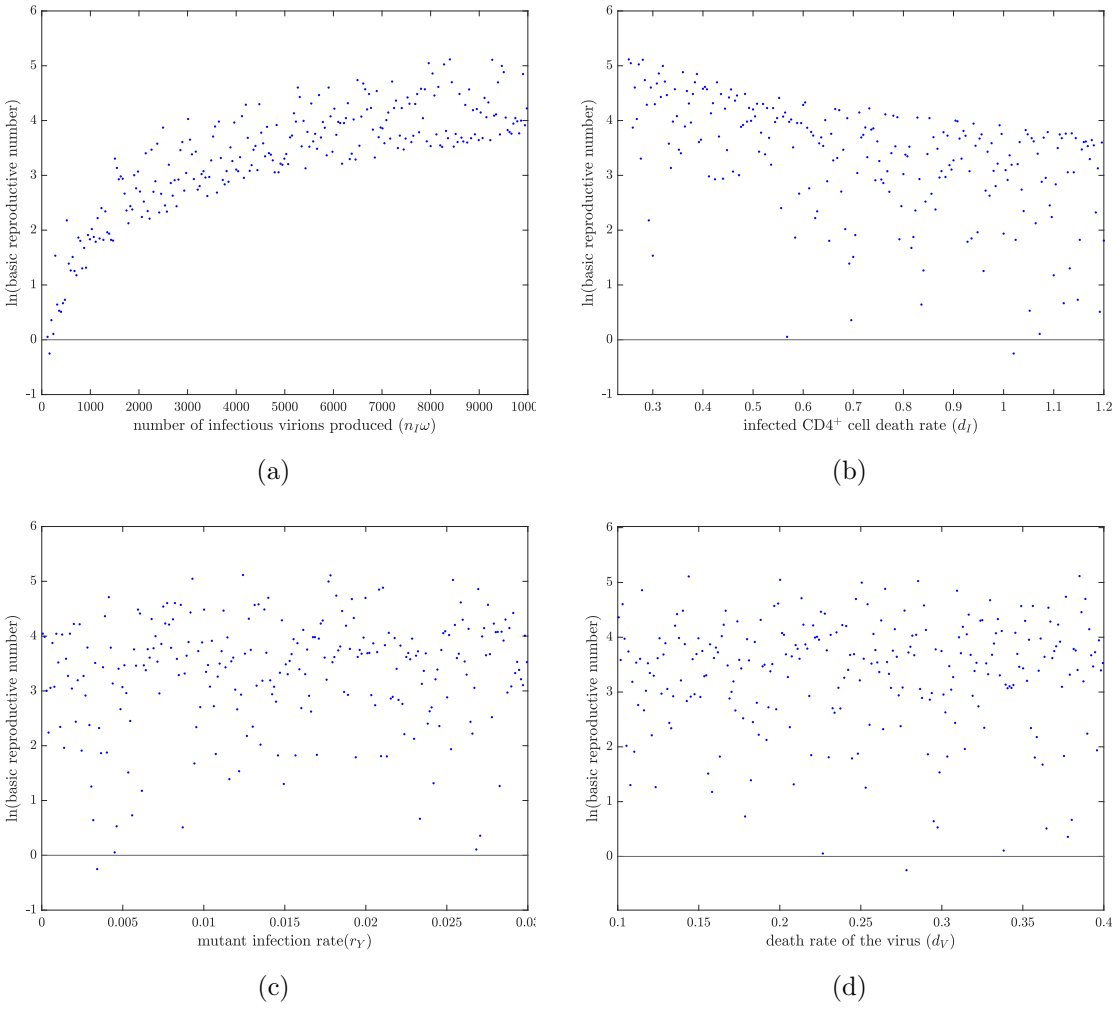

Figure 5.15: Sensitivity analysis for Region 3. (a) The effect of the number of infectious virions produced per day from an infected CD4$^+$ T cell on $R_{0,3}$. (b) The effect of the death rate of infected CD4$^+$ T cells on $R_{0,3}$. (c) The effect of the mutant infection rate on $R_{0,3}$. (d) The effect of the death rate of the virus on $R_{0,3}$.

Table 5.4: Recommended first-line regimens by population as outlined in the World Health Organization's 2019 clinical guidelines for antiretroviral therapy [56]. 3TC: lamivudine; ABC: abacavir; ATV/r: atazanavir boosted with ritonavir; AZT: zidovudine; DRV/r: darunavir boosted with ritonavir; DTG: dolutegravir; EFV: efavirenz; FTC: emtricitabine; LPV/r: lopinavir boosted with ritonavir; NVP: nevirapine; RAL: raltegravir; TDF: tenofovir disoproxil fumarate. Special circumstances in which the preferred regimen would not be used is if it is not available or suitable due to significant toxicities, drug–drug interactions are anticipated or if drug procurement in the given country is challenging.

Population	Preferred first-line regimen	Alternative first-line regimen	Special Circumstances
Adults and adolescents (10+ years old)	TDF + 3TC (or FTC) + DTG	TDF + 3TC + EFV 400 mg[1]	TDF + 3TC (or FTC) + EFV 600 mg[1]
			AZT + 3TC + EFV 600 mg[1]
			TDF + 3TC (or FTC) + PI/r[1]
			TDF + 3TC (or FTC) + RAL
			TAF[2] + 3TC (or FTC) + DTG
			ABC + 3TC + DTG
Children (3–10 years)	ABC + 3TC + DTG	ABC + 3TC + LPV/r	ABC + 3TC + EFV (or NVP)
		ABC + 3TC + RAL[3]	AZT + 3TC + EFV[4](or NVP)
		TAF + 3TC (or FTC) + DTG	AZT + 3TC + LPV/r (or RAL)
Infants (0–3 years)	AZT + 3TC + RAL	AZT + 3TC + NVP	AZT + 3TC + LPV/r

[1] EFV-based ART should not be used in countries with national estimates of pretreatment resistance to EFV of 10% or higher. DTG-based ART is preferred. When unavailable, a boosted PI-based regimen should be used, where the choice of PI/r depends on programmatic characteristics.
[2] TAF can be considered for people with established osteoporosis and/or impaired kidney function.
[3] RAL should be used as an alternative regimen only if LPV/r solid formulations are not available.
[4] EFV should not be used for children younger than three years.

Table 5.5: Recommended second-line regimens by population as outlined in the World Health Organization's 2019 clinical guidelines for antiretroviral therapy [56]. 3TC: lamivudine; ABC: abacavir; ATV/r: atazanavir boosted with ritonavir; AZT: zidovudine; DRV/r: darunavir boosted with ritonavir; DTG: dolutegravir; EFV: efavirenz; FTC: emtricitabine; LPV/r: lopinavir boosted with ritonavir; NVP: nevirapine; RAL: raltegravir; TDF: tenofovir disoproxil fumarate.

Population	Failing first-line regimen	Preferred second-line regimen	Alternative second-line regimen
Adults and adolescents[1] (10+ years old)	TDF + 3TC (or FTC) + DTG[2]	AZT + 3TC + ATV/r (or LPV/r)	AZT + 3TC + DRV/r[3]
	TDF + 3TC (or FTC) + EFV (or NVP)	AZT + 3TC + DTG[2]	AZT + 3TC + ATV/r (or LPV/r or DRV/r) [3]
	AZT + 3TC + EFV (or NVP)	TDF + 3TC (or FTC) + DTG[2]	TDF + 3TC (or FTC) + ATV/r (or LPV/r or DRV/r) [3]
Children and Infants (0 – 10 years)	ABC + 3TC + DTG	AZT+ 3TC + LPV/r (or ATV/r[4])	AZT + 3TC + DRV/r[5]
	ABC (or AZT) + 3TC + LPV/r	AZT (or ABC) + 3TC + DTG	AZT (or ABC) + 3TC + RAL
	ABC (or AZT) + 3TC + EFV	AZT (or ABC) + 3TC + DTG	AZT (or ABC) + 3TC + LPV/r (or ATV/r[4])
	AZT + 3TC + NVP	ABC + 3TC + DTG	ABC + 3TC + LPV/r (or ATV/r[4] or DRV/r[5])

[1] Sequencing if PIs are used in first-line ART: ATV/r (or LPV/r or DRV/r depending on programmatic considerations) + TDF + 3TC (or FTC) and then AZT + 3TC + DTG in second-line ART.
[2] TAF (tenofovir alafenamide) can be used as an alternative NRTI in special situations for adults and adolescents.
[3] RAL + LPV/r can be used as an alternative second-line ART regimen for adults and adolescents.
[4] ATV/r can be used as an alternative to LPV/r for children older than three months, but the limited availability of suitable formulations for children younger than six years, the lack of a fixed-dose formulation and the need for separate administration of the ritonavir booster should be considered when choosing this regimen.
[5] DRV should not be used for children younger than three years and should be combined with appropriate dosing of ritonavir.

Chapter 6

Discussion

Strict adherence to HIV-1 antiretroviral therapy is crucial in maintaining viral suppression, minimizing the emergence of drug-resistant mutations and improving overall mental health and quality of life. Side effects to antiretroviral drugs, complexity of prescribed regimens and socio-economic status are among some of the determinants of health that can influence adherence. Since imperfect adherence facilitates drug resistance, it is important to understand the impact of drug holidays on virologic response.

Standard combination therapy models [46, 66, 67, 68, 69] typically consist of a system of ODEs to describe the interaction between susceptible cells, infected cells, non-infectious virions and infectious virions. Within these equations, they define $0 \leq \epsilon_R \leq 1$ to describe the inhibition of infection due to reverse transcriptase inhibitor use and $0 \leq \epsilon_P \leq 1$ to describe the inhibition of budding infectious virions due to protease inhibitor use. These models make the assumption that the drug is widely available within the body and the (average) efficacy varies between complete drug failure and complete inhibition. While this means the resulting model are quite simple and appealing due to their mathematical tractability, they fail to capture the vast variability in drug efficacy due to pharmacokinetics differences between each drug and within each patient. Another disadvantage is that the dynamics of drug behaviour are ignored. Ignoring both the pharmacokinetics and pharmacodynamics profiles of the antiretroviral drugs may result in misleading conclusions, especially in a model formulated to make predictions about the emergence of drug resistance .

In this thesis, we developed the first immunological model of the HIV-1 infected human immune system that integrates the unique mechanisms of action for NRTIs,

NNRTIs and PIs in multi-class ART. The models incorporates both a wild-type and a drug-resistant viral strain. Since the emergence of a mutant strain is highly dependent on drug levels, which vary with the drug dosage absorption, drug half life and dosing interval, our modelling approach integrates these pharmacokinetic factors; this enabled us to determine how many doses could be missed for each WHO-approved regimen, as well as the number of doses that needed to be taken in order to return to pre-interruption levels. These results are summarized in Table 5.3. We used impulsive differential equations to model the kinetics of drug action.

Overall, ART can tolerate fairly short drug holidays, as long as the patient starts at a high drug concentration, and diligently takes their medication following the break. The length of acceptable holidays will vary with each drug, as well as which other drugs are in the regimen and if the drugs are stopped synchronously or asynchronously. Using the available pharmacokinetic data, we determined that the maximum length of a drug holiday varies between one day (AZT+3TC+ATV/r) and five days (ABC+3TC+DRV/r and TDF+3TC+DRV/r), assuming drugs are stopped at the same time. The virologic cost of exceeding these recommendations is unacceptably high, as shown in Figure 5.5; the drug resistance accumulated during therapy interruption can take several weeks to be eliminated, even assuming perfect adherence after the interruption. These numerical results have also been mirrored in the clinical setting through various clinical trials. They may explain why studies looking at long-term treatment interruptions have failed to suppress viral replication.

We also demonstrated the varying virologic responses to different patterns of adherence within the same adherence strata; missing consecutive doses favours the emergence of drug resistance more than missing doses intermittently, as shown in Figures 5.7–5.9. The effect of inter-individual variability on the number of missable doses was also examined.

In addition to adherence, therapy outcome can depend on treatment expertise, previously conferred mutations and other host factors not considered in this thesis. We assumed that a dose is either taken, or not, precisely at the prescribed times. We ignore the fact that, in reality, a semi-adherent patient may choose to take a dose later than prescribed, or take twice the dosage amount at the next prescription time. Since our estimates are based on maximal concentrations, this could overestimate drug-exposure; as the number of missable doses is most sensitive to time between doses, as shown in Figure 5.10, this could influence the time a patient could safely continue a drug holiday. Lastly, we also assume that the change in drug concentration is instantaneous after a dose has been taken. While some drugs have a short time to peak concentration, others do not; however, many studies have shown that non-impulsive HIV models match the results of impulsive models with significant accuracy [2].

Many important future research directions may be guided by this thesis. For example, this includes expanding the model to account for latent viral reservoirs, which are anatomical sites in which a replication-competent strain of the virus accumulates

and remains dormant within the proviral DNA; as only actively-replicating virus is targeted by ART, these latently-infected reservoirs will persistent even when in the region of viral elimination. Cellular activation of these reservoirs can lead to virema rebound, if treatment is interrupted. The effect these viral reservoirs can have on viral suppression during therapy breaks should be further explored. Additionally, since certain drugs can upregulate another drug's half-life or IC_{50} values when taken concomitantly, another expansion of the model could take this specific pharmacokinetic effect into account.

The work in this thesis can also be useful in guiding the development of a model that accounts for the interactions between NRTIs and integrase inhibitors. The alarming rate at which resistance to NNRTIs is being observed, specifically in low and middle-income countries [70], threatens the success of the global scale-up of ART. In 2019, several of the WHO's recommended first-line regimens changed from NNRTI-based regimens, to those with either a PI or INSTI backbone. The switch reduces the threat posed by NNRTI resistance, due to the high genetic barrier to resistance of both PIs and INSTIs. The recommendations for drug-holiday length presented in this thesis, as well as similar recommendations for INSTI-containing regimens, are critical to curbing the spread of NNRTI resistance before the whole class becomes broadly ineffective: diversified multi-class regimen choices will preserve therapeutic options for patients on a failing first-line regimen.

The implications of understanding the adherence–drug resistance relationship are critical to achieving the global goal of ending the HIV/AIDS epidemic by 2030. However, suboptimal adherence remains a significant barrier to achieving these targets. Structured treatment interruptions, as outlined in this thesis, may increase adherence by minimizing treatment side effects and fatigue. In addition, the results may also serve as a guideline for physicians prescribing relief from drug-related side effects and patients who may have inadvertently started a drug holiday. It also provides a robust method by which to determine therapy guidelines for patients who are unwilling or unable to adhere completely.

The COVID-19 pandemic, caused by severe acute respiratory syndrome coronavirus 2 (SARS-CoV-2), represents another significant barrier to achieving the 2030 targets. The wide-spread lockdowns have significantly affected both the production and distribution of antiretroviral drugs, especially in low or middle-income countries. As a result of these disruptions, 73 countries are at risk of stock-outs, 24 of which are already experiencing a critically low stock of antiretrovirals [71]; this represents approximately 33% of people receiving ART globally. However, as an illustrative example, suppose a patient taking ABC+3TC+DRV/r was following the recommendations in this thesis: a drug holiday lasting 5 days and followed by continuous therapy for 15 days. Over a period of six months, this cycle could be repeated nine times, prolonging drug supply by an additional 45 days without compromising therapeutic response. As recent modelling has estimated that a six-month disruption of

antiretroviral therapy could cause more than 500,000 additional deaths from AIDS-related illnesses in sub-Saharan Africa alone in 2020–2021 [18], following cycles of treatment interruptions as outlined in this thesis (Table 5.3) could help reduce the percentage of these deaths attributable to the emergence of drug resistance.

Bibliography

[1] S.G. Deeks, S.R. Lewin, and D.V. Havlir. The end of AIDS: HIV infection as a chronic disease. *The Lancet*, 382(9903):1525–1533, 2017.

[2] R.J. Smith? Adherence to antiretroviral HIV drugs: how many doses can you miss before resistance emerges? *Proc. Biol. Sci.*, 273(1586):617–624, 2006.

[3] C. Janeway, P. Travers, M. Walport, and M. Shlomchik. *Immunobiology: the immune system in health and disease*. Taylor and Francis Group, London, 2006.

[4] F. Zanini, V. Puller, J. Brodin, A. Jan, and R.A. Neher. In-vivo mutation rates and the landscape of fitness costs. *Virus Evol*, 3(1), 2017.

[5] A. Ali, R.M. Bandaranayake, Y. Cai, N.M. King, M. Kolli, S. Mittal, J.F. Murzycki, M.N. Nalam, E.A. Nalivaika, A. Ozen, M.M. Prabu-Jeyabalan, K. Thayer, and C.A. Schiffer. Molecular Basis for Drug Resistance in HIV-1 Protease. *Viruses*, 2(11):2509–2535, 2010.

[6] World Health Organization. Hiv drug resistance report 2019. https://www.who.int/hiv/pub/drugresistance/hivdr-report-2019/en/, 2019.

[7] A. N. Phillips, J. Stover, V. Cambiano, F. Nakagawa, M.R Jordan, D. Pillay, M. Doherty, P. Revill, and S. Bertagnolio. Impact of HIV Drug Resistance on HIV/AIDS-Associated Mortality, New Infections, and Antiretroviral Therapy Program Costs in Sub–Saharan Africa. *J. Infect. Dis.*, 214(12):1826–1830, 2016.

[8] Y. Huang, H. Wu, and E.P. Acosta. Hierarchical Bayesian inference for HIV dynamic differential equation models incorporating multiple treatment factors. *Biom J*, 52(4):470–486, 2010.

[9] R.J. Smith? and B.D. Aggarwala. Can the viral reservoir of latently infected CD4(+) T cells be eradicated with antiretroviral HIV drugs? *J Math Biol*, 59(5):697–715, 2009.

[10] V. von Wyl, V. Cambiano, M.R. Jordan, S. Bertagnolio, A. Miners, D. Pillay, J. Lundgren, and A.N. Phillips. Cost-effectiveness of tenofovir instead of zidovudine for use in first-line antiretroviral therapy in settings without virological monitoring. *PLoS ONE*, 7(8):e42834, 2012.

[11] R.E. Miron and R.J. Smith? Modelling imperfect adherence to HIV induction therapy. *BMC Infect. Dis.*, 10:6, 2010.

[12] R.J. Smith and L.M. Wahl. Distinct effects of protease and reverse transcriptase inhibition in an immunological model of HIV-1 infection with impulsive drug effects. *Bull. Math. Biol.*, 66(5):1259–1283, 2004.

[13] D.D. Bainov and P.S. Simeonov. *Impulsive differential equations: periodic solutions and applications*. Longman Scientific and Technical, Burnt Mill, 1993.

[14] D.D. Bainov and P.S. Simeonov. *Impulsive Differential Equations: Asymptotic Properties of the Solutions*. World Scientific, Singapore, 1995.

[15] V. Lakshmikantham, D.D. Bainov, and P.S. Simeonov. *Theory of Impulsive Differential Equations*. World Scientific Publishing, Singapore, 1989.

[16] R.J. Smith and L.M. Wahl. Drug resistance in an immunological model of HIV-1 infection with impulsive drug effects. *Bull. Math. Biol.*, 67(4):783–813, 2005.

[17] M.W. Tang and R.W. Shafer. HIV-1 Antiretroviral Resistance. *Drugsl*, 72(9):1–25, 2012.

[18] UNAIDS. Seizing the moment: tackling entrenched inequalities to end epidemics. https://aids2020.unaids.org/report, 2020.

[19] World Health Organization. HIV/AIDS Key facts. https://www.who.int/news-room/fact-sheets/detail/hiv-aids, 2020.

[20] I.L. Chrystie and J.D. Almeida. The Morphology of Human Immunodeficiency Virus (HIV) by Negative Staining. *J Med Virol*, 25(3):281–288, 1998.

[21] J.G. Briggs, T. Wilk, R. Welker, H.G. Kräusslich, and S.D. Fuller. Structural organization of authentic, mature HIV-1 virions and cores. *EMBO J.*, 22(7):1707–1715, 2003.

[22] German Advisory Committee: Assessment of Pathogens Transmissible by Blood Subgroup. Human Immunodeficiency Virus (HIV). *Transfus Med Hemother.*, 43(3):203–222, 2016.

[23] J.M. Watts, K.K. Dang, R.J. Gorelick, C.W. Leonard, J.W. Bess, R. Swanstrom, and C.L. Burch nd K.M. Weeks. Architecture and Secondary Structure of an Entire HIV-1 RNA Genome. *Nature*, 460(7256):711–716, 2009.

[24] C.B. Wilen, J.C. Tilton, and R.W. Doms. HIV: Cell Binding and Entry. *Cold Spring Harb Perspect Med.*, 2(8), 2012.

[25] B. Lee, M. Sharron, L.J. Montaner, D. Weissman, and R.W. Doms. Quantification of CD4, CCR5, and CXCR4 levels on lymphocyte subsets, dendritic cells, and differentially conditioned monocyte-derived macrophages. *Pro. Nat.*, 96(9):15215–5220, 1999.

[26] R.W. Doms and J.P. Moore. HIV-1 Membrane Fusion. *J. Cell Biol.*, 151(2):f9–f14, 2000.

[27] T.E. Schlub, A.J. Grimm, R.P. Smyth, D. Cromer, A. Chopra, S. Mallal, V. Venturi, C.Waugh, J. Mak, and M.P. Davenport. Fifteen to Twenty Percent of HIV Substitution Mutations Are Associated with Recombination. *J. Virol*, 88(7):3837–3849, 2014.

[28] W.S. Hu and S.H. Hughes. HIV-1 reverse transcription. *Cold Spring Harb Perspect Med.*, 2(10):a006882, 2012.

[29] G.L. Beilhartz and M. Götte. HIV-1 Ribonuclease H: Structure, Catalytic Mechanism and Inhibitors. *Viruses*, 2(4):900–926, 2010.

[30] R. Craigie. The molecular biology of HIV integrase. *Future Virol.*, 7(7):679–686, 2012.

[31] R. Craigie and F.D. Bushman. HIV DNA Integration. *Cold Spring Harb Perspect Med.*, 2(7):a006890, 2012.

[32] O. Delelis, K. Carayon, A. Saïb, E. Deprez, and J.F.Mouscadet. Integrase and integration: biochemical activities of HIV-1 integrase. *Retrovirology*, 5(114), 2008.

[33] S. Hare, G.N Maertens, and P. Cherepanova. 3'-Processing and strand transfer catalysed by retroviral integrase in crystallo. *EMBO J.*, 31(13):3020–3028, 2012.

[34] N.T. Sebastian and K.L. Collins. Targeting HIV latency: resting memory T cells, hematopoietic progenitor cells, and future directions. *Expert Rev Anti Infect Ther.*, 12(10):1187–1201, 2014.

[35] R.D. Liu, J. Wu, R. Shao, and Y.H. Xue. Mechanism and factors that control HIV-1 transcription and latency activation. *J Zhejiang Univ Sci B.*, 15(5):455–465, 2014.

[36] K.A. Roebuck and M. Saifuddin. Regulation of HIV-1 Transcription. *Gene Expr.*, 8(2):67–84, 1999.

[37] W.I Sundquist and H.G Kräusslich. HIV-1 Assembly, Budding, and Maturation. *Cold Spring Harb Perspect Med.*, 2(7), 2012.

[38] N. Jouvenet, S.M. Simon, and P.D. Bieniasz. Visualizing HIV-1 assembly. *J. Mol. Biol.*, 410(4):501–511, 2012.

[39] S. Jing, Q. Zhao, and A.K. Debnath. Peptide and Non-peptide HIV Fusion Inhibitors. *Bentham. Sci.*, 8(8):563–580, 2002.

[40] A. Palani and J.R. Tagat. Discovery and Development of Small-Molecule Chemokine Coreceptor CCR5 Antagonists. *J. Med. Chem*, 49(10):2851–2857, 2006.

[41] A.D. Holec, S. Mandal, P.K.Prathipati, and C.J. Destache. Nucleotide Reverse Transcriptase Inhibitors: A Thorough Review, Present Status and Future Perspective as HIV Therapeutics. *Curr. HIV Res.*, 15(6):411–421, 2017.

[42] M.P. de Béthune. Non-nucleoside reverse transcriptase inhibitors (NNRTIs), their discovery, development, and use in the treatment of HIV-1 infection: a review of the last 20 years (1989-2009). *Antiviral Res.*, 85(1):75–90, 2009.

[43] W.G. Powderly. Integrase inhibitors in the treatment of HIV-1 infection. *J. Antimicrob. Chemother.*, 65(12):2485–2488, 2010.

[44] A.K. Patick and K.E. Potts. Protease inhibitors as antiviral agents. *Clin. Microbiol. Rev.*, 11(4):614–627, 1998.

[45] R.J. Pomerantz and D.L. Horn. Twenty years of therapy for HIV-1 infection. *Nat. Med.*, 9(7):867–873, 2003.

[46] A.S. Perelson, A.U. Neumann, M. Markowitz, J.M. Leonard, and D.D. Ho. HIV-1 dynamics in vivo: virion clearance rate, infected cell lifespan, and viral generation time. *Science*, 271(5255):1582–1585, 1995.

[47] A.S. Perelson, D.E. Kirschner, and R. De Boer. Dynamics of HIV infection of CD4 T cells virion:clearance rate, infected cell lifespan, and viral generation time. *Math Biosci.*, 114(1):81–125, 1993.

[48] R.E. Miron and R.J. Smith? Resistance to protease inhibitors in a model of HIV-1 infection with impulsive drug effects. *Bull. Math. Biol.*, 76(1):59–97, 2014.

[49] J.M. Heffernan, R.J. Smith?, and L.M. Wahl. Perspectives on the basic reproductive ratio. *J R Soc Interface*, 2(4):281–293, 2005.

[50] S. M. Blower and H. Dowlatabadi. Sensitivity and Uncertainty Analysis of Complex Models of Disease Transmission: An HIV Model, as an Example. *International Statistical Review*, 62(2):229–243, 1994.

[51] J. Lou, Y. Lou, and J. Wu. Threshold Virus Dynamics With Impulsive Antiretroviral Drug Effects. *J Math Biol.*, 65(4):623–652, 2012.

[52] S.S. Morse. Factors in the Emergence of Infectious Diseases. *Emerg. Infect. Dis.*, 1(1):7–15, 1995.

[53] O. Diekmann, J.A.P. Heesterbeek, and J.A. Metz. On the definition and the computation of the basic reproduction ratio R0 in models for infectious diseases in heterogeneous populations. *J. Math. Biol.*, 28(4):365, 1990.

[54] P. van den Driessche and J. Watmough. Reproduction numbers and subthreshold endemic equilibria for compartmental models of disease transmission. *Math. Biosci.*, 28:29, 2002.

[55] P. Hartman. *Ordinary Differential Equations: Second Edition.* Birkhäuser Boston, 675 Massachusetts Avenue, 1982.

[56] World Health Organization. Update of recommendations on first- and second-line antiretroviral regimens. https://apps.who.int/iris/bitstream/handle/10665/325892/WHO-CDS-HIV-19.15-eng.pdf?ua=1, 2019.

[57] The Strategies for Management of Antiretroviral Therapy (SMART) Study Group. CD4+ Count–Guided Interruption of Antiretroviral Treatment. *N. Engl. J. Med.*, 355(22):2283–2296, 2006.

[58] Trivacan ANRS 1269 Trial Group. Two-Months-off, Four-Months-on Antiretroviral Regimen Increases the Risk of Resistance, Compared with Continuous Therapy: A Randomized Trial Involving West African Adults. *J. Infect. Dis.*, 199(1):66–67, 2009.

[59] ANRS 162-4D Study Group. Four-days-a-week antiretroviral maintenance therapy in virologically controlled HIV-1-infected adults: the ANRS 162-4D trial. *J. Antimicrob. Chemother.*, 73(3):739–747, 2018.

[60] C.J. Cohen, A.E. Colson, A.G. Sheble-Hall, K. A. McLaughlin, and G.D. Morse. Pilot Study of a Novel Short-Cycle Antiretroviral Treatment Interruption Strategy: 48-Week Results of the Five-Days-On, Two-Days-Off (FOTO) Study. *HIV Clin. Trials*, 8(1):19–23, 2015.

[61] D. Yoong, A.M. Bayoumi, L. Robinson, B. Rachlis, and T. Antoniou. Public prescription drug plan coverage for antiretrovirals and the potential cost to people living with HIV in Canada: a descriptive study. *CMAJ*, 6(4):551–560, 2018.

[62] B.L. Genberg, I.B. Wilson, D.R. Bangsberg, K. Goggin J. Arnsten, R.H. Remien, J. Simoni, R. Gross, N. Reynolds, M. Rosen, and H. Liu. Patterns of antiretroviral therapy adherence and impact on HIV RNA among patients in North America. *AIDS*, 26(11):1415–1423, 2013.

[63] J.J Parienti, M. Das-Douglas, V. Massari, D. Guzman, S.G. Deeks, R. Verdon, and D.R. Bangsberg. Not All Missed Doses Are the Same: Sustained NNRTI Treatment Interruptions Predict HIV Rebound at Low-to-Moderate Adherence Levels. *PLoS One*, 3(7):e2783, 2008.

[64] C.E. Golin, H. Liu, R.D. Hays, L.G. Miller, C.K. Beck, J. Ickovics, A.H. Kaplan, and N.S. Wenger. A prospective study of predictors of adherence to combination antiretroviral medication. *J Gen Intern Med*, 17(10):756–765, 2002.

[65] K.K. Byrd, J.G. Hou, R. Hazen, H.Kirkham, S. Suzuki, P.G. Clay, T.Bush, N.M. Camp, P.J. Weidle, and A. Delphino. Antiretroviral adherence level necessary for HIV viral suppression using real-world data. *J Acquir Immune Defic Syndr*, 8(3):245–251, 2019.

[66] R.M. Anderson and R.M. May. Epidemiology parameters of HIV transmission. *Nature*, 333(6173):514–519, 1988.

[67] A.R. McLean and M.A. Nowak. Competition between zidovudine sensitive and resistant strains of HIV. *AIDS*, 6(1):71–79, 1992.

[68] L.M. Wei, S.K. Ghosh, M.E. Taylor, V.A. Hohnson, E.A. Emini, P. Deutsch, J.D. Lifson, S. Bon hoeffer, M.A. Nowak, B.H. Hahn, M.S. Saag, and G.M. Shaw. Viral dynamics in HIV-1 infection. *Nature*, 373(6510):117–122, 1995.

[69] A.S. Perelson and P.W. Nelson. Mathematical analysis of HIV-1 dynamics in vivo. *SIAM Rev.*, 41(1):3, 1999.

[70] World Health Organization. HIV drug resistance report 2019. *Virol. J.*, 2019.

[71] World Health Organization. The cost of inaction: COVID-19-related service disruptions could cause hundreds of thousands of extra deaths from HIV. https://www.who.int/news/item/11-05-2020-the-cost-of-inaction-covid-19-related-service-disruptions-could-cause-hundreds-of-thousands-of-extra-deaths-from-hiv, 2020.